Chemical Physics Reviews

Layer-by-layer assembly of metal-organic framework thin films: Fabrication and advanced applications

Cite as: Chem. Phys. Rev. 4, 011305 (2023); https://doi.org/10.1063/5.0135019
Submitted: 15 November 2022 • Accepted: 05 January 2023 • Published Online: 10 February 2023

Dong-Hui Chen, Hartmut Gliemann and Christof Wöll

Chemical Physics Reviews REVIEW scitation.org/journal/cpr

Layer-by-layer assembly of metal-organic framework thin films: Fabrication and advanced applications

Cite as: Chem. Phys. Rev. 4, 011305 (2023); doi: 10.1063/5.0135019
Submitted: 15 November 2022 · Accepted: 5 January 2023 ·
Published Online: 10 February 2023

Dong-Hui Chen, Hartmut Gliemann, and Christof Wöll[a)]

AFFILIATIONS

Institute of Functional Interfaces (IFG), Karlsruhe Institute of Technology (KIT), Hermann-von-Helmholtz-Platz 1, 76344 Eggenstein-Leopoldshafen, Germany

[a)]Author to whom correspondence should be addressed: christof.woell@kit.edu

ABSTRACT

Metal-organic frameworks (MOFs) are a class of crystalline porous coordination materials, which are assembled from inorganic nodes and organic linkers. Numerous applications, such as gas storage, molecule separation, catalysis, optical sensing, and charge transport, benefit from the outstanding properties of MOF materials. More advanced applications, e.g., in the electronics and optoelectronics area, demand homogeneous and monolithic MOF thin films. Recent studies demonstrated that surface-mounted MOFs (SURMOFs) are well suited to fulfill the requirements for the integration of MOFs into devices. As a crystalline thin-film material with tunable thickness, SURMOFs have been widely used in the optimization of chromophore stacking, electrical transport, stimuli-response, etc. The fabrication of SURMOFs is carried out employing a layer-by-layer (LbL) assembly technique, and it can yield MOF thin films with a well-defined orientation, tunable thickness, and editable crystalline heterostructure. We summarize the LbL assembly methods for SURMOF fabrication and the realization of advanced SURMOF architectures, including optical and electronic applications as well as the integration of photoactive SURMOFs and SURMOF-derived materials in technical devices. We conclude with a discussion of the challenges and prediction of the future of SURMOF materials.

TABLE OF CONTENTS

I. INTRODUCTION

Metal-organic frameworks (MOFs) were introduced in 1995 by Yaghi and co-workers[1] and are characterized by their high crystallinity and porosity (up to 10 000 m^2/g).[2,3] MOFs generally consist of inorganic node components—metal ions or metal ion-containing clusters—and organic linker molecules. The linker molecules have two or more functional sites that coordinatively bind to the node metal ions or ion-containing clusters. MOFs are usually prepared as bulk material by hydrothermal or solvothermal synthesis processes, where a

solution containing the ionic component and the linker is kept at elevated temperatures for several hours under increased pressure. When applying appropriate reaction conditions, a highly crystalline MOF powder precipitates. Due to the huge number of available nodes and linker building blocks, it is difficult to provide an upper limit for the number of different MOF crystal structures. More than 100 000 different MOF structures are known in the literature.[2] As the geometry of the pores is determined by the used linkers—e.g., in terms of the pore size and pore shape—the building block principle offers an excellent opportunity to tailor MOF materials according to the application. In a first systematic study, Eddaoudi *et al.* used linker molecules with different lengths to produce bulk MOFs with different pore sizes.[4] An overview of the historical evolution of porosity and the activation of MOFs is given by Farha *et al.*[2] MOF-based bulk materials display outstanding properties for applications in many technical fields, such as gas storage or fixed-bed-based gas filtering and separation.[5–8] For those applications, the powder form of MOFs is well suited since filling of the corresponding columns or containers is rather straightforward. However, a number of more advanced, emerging applications of MOFs emerging require the fabrication of MOF thin films or coatings. In this context, the application potential of MOF powders is limited due to the low orientation and adhesion of MOF particles on substrates as well as the large roughness of the resulting layers. In addition, thin films made from MOF particles show low transparency, an obvious disadvantage, e.g., when coating optical glasses. Therefore, much effort has been directed toward coating substrates with well-defined, homogeneous MOF-based layers. Several review papers provide an overview of MOF thin film deposition on different supporting substrates.[9–11] In one of the most obvious methods, *in situ* solvothermal growth, substrates are immersed in a precursor solution containing the inorganic compound and the linker, resulting in the deposition of a polycrystalline MOF film. Because of the large roughness and the low structural quality of the resulting films, a number of other, more advanced approaches for coating substrates with MOFs have been developed. Virmani *et al.* reported on vapor-assisted conversion (VAC) to grow several MOFs of the UiO class on gold-coated glass and silicon substrates. Here, the first step is to spread a precursor solution on a substrate, which is then stored in a saturated atmosphere of a solvent.[12] MOF coatings can also be prepared by immersing a solid material, e.g., ZnO, into a solution of the linker molecule, such as 1-methylimmidazole. The MOF layer is then formed by the coordination of the Zn ions at the ZnO interface by the linker molecule. In that way, the ZnO acts as a sacrificial substrate and is consumed with progressing MOF growth.[13] This method is similar to the process which has been introduced by Yaghi *et al.*, where silver particles were first coated with alumina and then immersed in a solution with the linker 4,4′,4″,4‴-(porphyrin-5,10,15,20-tetrayl)tetrabenzoic acid (H_4TCPP) to form the MOF [$Al_2(OH)_2$TCPP].[14]

The substantial impact of MOF thin films in numerous application fields has been the topic of several recent reviews,[15] including electrochemical approaches.[16–18] This review article gives a comprehensive overview of MOF-based thin films which are used as active materials in photovoltaics and catalysis (e.g., CO_2 reduction and water splitting), in electronics (e.g., as memristors, field effect transistors, dielectrics or thermoelectric devices), as energy storage materials for batteries and supercapacitors or as membranes. Although thick MOF layers can be achieved with those coating techniques—which is why they can be seen as very effective—there are several drawbacks that limit their application. One disadvantage, e.g., of solvothermal deposition, is the missing orientation of the MOF material. Particularly for investigating diffusion processes of the guest molecule in the framework, well-oriented MOF layers are required to (1) exclude any influence of polycrystalline morphology on the diffusion behavior and (2) correlate the experimental results with theoretical calculations—this is much easier when the experimentally produced MOF material is close to the theoretically ideal geometry. This is also very important when investigating the electrical conductivity of MOFs. In addition, it is hardly possible to control the thickness of the layers in the range of a few nanometers with the methods mentioned above.

Therefore, alternative techniques needed to be developed to face the following challenges:

(1) Is it possible to develop a process that allows the growth of highly oriented MOF-based thin films with a thickness that can be controlled in the range of a few nanometers?
(2) To what extent is it possible to create heteroepitaxial MOF layers?
(3) What is the best way to render electrical conductivity to MOF thin films?
(4) How can the defect density in MOF thin films be reduced?
(5) Which are the best methods to reduce the roughness of MOF thin films?
(6) Are there strategies to fabricate MOF thin films with guests (C_{60}, semiconductor or metal nanoparticles, proteins) loaded in the pores? And to yield loaded/unloaded hetero-multilayers?

In the following, we will demonstrate that layer-by-layer (LbL) assembly fulfills virtually all of these requirements.

The LbL assembly technique was first introduced by Langmuir and Blodgett in 1937 for depositing stearate films prepared at the air–water interface onto different types of solid substrates.[19] As a powerful liquid-phase technique, LbL assembly can be utilized to generate multilayer thin films and control their thicknesses in the nanometer regime.[20,21] In the past decades, LbL assembly has been widely used for the deposition of various molecular materials, including bipolar amphiphiles,[22] biomacromolecules,[23,24] two-dimensional (2D) materials,[21] and nanoparticles.[25] The stacking of the layers gives rise to a periodicity perpendicular to the substrate, which can be probed by x-ray diffraction (XRD).[26] Also, the structure within the layers can be probed by XRD, but the multilayers do not exhibit a 3D crystalline structure, i.e., there is no fixed relationship between the structures of adjacent layers. Subsequently, the LbL method has also been used for the assembly of multilayers of appropriately functionalized thiols[27] and polymers.[22] Also, in the latter two cases, the resulting multilayers do not show crystallinity in all three dimensions.

In this review, we focus on MOFs as the basis for applying the LbL method to the growth of 3D crystalline MOF thin films and for integrating the loading of guests into the LbL process. The first report on the LbL growth of crystalline and oriented HKUST-1-based MOF thin films was published in 2007.[28] In this pioneering work, Au substrates modified by self-assembled monolayers (SAMs)[15,29,30] were successively dipped by hand into four reservoirs containing (1) metal salt solution (Cu acetate in ethanol), (2) rinsing solution (ethanol), (3) organic linker solution (benzene-1,3,5-tricaboxylic acid in ethanol), and (4) rinsing solution (ethanol). These four dipping sub-steps

formed one complete deposition cycle and should—theoretically—result in an increase in the surface-mounted MOF (SURMOF) thickness by exactly one SURMOF layer. The rinsing steps are required to (1) avoid any cross contamination of the linker or metal ion solution during dipping and (2) inhibit any formation of MOF nanocrystals on the substrate surface due to the reaction between residual linker molecules or metal ions on the substrate or inside the pores of the grown SURMOF layer. XRD data of these materials revealed sharp diffraction peaks detected using out-of-plane or in-plane scattering geometries, arising from the planes oriented parallel or perpendicular to the substrate, respectively. As will be described, the pores of SURMOFs can be loaded with molecules or clusters. One option for filling the pores is to immerse the SURMOF-coated substrate in a solution containing the molecules or clusters. However, what about the case when the guest molecules or clusters are too big to pass through the pore apertures? In this case, the encapsulation approach can be employed by implementing two more sub-steps during the SURMOF deposition cycle. After treatment with the metal ion solution, the sample is dipped or treated with the solution of the guest molecule or cluster, followed by a rinsing step. The guest molecule can now occupy the open pores of the structure. As soon as the sample is treated with the linker solution during the next sub-step, the guest will be "captured" inside the closed pore.

Note that LbL synthesis is strikingly different from conventional MOF synthesis, which is done using solvothermal methods applied to mixtures of the reactants and heating to temperatures typically above 150 °C.[31] In the following, MOF thin films fabricated using the LbL method will be referred to as SURMOFs.

While the popular MOF HKUST-1 was synthesized in the first realization of a SURMOF, in later work, inspired by the success of SURMOF fabrication approaches, numerous other types of MOFs were successfully grown as SURMOFs using the LbL technique. In addition, numerous variants of the original dipping method were introduced to deposit SURMOFs on a huge variety of substrates. Here, we focus on the most popular SURMOF fabrication methods using the LbL approach, namely, dipping,[28] pumping,[32] spraying,[33] and spin coating,[34] see Fig. 1.

As described above, the first LbL deposition of SURMOF thin films was performed manually. Since then, fully automated robot systems operated inside a glovebox have been introduced, allowing environmental conditions to be controlled in terms of humidity and temperature. In addition, nitrogen can be used as an inert gas during synthesis to avoid the influence of oxygen.[35] The resulting SURMOF quality in terms of crystallinity, thickness, and orientation is strongly dependent on the immersion and rinsing times, which must be controlled during the deposition process. Also, the application of ultra-sonification can be important to improve the roughness and transparency of SURMOF layers.[36]

The pump LbL method adopts the above-mentioned strategy of exposing a substrate to different solutions in an alternating fashion. Instead of immersing and then removing the substrate from different reservoirs containing synthesis or rinsing solutions, in the pump system, functionalized substrates are placed inside a temperature-controlled double-walled glass flow reactor. Three pumps inject a metal salt solution, organic solution, and rinsing solvent into the reactor, respectively. A programmable controller is used to steer the sequence of the pump operations as well as the immersion and rinsing times. An additional pump removes the corresponding solution before the next solution is injected.[32]

A very similar approach is the application of commercially available quartz crystal micro-balance (QCM) systems combined with an auto sampler.[37] The sampler feeds the QCM sensor cell with the different reaction and rinsing solutions. The LbL growth of the SURMOF thin film on the QCM sensor surface can be observed online by

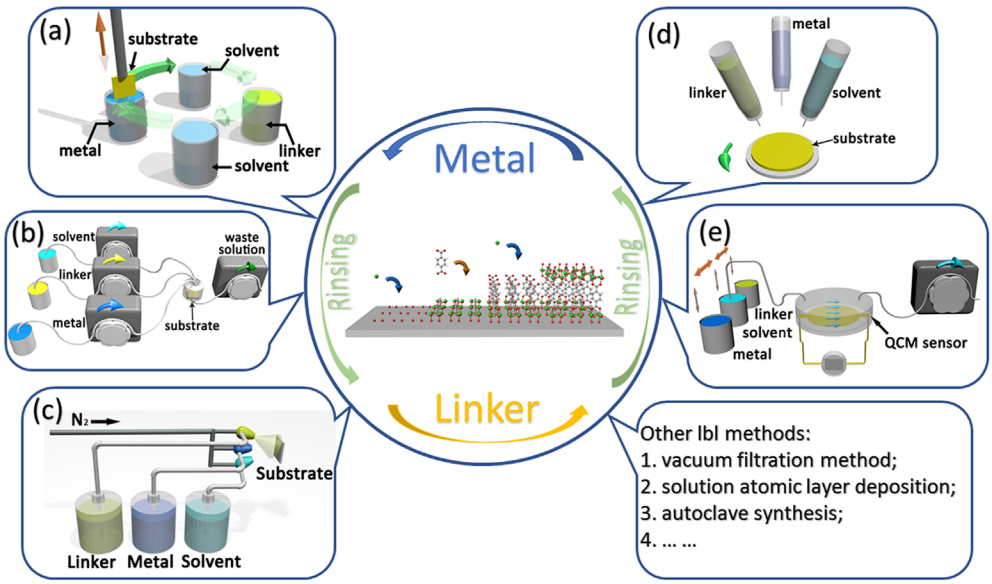

FIG. 1. Schematic illustration of the layer-by-layer assembly of SURMOFs: (a) dipping method, (b) pumping method, (c) spray method, (d) spin coating method, and (e) LbL synthesis on QCM system.

monitoring the mass change of the functionalized QCM chip.[37] In addition to allowing the LbL growth to be monitored, the QCM system can additionally be used to investigate the loading of the SURMOF pores with guest molecules, either in the gas phase or in liquid. The increase in mass during the loading process can provide valuable information about loading kinetics and the absolute mass of the species loaded inside the SURMOF pores.[38]

The spray LbL method employs a specially designed nozzle system that transforms the metal salt and organic linker solutions into aerosols so they can be sprayed on the substrate surface.[33] The metal salt solution and the organic linker solution are successively sprayed on the substrate while pure solvent is sprayed after each step for rinsing. The spray LbL method is a high-throughput fabrication process for depositing homogenous and uniform SURMOFs and is much faster than, e.g., the dipping or pump LbL approaches.

The spin-coating LbL method is carried out on a spin-coating machine, where the different solutions and rinsing liquids are dropped successively on a rotating chemically functionalized substrate that is fixed by a vacuum chuck on a rotator rotating at a certain angular velocity.[34] The application of the droplets can be made either by hand or by using fully automated micro syringes. The centrifugal force induces the dripping liquid to spread homogeneously on the surface. Spin coating is a facile method to generate SURMOFs with low reactant and solvent consumption. In the dipping and pump LbL approaches, the immersion times of the substrate in the corresponding reaction and rinsing solutions are relevant for SURMOF quality, but with spin coating, the drop volumes as well as the rotation speed and rotation time are used to optimize SURMOF growth.

When comparing the four above-mentioned approaches for preparing SURMOF-based thin films, we can identify advantages and drawbacks for every method. In dipping- or pump-based synthesis, every deposition sub-step is time consuming and can take up to 15 min. The increase in thickness of the SURMOF per deposition cycle corresponds to exactly one layer, and the final SURMOF shows a perfect orientation. This "real" LbL deposition was proven by using a surface plasmon resonance (SPR) device, where the SURMOF growth is carried out on the sensor gold surface in a flow cell, while the shift of the gold plasmon resonance band is determined at the same time.[28] The result confirms that an exact control of the thickness is possible and that challenge 1 mentioned above is solved. In contrast, with the spray method, one complete deposition cycle consisting of four sub-steps that take only a few minutes, and the average increase in thickness correlates with about ten SURMOF layers. However, spray-coated SURMOFs exhibit a lower orientation compared with the SURMOFs prepared by the dipping or pump method. It is found that, for each SURMOF type, one specific deposition approach results in an optimized quality. It was shown that heteroepitaxial SURMOF coatings (see challenge 2) can be realized just by switching from one linker molecule to another during the SURMOF synthesis.[39] To reduce the defect density on the molecular and atomic level (challenge 4), as a start an approach is needed to detect and to quantify defects in a SURMOF structure. One option is to use carbon monoxide as a probe molecule which shows different spectral positions of the IR absorption bands as a function of the oxidation state, e.g., of the Cu ion in a NOTT-100 MOF,[40] where it was shown that the defect density can be tuned by temperature. Reducing defects in terms of producing closed, highly transparent and homogenous SURMOF layers without pinholes can be achieved by using additional techniques during synthesis such as ultrasonic devices. With this approach, highly transparent SURMOF films have been produced without scattering effects visible on the SURMOF film.[36] The lbl method offers the opportunity to implement clusters, or big molecules inside the pores, although the guest species are not able to pass the pore apertures during a post-synthetic diffusion-driven loading of the MOF host structure due to steric hindrance. In this case, the guest molecules or clusters are offered during the SURMOF synthesis, where they are implemented inside the semi-finished pores.[41] Although many of the above-mentioned challenges are solved, some need to be faced in future. Roughness optimization is one important step toward high quality SURMOF coatings, when thinking applications where roughness on the nm scale might have significant influence as, e.g., in the performance of optical devices such as MOF-based micro cavities.[42]

Recently, other variants of LbL methods for MOF thin-film growth have been reported, such as the vacuum filtration method for 2D MOFs,[43] solution atomic layer deposition,[44] and autoclave synthesis.[45]

The use of SAMs to functionalize substrate surfaces for SURMOF growth creates the option to produce SURMOF patterns, e.g., by using micro-contact printing.[46] For this approach, a polymer stamp that is wetted with a solution containing a thiol terminated, e.g., with an –OH or –COOH group is used to create a SAM pattern on a gold surface. On those surface areas, which are in contact with the stamp, the SAM molecules are transferred to the surface. The non-coated areas can be refilled after the printing step by dipping the substrate in a solution with the second thiol which is terminated, e.g., with a $-CH_3$ group. This acts as a passivator for SURMOF growth.[47] Then, the LbL process is started for the SURMOF growth. For smaller structures, atomic force microscopy-based patterning can be applied (Table I).[48]

II. OPTICAL APPLICATION OF SURMOFs

To some extent, inspired by the work of Kuhn[202] for optical applications of Langmuir–Blodgett films, huge flexibility can be obtained by assembling crystalline materials from building blocks, metal nodes, and organic ligands. In this way, numerous MOF materials have been designed and prepared for various optical applications, such as light-emitting materials,[203–205] optical sensors,[206] nonlinear optical materials,[207] and upconversion (UC) materials.[208] The three most popular strategies to render photoactivity to MOFs are (1) using functionalized chromophores as linker molecules,[208,209] (2) utilizing unique metal ions or clusters as metal nodes,[210,211] and (3) loading guest molecules with special optical features into the pores of the MOF.[212,213] However, due to the scattering effect, integrating the powder form of MOFs into optical devices is not straightforward. By precisely controlling the thickness and quality in terms of orientation, crystallinity, and roughness, SURMOF materials can potentially be used to fabricate coatings for large-scale optical devices. In this section, we introduce SURMOFs for optical applications that benefit from editable manufacturing by the liquid-phase epitaxy LbL approach. We will also mention interfaces between different types of MOFs, as these are important for some optical applications, e.g., photon upconversion.[175]

A. Optimizing chromophore assemblies and controlling aggregation

Intermolecular interactions between π-conjugated organic chromophores strongly depend on the packing arrangement; thus, the

TABLE I. Summary of SURMOFs by the LbL assembly fabrication.

MOF type	LbL method	Solvent	Oriented growth and direction		Application	Ref.
$[Co(TCPP)]_n$	Dipping	Ethanol	No		Solar cells	49
$[Co(TCPP)]_n$	Spin coating	Ethanol	Yes	[011]	Nonlinear optical application	50
$[Cu(BDC)]_n$	Spray	Ethanol	Yes	[001]	Conductive SURMOFs	51
$[Cu(BDC)]_n$	Spray	Ethanol	Yes		Graphene transistors	52
$[Cu(BDC)]_n/[Cu(NDC)]_n/[Cu(BPDC)]_n$	Spray	Ethanol	Yes		Heterostructure SURMOFs	39
$[Cu(BDC)]_n/[Zn(BDC)]_n$	Spray	Ethanol	Yes		Antifouling coatings	53
$[Cu(BDC)_2]_n$	Pump/spray	Ethanol	Yes		Biocompatibility	54
$[Cu(BDC)_2]_n$	Spray	Ethanol	Yes		Magnetic behavior	55
$[Cu(BPDC)]_n$	Dipping	Ethanol	Yes		SAMs effect	56
$[Cu(DA\text{-}SBDC)]_n$	Dipping	Ethanol	Yes		SURGELs	57
$[Cu(DA\text{-}SBDC)]_n$	Dipping	Ethanol	Yes		Cell adhesion	58
$[Cu(DA\text{-}SBDC)]_n$	Dipping	Ethanol	Yes		Gas separation	59
$[Cu(QPDC)]_n$	Spray	Ethanol	Yes	[001]	Encapsulation of Au_{55} clusters	60
$[Cu(TCNQ)]_n$	Dipping	Ethanol	Yes		Electrically conductive SURMOFs	61
$[Cu(TCPP)]_n$	Dipping	Ethanol	Yes	[001]	Optical limiting	62
$[Cu_2(AB\text{-}BPDC)_2(BiPy)]_n$-on-$[Cu_2(BPDC)_2(BiPy)]_n$	Pump	Ethanol	Yes	[001]	Photoswitching release molecular	63
$[Cu_2(atBDC)_2(dabco)]_n/[Cu_2(BDC)_2(dabco)]_n$	Pump	Ethanol	Yes	[001]	Guest loading	64
$[Cu_2(AzoBDC)_2(dabco)]_n$	Dipping	Ethanol	Yes		Photoswitching separation	65
$[Cu_2(AzoBPDC)_2(AzoBiPyB)]_n$	Pump	Ethanol	Yes		Photoswitching separation	66
$[Cu_2(BDC)_2(AzoBiPyB)]_n/[Cu_2(DMTPDC)_2(AzoBiPyB)]_n$	Pump	Ethanol	Yes		Photoswitching SURMOFs	67
$[Cu_2(BDC)_2(bipy)]_n$	pump	Ethanol	Yes	[100]/[001]	Growth mechanism	68
$[Cu_2(BDC)_2(dabco)]_n/[Cu_2(C4H4BDC)_2(dabco)]_n/[Cu_2(BrBDC)_2(dabco)]_n/[Cu_2(NO2BDC)_2(dabco)]_n/[Cu_2(F4BDC)_2(dabco)]_n$	Pump	Ethanol	Yes	[100]/[001]	Growth mechanism by mixing linkers strategy	69
$[Cu_2(BDC)_2(dabco)]_n/[Cu_2(adc)_2(dabco)]_n$	Dipping	Ethanol	Yes	[001]	Photoswitching conductive SURMOFs	70
$[Cu_2(BDC)_2(dabco)]_n/[Cu_2(NH_2BDC)_2(dabco)]/[Cu_2(F4BDC)_2(dabco)]_n$	Spray	Ethanol	Yes		Triboelectric nanogenerator	71
$[Cu_2(BDC)_2]_n/[Cu_2(BPDC)_2]_n/[Cu_2(TPDC)_2]_n/[Cu_2(QPDC)_2]_n/[Cu_2(P(EP)_2DC)_2]_n/[Cu_2(PPDC)_2]_n$	Spray	Ethanol	Yes		Fabrication strategy	72
$[Cu_2(BDC)_2]_n/[Zn_2(BDC)_2]_n$	Spray	Ethanol	Yes	[010]	Oxidative polymerization	73
$[Cu_2(DCam)_2(AzoBiPyB)]_n$	Dipping	Ethanol	Yes	[001]	Photoswtiching enantioselectivity	74
$[Cu_2(DCam)_2(dabco)]_n/[Cu_2(DCam)_2(BiPy)]_n/[Cu_2(DCam)_2(BiPyB)]_n/$ HKUST-1/$[Cu(BDC)]_n/[Cu(BPDC)]_n$	Spray	Ethanol	Yes		Enantioselective QCM sensor array	75

TABLE I. (*Continued.*)

MOF type	LbL method	Solvent	Oriented growth and direction		Application	Ref.
$[Cu_2(Dcam)_{2x}(Lcam)_{2-2x}(dabco)]_n$	Dipping	Ethanol	Yes	[001]/[110]	Chiral SURMOFs	76
$[Cu_2(DMTPDC)_2(AzoBiPyB)]_n$/ $[Cu_2(AzoBPDC)_2(dabco)]_n$/ $[Cu_2(BDC)_2(AzoBiPyB)]_n$	Pump	Ethanol	Yes		Photoswitching uptake	77
$[Cu_2(e\text{-}BPDC)_2(dabco)]_n$	Dipping	Ethanol	Yes	[100]	Photomodulated conductive SURMOFs	78
$[Cu_2(F_2AzoBDC)_2(dabco)]_n$	Dipping	Ethanol	Yes		Photoswitching conductive SURMOFs	79
$[Cu_2(F_2AzoBDC)_2(dabco)]_n$	Dipping	Ethanol	Yes		Photomodulatable refractive index	80
$[Cu_2(F_2AzoBDC)_2(dabco)]_n$	Dipping	Ethanol	Yes		switchable selectivity for VOCs	81
$[Cu_2(F_4BDC)_2(dabco)]_n$	Dipping	Ethanol	Yes	[100]	Growth mechanism	82
$[Cu_2(F_4BDC)_2(dabco)]_n$	Pump	Ethanol	No		Seeding fabrication	83
$[Cu_2(FBDC)_2(dabco)]_n$	Dipping	Ethanol	Yes	[001]	Synthetic conditions	84
$[Cu_2(NDC)_2(dabco)]_n$	Pump	Ethanol	Yes	[001]	Selective modification	85
$[Cu_2(NDC)_2(dabco)]_n$	Dipping	Ethanol	Yes	[001]	Guest loading	38
$[Cu_2(NH_2BDC)_2(dabco)]_n$-on-$[Cu_2(BDC)_2(dabco)]_n$/ $[Cu_2(NDC)_2(dabco)]_n$-on-$[Cu_2(NH_2BDC)_2(dabco)]_n$-on-$[Cu_2(BDC)_2(dabco)]_n$	Pump	Ethanol	Yes	[001]	Heterostructured SURMOFs	86
$[Cu_2(NH_2BDC)_2(dabco)]_n$-on-$[Cu_2(BDC)_2(dabco)]_n$	Pump	Ethanol	Yes	[001]	Post-synthetic modification	87
$[Cu_3(HHTP)_2]_n$	Spray	Ethanol	Yes		Conductive SURMOFs	88
$[Cu_3(HHTP)_2]_n$	Spray	Ethanol	Yes	[001]	Conductive SURMOFs	89
$[Cu_3(HHTP)_2]_n$	Spray	Ethanol	Yes	[001]	Growth mechanism	90
$[Cu_2(TPDC)_2]_n$/ $[Cu_2(BA\text{-}TPDC)_2]_n$	Immersion	Ethanol	No		SURGELs	91
HKUST-1 ($[Cu_3(BTC)_2]_n$)	Dipping	Ethanol	Yes	[100]	SURMOF fabrication	28
HKUST-1	Dipping	Ethanol	Yes	[100]/[111]	Growth mechanism	92
HKUST-1	Dipping	Ethanol	Yes	[100]	Growth mechanism	93
HKUST-1	Dipping	Ethanol	Yes	[100]	Guest loading	37
HKUST-1	Spray	Ethanol	Yes	[111]	SURMOF fabrication	33
HKUST-1	Pump	Ethanol	Yes	[111]	SAM patterning	47
HKUST-1	Spray	Ethanol	Yes	[100]	SAM effect	85
HKUST-1	pump	Ethanol	Yes		Electrochemical application	94
HKUST-1	Dipping	Ethanol	Yes		Optical applications	95
HKUST-1	Spray	Ethanol	Yes	[100]	Control of defects	96
HKUST-1	Spray	Ethanol	Yes	[111]	SAM patterning	48
HKUST-1	Spray	Ethanol	Yes	[100]	Guest loading	97
HKUST-1	Spray	Ethanol	Yes	[111]	Nanomechanical investigation	98
HKUST-1	Spray	Ethanol	Yes	[100]	Optical sensing	99
HKUST-1	Dipping	Ethanol	Yes	[100]	Optical applications	36
HKUST-1	Spray	Ethanol	Yes	[111]	Loading; electrically conductive SURMOFs	100
HKUST-1	Spray	Ethanol	Yes	[001]	Anisotropic thermal expansion	101

TABLE I. (*Continued.*)

MOF type	LbL method	Solvent	Oriented growth and direction		Application	Ref.
HKUST-1	Pump	Ethanol	Yes	[100]	Resistive switching nanodevices	102
HKUST-1	Spray	Ethanol	Yes	[100]	Guest loading	103
HKUST-1	Dipping	Ethanol	Yes		Control of defects	104
HKUST-1	Dipping	Ethanol	Yes		Nanoscale morphology	105
HKUST-1	Dipping	Ethanol	Yes	[111]	Organic field-effect transistor	106
HKUST-1	Spray	Ethanol	Yes	[111]	Catalysis	107
HKUST-1	Dipping	Ethanol	Yes	[111]	Guest loading; photoswitching uptake	108
HKUST-1	Spray	Ethanol	Yes	[100]	Electrically conductive SURMOFs	109
HKUST-1	Spray	Ethanol	Yes		Guest loading	110
HKUST-1	Spray	Ethanol	Yes		Separation	111
HKUST-1	Dipping	Ethanol	Yes		Dye uptake	112
HKUST-1	Spray	Ethanol	Yes	[111]	Loading; enantioselective adsorption	113
HKUST-1	Dipping	Ethanol	Yes	[100]	Control of defects	35
HKUST-1	Dipping	Ethanol	Yes	[111]	Morphology of SURMOFs	114
HKUST-1	Dipping	Ethanol	Yes	[100]	Growth mechanism	115
HKUST-1	Dipping	Ethanol	Yes		Growth mechanism	116
HKUST-1	Immersion and separate	Ethanol	No		Photocatalysis	117
HKUST-1	Dipping	Ethanol	Yes		Morphological crystal engineering	118
HKUST-1	Dipping	Ethanol	Yes		Morphological crystal engineering	119
HKUST-1	Dipping	Ethanol	Yes	[111]	Biological applications	120
HKUST-1	Dipping	Ethanol	Yes	[100]	Guest loading conductivity	121
HKUST-1	Dipping	Ethanol	Yes	[100]/[111]	Optimized growth	122
HKUST-1	Dipping	Ethanol	Yes		Optimized growth	123
HKUST-1	Spin coating	Ethanol	Yes	[111]	Dye adsorption; water oxidation	124
HKUST-1	Pump	Ethanol	Yes	[100]/[111]	Ambipolar resistive	125
HKUST-1	Dipping	Ethanol	Yes	[111]	SURMOF on polymer	126
HKUST-1	Dipping	Ethanol	Yes	[100]/[111]	Gas sorption	127
HKUST-1	Pump	Ethanol	Yes	[100]	Defect creation	128
HKUST-1	Pump	Ethanol	Yes	[111]	SAM patterning	129
HKUST-1	Pump	Ethanol	Yes		Negative differential resistance	130
HKUST-1	Spray	Ethanol	Yes	[100]/[111]	Growth method	131
HKUST-1	Spray	Ethanol	Yes		Reversible photoalignment	132
HKUST-1	Dipping	Ethanol	Yes		Tracking of heat release	133
HKUST-1	Dipping	Ethanol	Yes	[111]	Hybrid electronics	134
HKUST-1	Spray	Ethanol	Yes	[001]	Conductive SURMOFs	136
HKUST-1/$[Cu_2(NDC)_2(dabco)]_n$	Pump	Ethanol	Yes	[111]/[001]	Heterostructure SURMOFs	137
HKUST-1/$[Cu_2(NDC)_2(dabco)]_n$	Pump	Ethanol	Yes	[100]/[200]	Heterostructure SURMOFs	138
HKUST-1/$[Cu(BDC)]_n$	Spray	Ethanol	Yes	[100]	Dielectric; optical properties	139
HKUST-1/$[Cu(BDC)]_n$	Pump	Ethanol	Yes		Heterostructure; adsorption	140

TABLE I. (*Continued.*)

MOF type	LbL method	Solvent	Oriented growth and direction		Application	Ref.
HKUST-1	Spray	Ethanol	Yes	[100]	Optical resonator	135A
HKUST-1	Spray	Ethanol	Yes	[100]	Fabry-Pérot cavity	135B
HKUST-1	Spray	Ethanol	Yes	[100]	Photonic Crystals	135C
HKUST-1/$[Cu(BDC)]_n$/ $[Cu(BPDC)]_n$/ $[Cu_2(DCam)_2(dabco)]_n$/ $[Cu_2(DCam)_2(BiPy)]_n$/ $[Cu_2(DCam)_2(BiPyB)]_n$	Spray	Ethanol	Yes		QCM sensor array	141
HKUST-1/$[Cu(BDC)]_n$/ $[Cu(BPDC)]_n$	Spray	Ethanol	Yes		QCM loading sensors	142
HKUST-1/$[Cu(BPDC)]_n$/ $[Cu_2(BDC)_2(dabco)]_n$	Spray	Ethanol	Yes		Conductive SURMOFs	143
HKUST-1/$[Cu_2(BDC)_2]_n$/ $[Cu_2(BDC)_2(dabco)]_n$	Pump	Ethanol	Yes		Water as growth modulator	144
HKUST-1/$[Cu_3(NH_2\text{-}BTC)_2]_n$	Spray/pump	Ethanol	Yes	[100]	Guest loading	145
HKUST-1/$[Zn(TPP)]_n$	Spray	Ethanol	Yes		Lithography	146
HKUST-1/ZIF-8	Dipping	Ethanol/Methanol	Yes	[001]	Adsorption	147
HKUST-1/ZIF-8/$[Cu(BDC)]_n$	Spin coating	Ethanol/Methanol	Yes		SURMOF fabrication	34
$[K(\gamma\text{-cyclodextrin})]_n$	Dipping	Water/Methanol	Yes	[110]	Peptide-enantiomers sensing	148
$[Ln2(X4\text{-}BDC)_3]_n$ (X = H, F, Cl, Br)	Dipping	Ethanol	Yes		Optical applications	149
MOF-76 ($[Ln(BTC)]_n$)	Pump	Ethanol	Yes	[001]	Tunable energy transfer	150
MOF-76	Pump	Ethanol	Yes	[001]	White light emission	151
MIL-68(In)	Pump	DMF	Yes	[010]	Optical sensing	152
$[Ni/Co(BDC)]_n$	Pump	Ethanol	Yes	[200]	Electrocatalysis	153
$[Ni/Fe(BDC)]_n$	Pump	Ethanol	Yes	[200]	Electrocatalysis	154
$[Ni/Fe(BDC)]_n$	Pump	Ethanol	Yes	[200]	Electrocatalysis	155
$[Ni\|Fe(BDC)]_n$	Pump	Ethanol	Yes	[200]	Electrocatalysis	156
NU-901 ($[Zr(1,3,6,8\text{-Tetra}(4\text{-carboxylphenyl})pyrene)]_n$)	Dipping	DMF	Yes	[110]	Circularly polarized luminescence	157
UiO-66-NH_2 ($[Zr_6O_4(NH_3\text{-}BDC)]_n$)	Dipping	DMF	No		Growth method	158
UiO-66-NH_2	Dipping	DMF	No		Stability	159
UiO-66-NH_2	Dipping	DMF	Yes		Hydrogen separation	160
UiO-66-NH_2	Pump	Ethanol	Yes	[510]	Fabrication method	161
UiO-66 ($[Zr_6O_4(BDC)]_n$)	Pump	Ethanol	Yes	[510]	Growth method	162
ZIF-8 ($[Zn(2\text{-methyl-}1H\text{-imidazole})]_n$)	Dipping	Methanol	Yes	[001]	Gas separation	163
ZIF-8	Dipping	Methanol	Yes	[001]	Gas separation	164
ZIF-8	Pump	Methanol	Yes	[001]	Growth mechanism	165
ZIF-8	Dipping	Methanol	Yes	[001]	Gas adsorption	166
$[Zn(2,20\text{-bipyridine-}5,50\text{-dicarboxylic acid}(Re(CO)_3Cl))]_n$	Spray	Ethanol	Yes	[100]	Electrocatalytic device	167
$[Zn(3,9\text{-perylenedicarboxylic acid})]_n$	Spray	Ethanol	Yes	[001]	Guest loading; up-conversion	168
$[Zn(3,9\text{-perylenedicarboxylic acid})]_n$	Spray	Ethanol	Yes		Solar cells	169
$[Zn(3,9\text{-perylenedicarboxylicacid})]_n$	Spin coating	Ethanol	Yes		Structure analysis	170

TABLE I. (*Continued.*)

MOF type	LbL method	Solvent	Oriented growth and direction		Application	Ref.
[Zn(5,15-bis(4-azidophenyl)-10,20-bis(4-carboxyphenyl)porphyrin)]$_n$	Spray	Ethanol	Yes	[001]	Antimicrobial activity polymer	171
[Zn(5,15-bis(4-azidophenyl)-10,20-bis(4-carboxyphenyl)porphyrin)]$_n$	Spin coating	Ethanol	Yes		Electrocatalytic device	172
[Zn(ADB)]$_n$	Spin coating	Ethanol	Yes		Optical application	173
[Zn(ADB)]$_n$	Spin coating	Ethanol	Yes		Optical application	174
[Zn(ADB)]$_n$/[Zn(DPP)]$_n$	Spin coating	Ethanol	Yes	[010]	Chromophore assemblies	154
[Zn(ADB)]$_n$/[Zn(TPP)]$_n$	Spray	Ethanol	Yes		Upconversion; heterojunctions	175
[Zn(BAB-TPDC)$_2$]$_n$/[Zn(BMB-TPDC)$_2$]$_n$	Dipping	Ethanol	Yes		SURMOF-derived polymer	176
[Zn$_2$(BA-BDC)$_2$(dabco)]$_n$	Pump	Ethanol	Yes	[100]	Polymer gels	177
[Zn(bianthryl linker)]$_n$	Spin coating	Ethanol	Yes	[010]	Photoinduced topotactic transformation	178
[Zn(cNDI)]$_n$	Spray	Ethanol	Yes		Optical application	179
[Zn(cNDIs)]$_n$	Spin coating	Ethanol	Yes	[100]	Chromophore aggregates	180
[Zn(cNDIs)]$_n$	Spin coating	Ethanol	Yes	[010]	Optical application	181
[Zn(cNDIs)]$_n$/[Zn(TPE)]$_n$	Spin coating	Ethanol	Yes	[010]	Photoinduced delamination	182
[Zn(DPA-TPE)]$_n$	Spin coating	Ethanol	Yes	[010]	Optical applications	183
[Zn(N$_3$-BPDC)$_2$(dabco)]$_n$	Spray	Ethanol	Yes	[001]	SAMs patterning	184
[Zn(porphyrin linkers)]$_n$	Spin coating	Ethanol	Yes	[010]	Computational screening porphyrinic linkers	185
[Zn(silicon phthalocyanine)]$_n$	Spray	Ethanol	Yes	[001]	Optical QED cavities	42
[Zn(TCPP(Zn))]$_n$	Dipping	Methanol/Water	Yes		Growth mechanism	186
[Zn(TCPP)(Dabco)]$_n$	Pump	Ethanol	Yes		Optical application	187
[Zn(TCPP)]$_n$	Pump	Ethanol	Yes	[001]	Solar cells	188
[Zn(TCPP)]$_n$	Dipping	Ethanol	No		Molecular recognition	189
[Zn(TPE-BDC)]$_n$	Spin coating	Ethanol	Yes	[010]	Controlling oxidative photocyclization	190
[Zn(TPP(Pd))]$_n$	Spray	Ethanol	Yes		Illumination effects	191
[Zn(TPP(Pd))]$_n$	Spray	Ethanol	Yes	[001]	Optical application	192
[Zn(TPP(Zn))]$_n$	Spray	Ethanol	Yes		Optical application	193
[Zn(TPP)]$_n$	Spray	Ethanol	Yes		Optical application	194
[Zn$_2$((+)cam)$_2$(dabco)]$_n$/[Zn$_2$((-)cam)$_2$(dabco)]$_n$	Pump	Ethanol	Yes	[110]/[001]	Enantioselective adsorption	195
[Zn$_2$(adc)$_2$(dabco)]$_n$	Dipping	Ethanol	Yes	[110]	SAM effect	46
[Zn$_2$(BDC)$_2$(4,4'-bipy)]$_n$	Dipping	Ethanol	Yes	[001]	Controlling interpenetration	92
[Zn$_2$(BDC)$_2$(H2O)$_2$]$_n$/[Cu$_2$(BDC)$_2$(H2O)$_2$]$_n$	Pump	Ethanol	Yes	[100]	SURMOF-2 fabrication	32
[Zn$_2$(BDC)$_2$]$_n$	Spray	Ethanol	Yes		Guest loading; optical application	196
[Zn$_2$(BDC)$_2$]$_n$	Spray	Ethanol	Yes		Guest loading; optical application	197
[Zn$_2$(Lcam)$_2$DAP]$_n$	Pump	Ethanol	Yes	[001]	Circularly polarized luminescence	198
[Zn$_2$(N$_3$-BDC)$_2$(dabco)]$_n$	Dipping	Ethanol	Yes	[001]	Post-synthetic modification	199
[Zn$_2$(TCPP)]$_n$	Dipping	Ethanol	Yes		Absorption	200

TABLE I. (*Continued.*)

MOF type	LbL method	Solvent	Oriented growth and direction		Application	Ref.
$[Zn_4O(dmcapz)_3]_n$/ $[Zn_4O(BDC)_3]_n$	Pump	Ethanol	Yes	[100]	Sorption	201

collective optical behavior of crystallized chromophores strongly depends on the structure of the corresponding molecular solids.[214] Because of their huge structural variability, MOF materials, in general, provide an excellent platform for controlling the aggregation of the chromophores. As a type of MOF material, SURMOFs not only inherit the features of MOFs in controlling the aggregation of chromophores but also offer a SURMOF-2 type structure, which can be obtained only in SURMOF thin films by the LbL method.[72,215] The assemblies in SURMOF-2 type structures lead to a short distance between two neighboring chromophores and a planar-oriented chromophore packing, that is, nearly parallel to the substrate.[32] Moreover, fabricating SURMOFs on colorless and transparent substrates (e.g., quartz glasses) offers a convenient opportunity to observe and characterize the photophysical properties of various π-conjugated organic chromophores.

An interesting example that exploited the tunability of MOF structures was the optimization of naphthalene-based chromophore assemblies. In 2017, core-substituted naphthalene diimide (cNDI)-based linkers were assembled into Zn-SURMOF-2 type MOF thin films.[179] The periodic one-dimensional (1D) stacked chromophores in this 2D SURMOF structure induced highly unusual photophysical properties. The decay of an excitation in a monomer led to bright fluorescence in solution. Assembly into a SURMOF yielded packing motifs in which the corresponding transition dipoles were arranged in a parallel fashion. As a result, a coupled excitonic state was formed, which led to a quenching of the excitation. Assembly into a SURMOF, thus, yielded an H-aggregate. However, when the NDI-based linker was modified by adding a so-called steric control unit (SCU), a special type of arrangement resulted in the unusual formation of J-aggregates in SURMOFs. These then exhibited high quantum yield and fluorescence lifetime. Afterward, the same group applied computational methods to

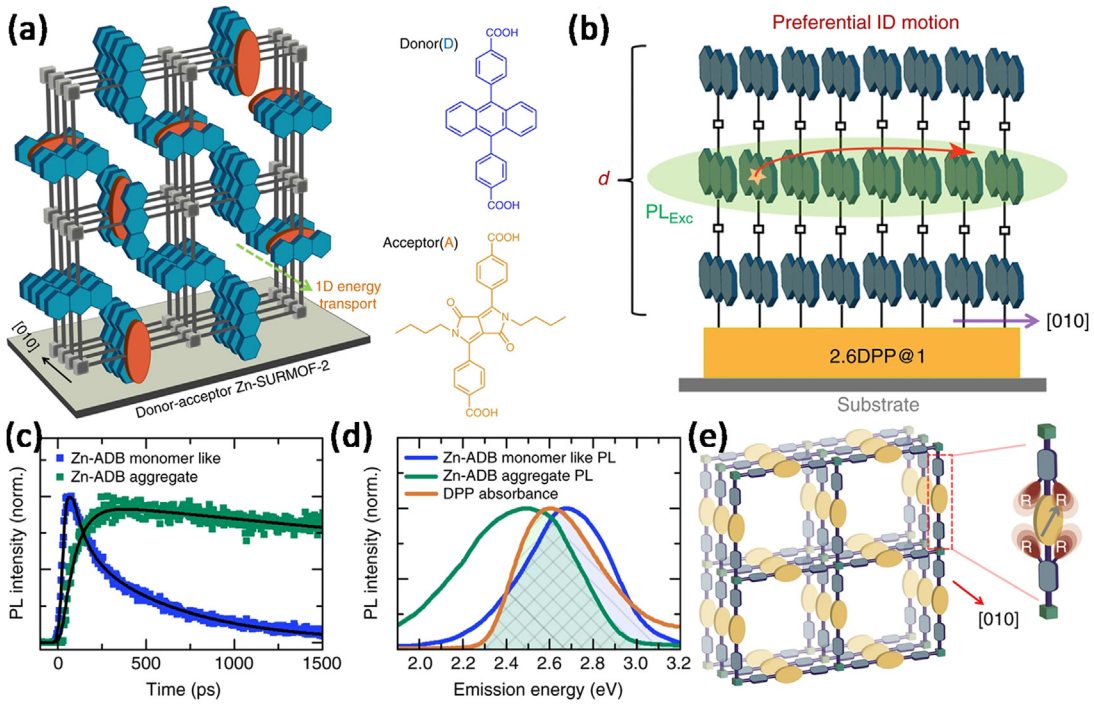

FIG. 2. (a) Schematic illustration of anisotropic architecture of a donor–acceptor Zn-SURMOF-2 with a mixed-linker strategy. The anthracene chromophores (blue) are stacked along the [010] direction as donor and the DPP linkers (orange) are homogeneously mixed in SURMOF; (b) schematic representation of the bilayer SURMOF and the energy transfer path of PL_{Exc} state; (c) decay and rise of the PL_{Mon} and PL_{Exc} states, respectively; and (d) PL spectra of the donor PL_{Mon} and PL_{Exc} states together with the acceptor DPP absorption. [(a)–(d)] Reproduced with permission from Haldar *et al.*, Nat. Commun. **9**, 1 (2018). Copyright 2018 Springer Nature.[216] (e) Schematic illustration of a Zn-SURMOF-2 showing the stacked chromophores along the [010] direction. The schematic illustration on the right illustrates the linker with the steric control unit. Reproduced with permission from Haldar *et al.*, Nat. Commun. **10**, 1 (2019). Copyright 2019 Springer Nature.[180]

search for more SCUs, aiming to obtain brighter emissions.[180] A library of NDI-based MOF linkers with different SCUs was created to change the molecular packing, and the best SCU was predicted using computational methods. With the theoretical prediction, the packing was modified to yield an angle of 60° between the transition dipoles. As a result, the excitonic changed completely, yielding a J-aggregate with pronounced fluorescence. Thus, this study demonstrated the huge potential of computer-based approaches to design and realize new SURMOF materials with bespoke photophysical properties by controlling the aggregation geometry of chromophores.

Another unique property of photoactive SURMOFs is the ability to realize anisotropic energy transport. The oriented nature of the SURMOFs allows chromophore packings that lead to a highly directional transport of the exciton parallel to the substrate surface.[216] As shown in Fig. 2, a highly anisotropic, 1D anthracene chromophore stacks in a Zn-SURMOF-2 type structure leads to the formation of two excited states: monomer-related photoluminescence and excimer-related photoluminescence. The two excited states can be distinguished by the different photoluminescence energies and lifetimes. By growing these highly oriented, crystalline SURMOFs, the authors demonstrated that the energy transfer for excimer-related photoluminescence proceeds in the crystallographic [010] direction, which follows the 1D anthracene chromophore stacks parallel to the substrate. In contrast, the monomer-related photoluminescence can diffuse in the [100] direction perpendicular to the substrate. The ability to fabricate SURMOFs with anisotropic exciton transport by controlling aggregation of the chromophores creates the huge potential for application in energy harvesting. Note that such directional transport is difficult to achieve for MOF powder materials.

Howard and co-workers introduced SURMOFs with enhanced photoluminescence using two approaches: mixing two linkers having an equivalent length or loading efficient acceptors as guest molecules, as shown in Fig. 3.[173] In the first approach, the anthracene based organic linker was mixed with an optically inert linker of equivalent length. The chromophore assemblies in the SURMOFs were optimized and the internal photoluminescence quantum yield (PLQY) was found to increase. However, the cost of this approach is a decrease in absorption and excited-state transport properties. The second approach introduced coumarin 343 (C343) as a guest acceptor molecule in the anthracene-based SURMOFs. The carboxylic group of C343 led to a strong interaction within the chromophore aggregation, and the aggregate states in SURMOFs brought more energy to the C343 acceptors. Thus, the internal and external PLQY were enhanced without sacrificing excited-state transport properties. Moreover, the C343 at SURMOFs were investigated as an emitter layer for triplet–triplet annihilation (TTA) upconversion. The upconversion quantum yield of the sensitizer/emitter SURMOF heterostructure was enhanced by optimizing the chromophore assemblies.

Subsequently, the same group used SURMOFs as a host material and applied a simple drop-casting approach to load tetraphenylethylene (TPE)-based chromophores, which show aggregation-induced emissions (AIE).[197] Various concentrations of the AIE chromophore

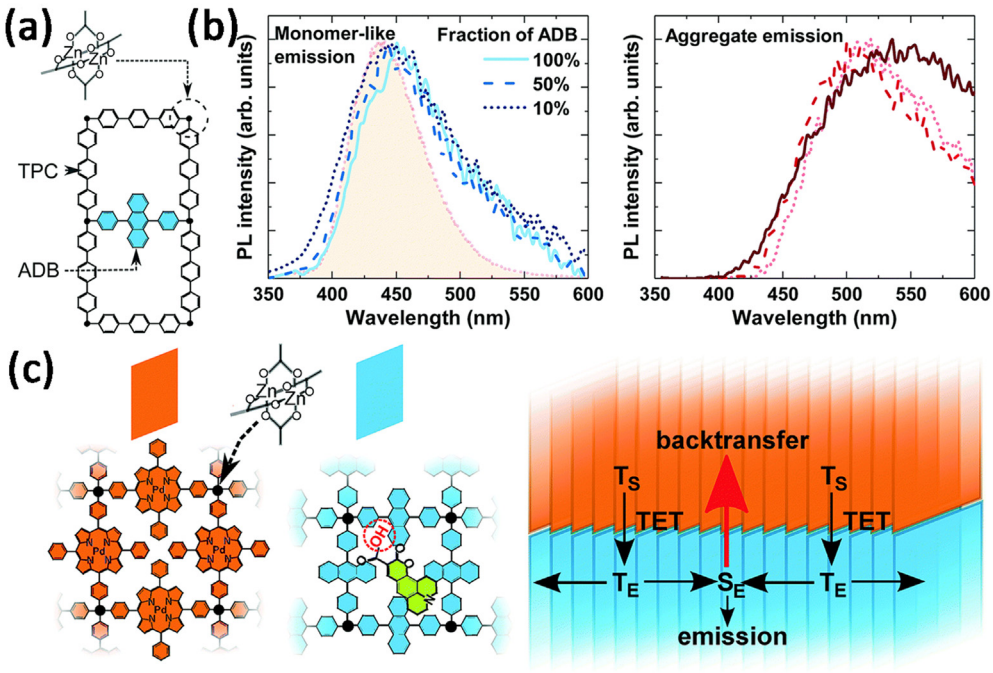

FIG. 3. (a) Schematic illustration of the SURMOF fabricated from zinc paddle-wheel units coordinated by ADB linkers and TPC linkers; (b) the emission spectra of the monomer-like and aggregated state for the various blend ratios in SURMOFs. The emission spectrum of ADB linkers in ethanol is plotted as a filled curve for comparison; and (c) schematic representation of the bilayer SURMOF heterostructure with the flow of triplet excitons transferred across the SURMOF interface. The sensitizer triplets (T_S) generated in the Pd-DCP SURMOF (orange sheets) can transfer across the interface and create emitter triplet states (TE) on the C343 at ADB SURMOF (blue sheets). Reproduced with permission from Oldenburg *et al.*, Phys. Chem. Chem. Phys. **20**, 11564 (2018). Copyright 2018 Royal Society of Chemistry.[173]

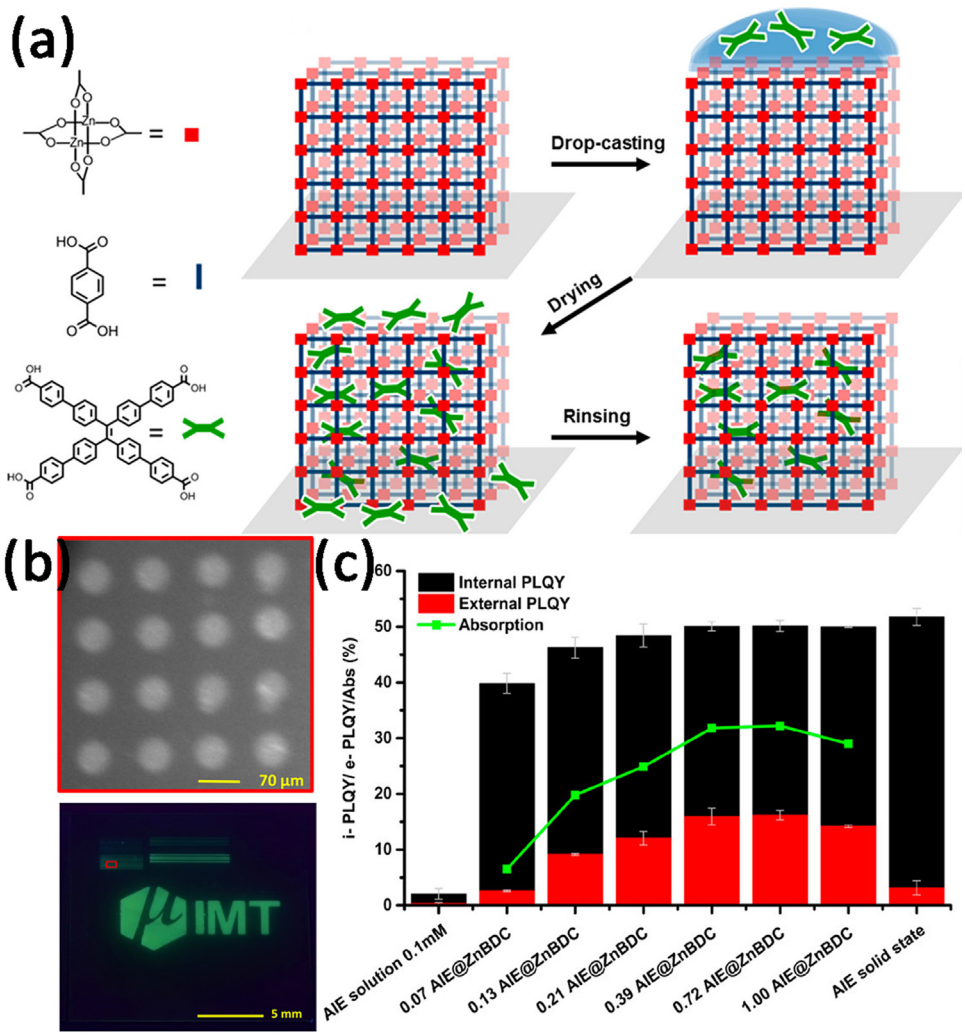

FIG. 4. (a) Schematic illustration of the AIE chromophore loading into SURMOF by drop-casting. An ethanolic solution of the AIE chromophore is drop cast onto the SURMOF. After drying, the surface is rinsed by ethanol to remove AIE chromophores outside the pore of SURMOF. (b) Top: Magnified image of an inkjet printing pattern with circular features of 70 μm; Bottom: Photograph of AIE chromophores printed SURMOF under 365 nm UV light. (c) The internal and external photoluminescent quantum yield of the AIE-loaded SURMOFs compared with the AIE chromophore (in solution and in the solid-state). The green curve shows the percentage of absorption in the SURMOFs loaded with different densities of AIE chromophores. Reproduced with permission from Baroni *et al.*, ACS Appl. Mater. Interfaces **10**, 25754 (2018). Copyright 2018 American Chemical Society.[197]

were loaded into SURMOFs and characterized for the photoluminescent quantum yield. As shown in Fig. 4, the results demonstrated that the SURMOF structure constrains the AIE-chromophore molecular conformation. A high quantum efficiency of AIE chromophores was achieved in the SURMOF structure, even at low loading densities. With increasing loading density of AIE molecules in SURMOFs, the photophysical nature of the AIE chromophore was modified by chromophore aggregation. The absorption and emission spectra were tuned, but the high photoluminescence quantum yield (PLQY = 50% for AIE chromophore) was maintained. This work also demonstrated patterns with 70 μm feature sizes, which could be created by inkjet printing the AIE chromophore onto the SURMOFs.

The possibility of controlling chromophore aggregation can be used to fabricate electroluminescent SURMOFs from linkers containing diphenylamine-tetraphenylethylene (DPA-TPE) chromophores.[183] Due to vibrational quenching, the DPA-TPE chromophore is nonemissive in its solvated state. Turning the DPA-TPE chromophore into a ditopic linker enabled the fabrication of Zn-(DPA-TPE) SURMOFs by the LbL approach. The SURMOFs exhibited pronounced green electroluminescence with low onset voltages, since the intermolecular interactions between adjacent chromophores strongly reduced the vibrational quenching present for the free molecule. In particular, the torsional vibrations were strongly affected by the packing. A small reorganization energy and the lowering of the triplet-singlet energy gap within the SURMOF led to thermally activated delayed fluorescence (TADF), as demonstrated by measurements at different temperatures. Although the quenching of the vibrations would also be expected to occur in bulk (powder) MOF materials, the advantage of the SURMOF approach is that the fabrication of the device is greatly simplified, since the substrate used for the LbL process can already act as the first electrode.

B. Tuning the antenna effect in lanthanide-based fluorescence

In this section, we focus on the tunable energy transfer in lanthanide-based SURMOFs (Ln-SURMOFs). An attractive feature of lanthanide-based materials is the high color purity of their light emission—independent of the linker coordinated to the lanthanide

ion—based on the intraconfigurational f–f transition. This high purity can be explained by the very effective shielding of the partially filled 4f shell by the closed $5s^2$ and $5p^6$ shells, resulting in a very low influence of any ligand coordinated in the lanthanide ion electron configuration.[217] However, because of the forbidden f–f transition in lanthanide atoms, inefficient absorption occurs under excitation light with weak emission profiles. Weissman discovered that, with the help of organic ligands, the lanthanide-based coordinated compounds exhibit remarkably enhanced absorption and increased emission intensity.[218] The organic ligands work as light absorption antennae in these lanthanide-based coordinated compounds, and this effect is called the "antenna effect."[219–221] As lanthanide-based MOFs (Ln-MOFs) are members of the lanthanide-based coordinated compounds, the antenna effect also plays a significant role in the photoluminescent properties of Ln-MOFs. However, unwanted energy transfer always occurs in mixed lanthanide ions MOFs [e.g., energy transfer from Tb(III) to Eu(III)]. A few studies used an epitaxial growth strategy to prepare hetero-Ln-MOF single crystals to control the antenna effect successfully.[222,223] However, complicated single-crystal growth and a large particle size limit the potential for thin-film fabrication. In this context, lanthanide-containing SURMOF thin films attracted considerable interest for studying the antenna effect and energy transfer.

Loading or encapsulating lanthanide coordination compounds as guest molecules into the pores of SURMOFs is the most straightforward strategy for combining the photoluminescent properties of lanthanide compounds with the advantages of SURMOFs. A Ln-complex, $Eu(bzac)_3bipy$ (bzac = 1-benzoylacetone, bipy = 2,2′-bipyridine), was loaded into HKUST-1 by simply immersing the MOF thin films into the ethanolic $Eu(bzac)_3bipy$ solutions.[95] In this case, the Ln-complex diffused through the pore apertures of HKUST-1 without steric hindrance. In another example, the encapsulation approach was applied to load Ln-compounds, $Ln(pdc)_3$ (H_2pdc = pyridine-2,6-dicarboxylic acid, Ln = Eu, Tb and Gd), into SURMOF thin films during LbL assembly.[224] A careful photophysical characterization revealed the efficient energy transfer between the BTC organic linker of the HKUST-1 MOF and the trivalent lanthanide ions. Therefore, the SURMOF backbone also contributed to the above-mentioned antenna effect, increasing the efficiency of energy transfer to the embedded Ln ions.

In principle, white light emission also can be obtained by immersing SURMOFs in a solution containing several different Ln-compounds with red, green, and blue emissions. However, to our knowledge, such an approach has not yet been reported.

Another approach for exploiting Ln ions to render photophysical functionality to SURMOFs is using Ln-containing nodes for SURMOF fabrication. While the first Ln-node-containing MOF was reported by Yaghi *et al.*,[225] the first Ln-based SURMOF was presented in 2019.[150] As shown in Fig. 5, we fabricated oriented, crystalline thin films based on the MOF-76 class of crystalline coordination networks. After fabricating different SURMOFs, each containing only one type of Ln-ion, next we used mixtures of Ln-ions for the metal-source step in the LbL process with the aim of producing white light–emitting SURMOFs. While this approach was shown to be possible in principle, we found it easier to realize hetero-trilayers with different Eu-, Tb-, and Gd-SURMOFs stacked on top of each other. We demonstrated

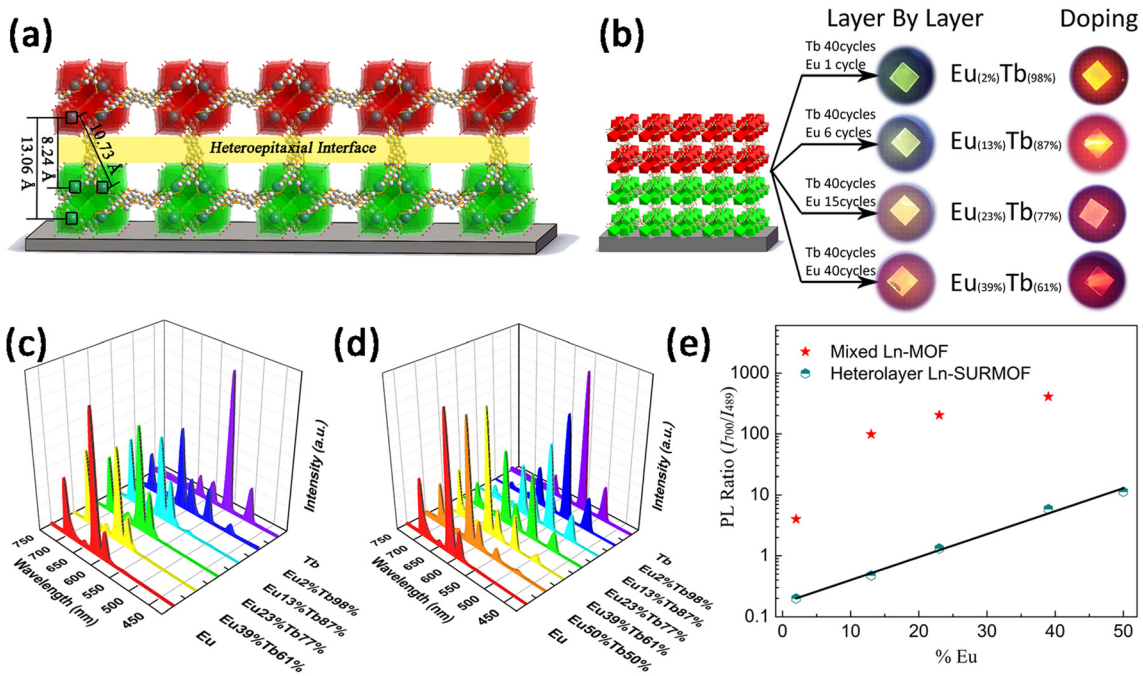

FIG. 5. (a) Schematic illustration of the heteroepitaxial interface between Tb and Eu; (b) (left) structure of Eu/Tb-SURMOF on substrate and (right) photoluminescent color comparison between the SURMOFs fabricated by the LbL assembly approach and the doping method; (c) emission spectra of Ln-SURMOFs fabricated by doping Eu/Tb method; and (d) emission spectra of Ln-SURMOFs fabricated by the LbL assembly approach; (e) ratio between the intensity of the Eu(III) peak (700 nm) and the Tb(III) peak (489 nm) in mixed Ln-MOF and heterolayer Ln-SURMOF. Reproduced with permission from Chen *et al.*, Adv. Funct. Mater. **29**, 1903086 (2019). Copyright 2019 Wiley-VCH.[150]

that the Eu(III)-SURMOF can be deposited on top of the Tb(III)-SURMOF in a heteroepitaxial growth process, maintaining the same crystallinity and orientation of the MOF-76 crystalline thin films.

The thickness of each layer in such heteroepitaxial Tb(III)-Eu(III)-SURMOFs can be further precisely optimized by adjusting the number of steps in the LbL fabrication process, thus tuning the emission color of the Ln-MOF bilayers. A specific advantage to using such a hetero-multilayer architecture instead of simply mixing the metals is the suppression of direct Tb(III)-to-Eu(III) energy transfer. This is an unwanted phenomenon occurring between neighboring Ln ions. In the multilayers, this process is strongly reduced, since different types of Ln ions are in direct vicinity to each other only at the interfaces within the hetero-multilayer. The reduction of energy transfer from Tb(III) to Eu(III) in the heteroepitaxial bilayer architecture of Tb(III)-Eu(III)-SURMOFs, thus, allowed a straightforward modulation of the emission color, removing the need for trial-and-error approaches when using the mixture strategy.

Ln-SURMOF thin films were also employed to provide a platform for systematically studying the photophysics governing the antenna effects of the lanthanide compound. Santos and co-workers demonstrated that the photoluminescent properties (including the antenna effects) of Ln-SURMOFs can be tuned by modifying their organic linkers. The terephthalic acid linker was modified by substitutions with halides (fluorine, chlorine, and bromine) at the 2,3,5,6 positions.[149] Calculations based on the different XRD patterns of tetrafluoro-, tetrachloro-, and tetrabromoterephthalic Ln-SURMOFs resulted in geometrically optimized molecular models, according to the molecular cluster model. The results demonstrated that the change in the lateral substitutes for the terephthalic acid linker, which sterically induces different dihedral angles, has drastic effects in both measured and calculated quantum yields and affects the Ln-SURMOFs' photophysical and structural properties. The theoretical model also revealed that the coordination symmetries of trivalent lanthanide twisted when coordinated with different halogen-substituted terephthalic acid compounds. Ln-SURMOFs with fluorine- and chlorine-

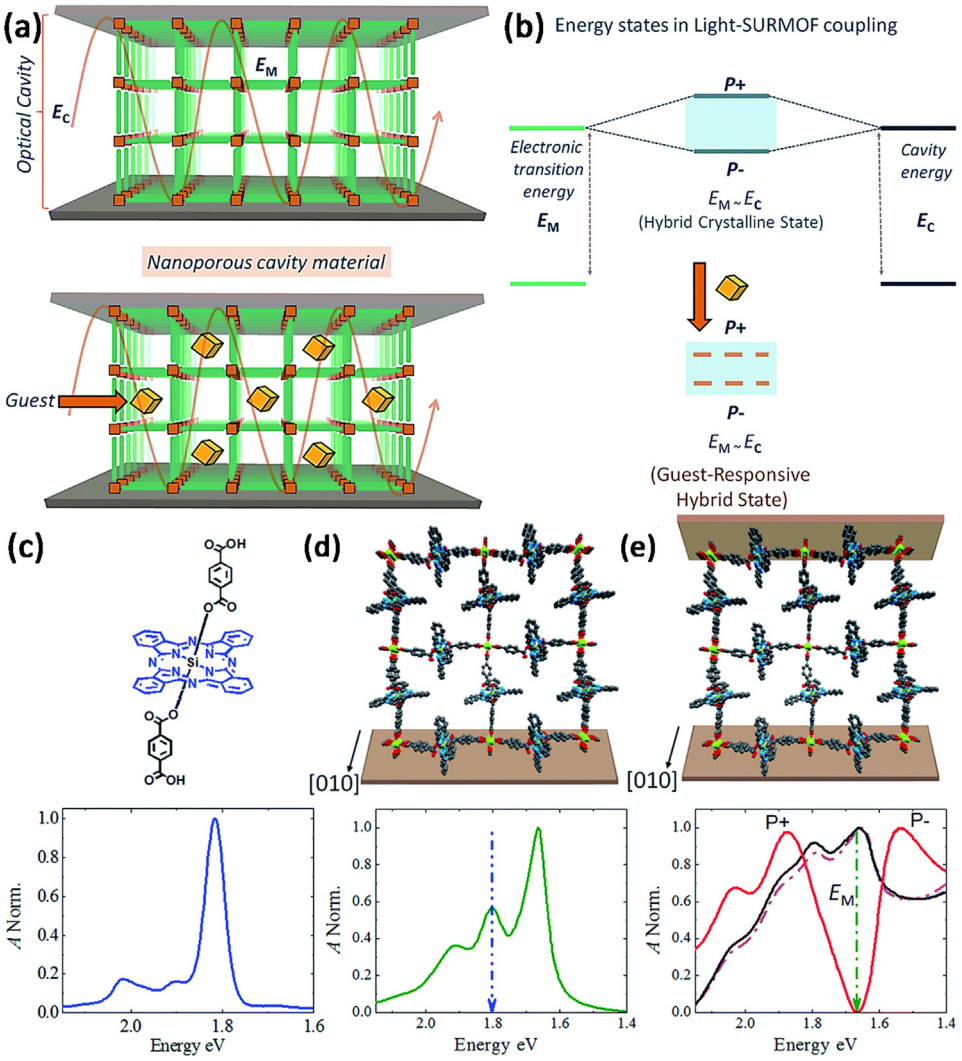

FIG. 6. (a) Schematic representation of the nanoporous SURMOF in an optical cavity and the guest responsive nature of the QED cavities; (b) hybrid energy states (P+ and P−) created by resonance of electronic transition energy (EM) and cavity energy (EC); (c) SiPc linker and its absorption spectrum; (d) Zn-SiPc SURMOF on Ag substrate and its absorption spectrum, the blue arrow corresponds to absorption maximum of SiPc linker; and (e) optical cavity of Zn-SiPc SURMOF and the absorption spectra with thicknesses of ∼210 (black), ∼300 (pink), ∼400 (red). EM is indicated by green arrow. Reproduced with permission from Haldar *et al.*, Chem. Sci. **11**, 7972 (2020). Copyright 2020 Royal Society of Chemistry.[42]

substituted linkers exhibited strong luminescence, whereas Ln-SURMOFs with a bromine-substituted linker had substantially suppressed luminescence. The construction of Ln-SURMOFs provides a versatile platform, not only because of their structural diversity and access to their unique photophysical properties, but also due to the possibility of different coordination symmetries of lanthanide centers.

C. Quantum-electrodynamical cavities

The special properties of SURMOFs are well suited to the fabrication of Fabry–Pérot interferometers used in obtaining optical quantum electrodynamical (QED) cavities. Using SURMOFs grown on a metal substrate that are then coated by a top mirror, it is possible to add porosity to the active medium in a QED device. The first demonstration of this approach was in 2020, when we realized optical QED cavities with a silicon phthalocyanine (SiPc)-based SURMOF as the active material.[42] As shown in Fig. 6, the total amount of Rabi splitting (~21%) reached in this work was impressive, which was in part due to the ability of SiPc chromophores to yield an efficient J-aggregate. The SURMOF QED exhibited an interesting additional functionality that guest species could be loaded and released from the additive medium between the mirrors, and this opened up the possibility of reversibly and continuously tuning the dielectric constant of the cavity. In addition, SURMOF-based QED devices can be used as optical sensors.

In 2022, Fernandez-Corbaton and co-workers presented a theoretical analysis based on a multi-scale approach that, starting from *ab initio* quantum mechanical molecular simulations, can compute the electromagnetic response of macroscopic photonic devices containing molecular materials.[226] This work suggested a refined interpretation of the effects occurring in the metal-clad SURMOFs and called for more work using other types of metals for the fabrication of the top and bottom mirrors.

D. Chiral SURMOFs for sensing and circular polarized luminescence

Thin films of chiral MOFs have substantial potential for applications in various fields, including gravimetric or optical sensing of enantiomers, demonstration of oriented circular dichroism, emission of circularly polarized light, and detection of the handedness of incident photons. Benefiting from the merits of LbL assembly, chiral SURMOFs for circularly polarized luminescence (CPL) were constructed with high orientation and homogeneity.

In 2012, Wöll, Fischer *et al.* presented the first enantiopure, highly oriented SURMOF thin films, $[Zn_2((+)cam)_2(dabco)]_n$ and $[Zn_2((-)cam)_2(dabco)]_n$ ((+)cam = (1R,3S)–(+)-camphoric acid (-)cam = (1S,3R)–(+)-camphoric acid, dabco = 1,4-diazabicyclo (2.2.2)octane).[195] The enantioselectivity of these SURMOFs was demonstrated by loading them with (2R,5R)-2,5-hexanediol and (2S,5S)-2,5-hexanediol enantiomeric probe molecules, respectively. As a result, significant differences in the absolute uptake and absorption rate were determined for the different SURMOFs. Later, Ulrich, Wöll, and co-workers prepared $[Cu_2((+)cam)_{2x}((-)cam)_{2-2x}(dabco)]_n$ and demonstrated that oriented circular dichroism (OCD) can be applied to characterize chiral SURMOFs in a straightforward fashion.[76] The ratio and orientation of the enantiomeric linkers were confirmed by the OCD results. Enantioselective enrichment was also observed by OCD when two chiral forms of ethyl lactate were loaded into the chiral SURMOFs.

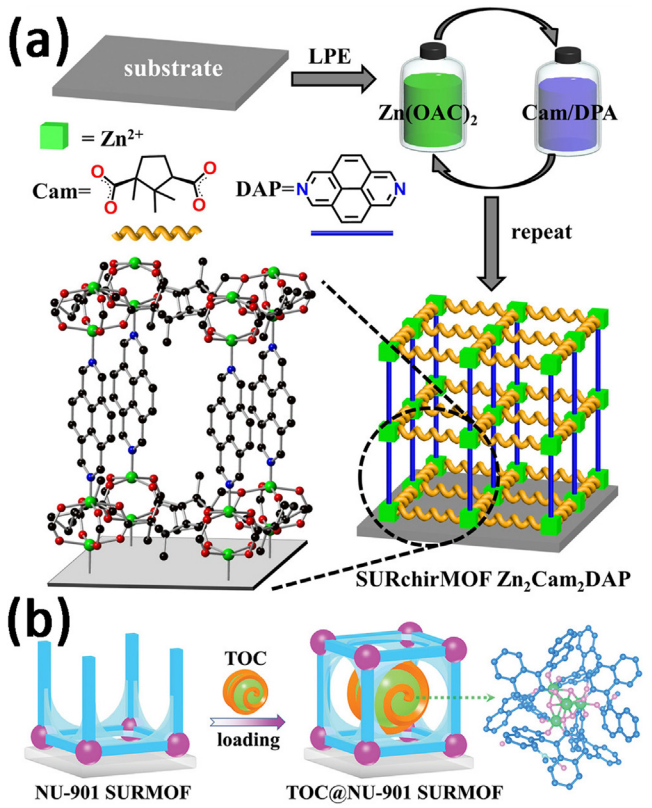

FIG. 7. (a) Schematic illustration of SURchirMOF grown on the substrate by LbL assembly approach along [001] direction. Reproduced with permission from Chen *et al.*, ACS Appl. Mater. Interfaces **11**, 31421 (2019). Copyright 2019 American Chemical Society.[198] (b) Schematic diagram of encapsulating chiral TOCs during LbL growth of NU-901 SURMOF. Reproduced with permission from Xiao *et al.*, Adv. Funct. Mater. **32**, 2204289 (2022). Copyright 2022 Wiley-VCH.[157]

In 2019, Xu, Gu *et al.* reported homochiral MOF thin films $[Zn_2Cam_2DAP]_n$ grown on functionalized substrates (named SURchirMOF-4) for their CPL property.[198] In this case, two different MOF ligands—a chiral camphoric acid (H_2Cam) and a luminescent chromophore, 2,7-diazapyrene (DAP)—were combined to yield SURMOFs with a pillared layer structure, see in Fig. 7(a). Circular dichroism, CPL, and enantioselective adsorption measurements revealed that the SURchirMOF-4 showed emission of circular polarized light. Furthermore, this MOF thin film had pronounced enantioselective adsorption for D- or L-methyl-lactate.

In 2022, Gu, Zhang *et al.* designed and fabricated another SURMOF exhibiting circularly polarized luminescence.[157] As shown in Fig. 7(b), in this work, chirality was rendered to the SURMOF by encapsulating chiral metal-organic clusters (MOCs) into an achiral photoluminescent NU-901 SURMOF. NU-901 is a highly stable MOF based on $Zr_6O_4(OH)_4$ nodes connected by pyrene-based linkers. The discovery of a LbL process to yield highly crystalline and oriented thin films is an important new development in the SURMOF field. Enantiopure titanium-oxo clusters (R/S-TOCs) were loaded into the

nanopores of the NU-901 SURMOF by utilizing the LbL encapsulation method. The chiral R/S-TOCs at NU-901 SURMOFs exhibited strong photoluminescent emission and remarkable CPL performance. The dissymmetry factor amounted to ± 0.025, a very high value. The excellent CPL performance of TOC at NU-901 SURMOFs resulted from the effective chiral induction and charge transfer caused by the strong π–π interactions between the chromophoric ligands of NU-901 SURMOF and the embedded chiral conjugated centers of the guest (R/S-TOC). The large cluster size of R/S-TOC prohibited indiffusion of this guest moiety by simple immersion into a solution, and only when using the LbL encapsulating strategy (see Sec. I) could a high loading rate be achieved.

E. Optical absorption and photo harvesting by porphyrin-based SURMOFs

Porphyrins are among the best molecular light absorber materials due to their large and unique π-aromatic system. Important properties in this context are their high-absorption cross section of Soret band excitations and distinct photophysical and electrochemical properties.[227,228] For applications in optical and optoelectronic areas, MOFs with porphyrin-based linkers have been utilized as a highly suitable platform in numerous works due to their flexible assembly and periodic structure.[219] However, MOF powders are poorly suited for optical or optoelectronic characterization of porphyrin-based materials, since there is typically considerable scattering of light by bulk particles. Particularly, for the investigation of electron transfer and transport properties, an oriented SURMOF is required to avoid any influence of the particulate character of a bulk MOF material in terms of grain boundaries or gaps between the bulk particles.

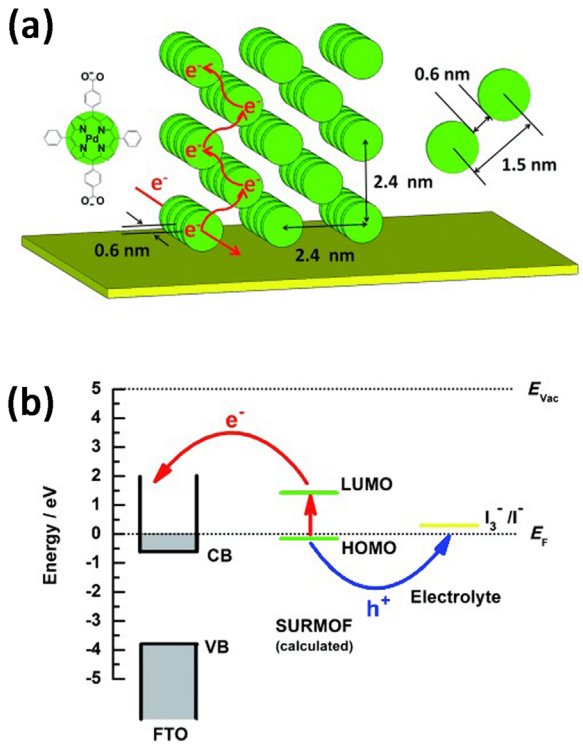

FIG. 8. (a) Schematic illustration of ordered arrays of porphyrin units in SURMOFs. (b) Schematic description of photon absorption and exciton separation process in the SURMOF photovoltaic device. Reproduced with permission from Liu *et al.*, Angew. Chem. Int. Ed. **54**, 7441 (2015). Copyright 2015 Wiley-VCH.[229]

The first porphyrin-based SURMOF was reported by Liu, Wöll *et al.*[229] Interestingly, a theoretical analysis revealed that the ordered arrays of porphyrins within the SURMOF-2 type structure exhibited a small dispersion of unoccupied and occupied electronic bands, yielding a small indirect bandgap, as shown in Fig. 8. Superior photophysical properties were demonstrated for this porphyrin-based SURMOF, including large charge-carrier generation efficiency and charge-carrier mobility. A prototype organic photovoltaic device was also fabricated with this porphyrin-based SURMOF. Later, the same group introduced electron-donating diphenylamine (DPA) groups into the porphyrin-based SURMOF-2 type structure as side groups.[230] This modified SURMOF exhibited improved absorption characteristics, especially a large photocarrier generation efficiency. In another study, Heine and Wöll *et al.* used a computational approach to identify porphyrin-based linkers to yield photoactive SURMOFs with predefined photophysical properties from an *in silico* library.[185] High-optical-quality SURMOFs with optimized photophysical properties were fabricated by LbL assembly using the selecting linkers. This approach demonstrated the enormous potential of computational screening methods with regard to fabricating porphyrin-based SURMOFs with bespoke photophysical properties.

The energy transfer between porphyrin-based chromophoric linkers within SURMOFs allows the study of anisotropic energy transport, a process that plays a crucial role in photoenergy conversion.[227,231] Farha and Hupp *et al.* tuned the distance between porphyrin chromophores in porphyrin-based pillar-layer SURMOFs by a solvent-assisted linker exchange strategy (Fig. 9).[187,232] The results demonstrated that shorter distances between porphyrin chromophores led to faster Förster-type exciton hopping in SURMOF materials. Hence, more hops occurred within the singlet excited state of porphyrin chromophores. Later, Howard and co-workers reported a palladium–porphyrin-based SURMOF and demonstrated that triplets in this porphyrin chromophores are very mobile.[192] Combined with experimental and theoretical results, a detailed analysis revealed that the triplet transfer rate can reach the order of 10^{10} S^{-1} in this palladium–porphyrin-based SURMOF. Sun and co-workers examined the relaxation processes of a porphyrin-based SURMOF by utilizing femtosecond time-resolved and steady-state spectroscopic techniques.[193] The results revealed the occurrence of ultrafast S_2–S_1 internal conversion and strong quenching in both S_2 and S_1 states. The strong quenching contributed to the spectral overlap of steady-state fluorescence spectra and absorption in the SURMOF. Howard and co-workers also investigated the effects of prolonged illumination on the palladium–porphyrin-based SURMOFs.[191] The results demonstrated that a stable photoproduct was formed that changed the photoresponse performance. Meanwhile, a short-lived cation–anion radical pair was formed when the mobile triplet excitons encountered the defect site, where a stable photoproduct formed under prolonged illumination.

In 2019, Xiang and Liu *et al.* designed a SURMOF-derived transparent $CoS_{1.097}$ at N-doped carbon film as a counter electrode in bifacial dye-sensitized solar cells (Fig. 10).[49] The materials were obtained from sulfuration of cobalt-porphyrin-based SURMOFs. This

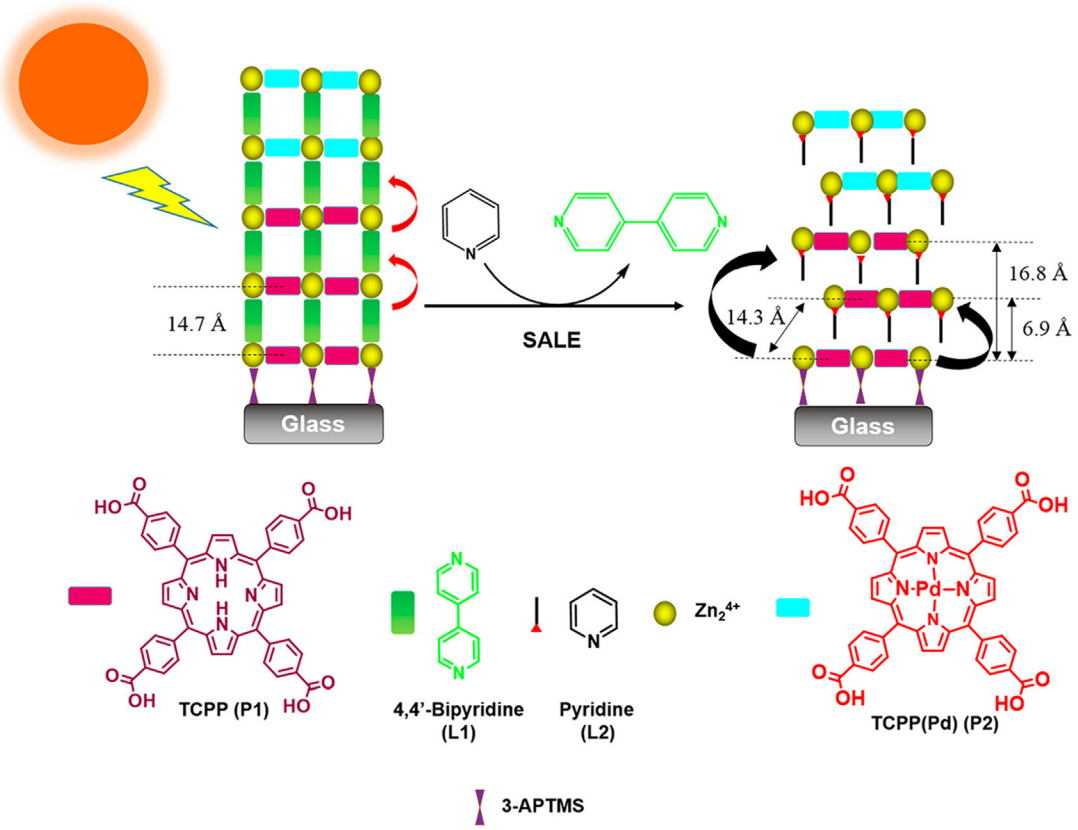

FIG. 9. Free base porphyrin linker TCPP and 4,4′-bipyridine were previously used to fabricate N cycles of SURMOFs, followed by N + 1 and N + 2 cycles by palladium porphyrin linker TCPP(Pd) and 4,4′-bipyridine. Solvent-assisted linker exchange was performed by replacing 4,4′-bipyridine by pyridine. Vertical distances are interlayer spacing (including layer thickness contributions to spacing). The indicated diagonal distance is the shortest interlayer point-dipole to point-dipole distance between porphyrin P1. Reproduced with permission from Goswami *et al.*, ACS Appl. Mater. Interfaces **10**, 34409 (2018). Copyright 2018 American Chemical Society.[187]

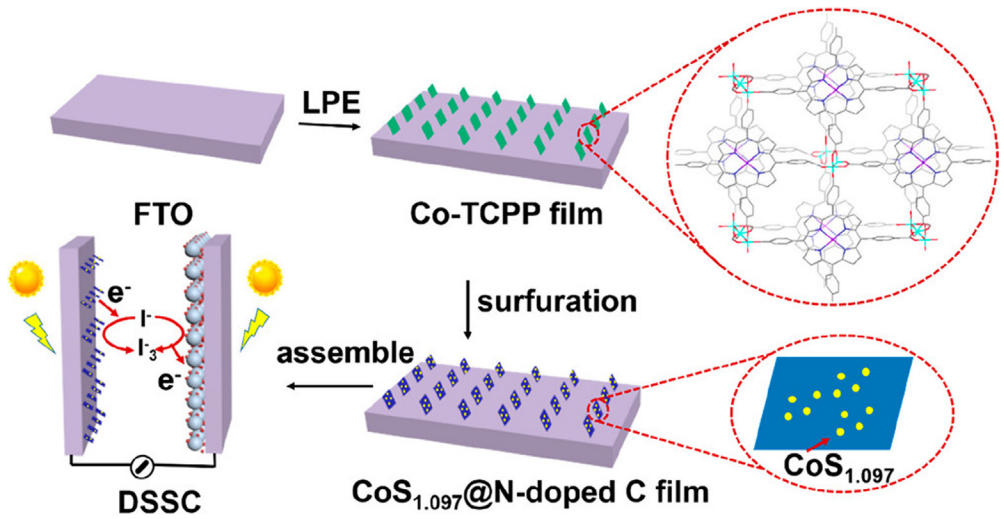

FIG. 10. Illustration of the preparation process for a SURMOF-derived transparent $CoS_{1.097}$ at N-doped carbon-film counter electrode for dye-sensitized solar cells. Reproduced with permission from Ou *et al.*, ACS Appl. Mater. Interfaces **11**, 14862 (2019). Copyright 2019 American Chemical Society.[49]

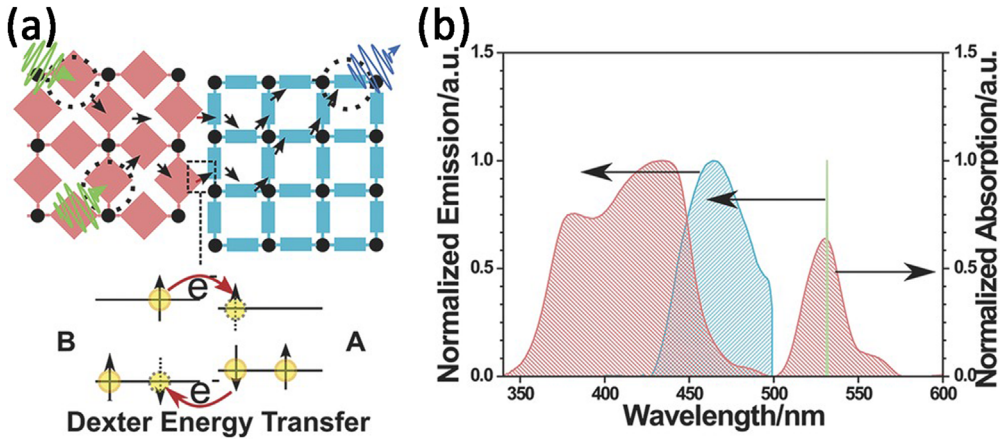

FIG. 11. (a) Schematic representation of triplet–triplet annihilation upconversion (TTA-UC). Two photons absorbed by the sensitizer SURMOF. Triplet states were created and transferred to the emitter SURMOF by a Dexter two-electron-exchange mechanism. Two triplets can annihilate and emit a higher-energy photon. (b) The absorption spectrum of the sensitizer SURMOF is shown in red. The excitation wavelength of the laser is at 532 nm (green). The up-converted emission is shown in blue. Reproduced with permission from Oldenburg *et al.*, Adv. Mater. **28**, 8477 (2016). Copyright 2016 Wiley-VCH.[175]

SURMOF-derived counter electrode did not require a tedious post-treatment procedure and exhibited higher power conversion efficiencies than platinum electrodes, which are high-cost materials.

Porphyrin chromophores are excellent candidates as a sensitizer moiety for triplet–triplet annihilation upconversion (TTA-UC) in SURMOFs. Richards and Howard fabricated a emitter–sensitizer–emitter heteroepitaxial SURMOF for TTA-UC, in which Pd(II) 5,15-diphenyl-10,20-di(4-carboxyphenyl) porphyrin was used as the sensitizer layer and 4,4′-(anthracene-9,10-diyl)dibenzoate was the emitter layer.[175] As shown in Fig. 11, dexter energy transfer processes were proposed to transfer the energy from the porphyrin-photosensitizer to the TTA layer. The TTA-UC thresholds were lower than 1 mW cm^{-2}. A later study from Liu, Sun *et al.* reported another strategy for TTA-UC based on SURMOFs.[168] A perylene-based SURMOF was fabricated on the substrate as an emitter, and platinum(II) octaethylporphyrin molecules were used as the sensitizer in acetonitrile solution. The photocurrent performance of the perylene-based SURMOF was enhanced with the presence of porphyrin molecules due to the TTA-UC mechanism.

Porphyrins also exhibit strong intrinsic nonlinear optical (NLO) properties. In 2019, Wang and Hu *et al.* demonstrated that porphyrin-based SURMOFs show third-order harmonic generation, with an NLO absorption coefficient of up to -10^{-3} cm/W, as shown in Fig. 12. This value is 7 orders of magnitude higher than that for porphyrin molecules in solvents.[50] Moreover, the interaction between one-photon saturable absorption, two-photon absorption, and two-photon saturable absorption led to tunable multistage NLO switching in the porphyrin-based SURMOFs.

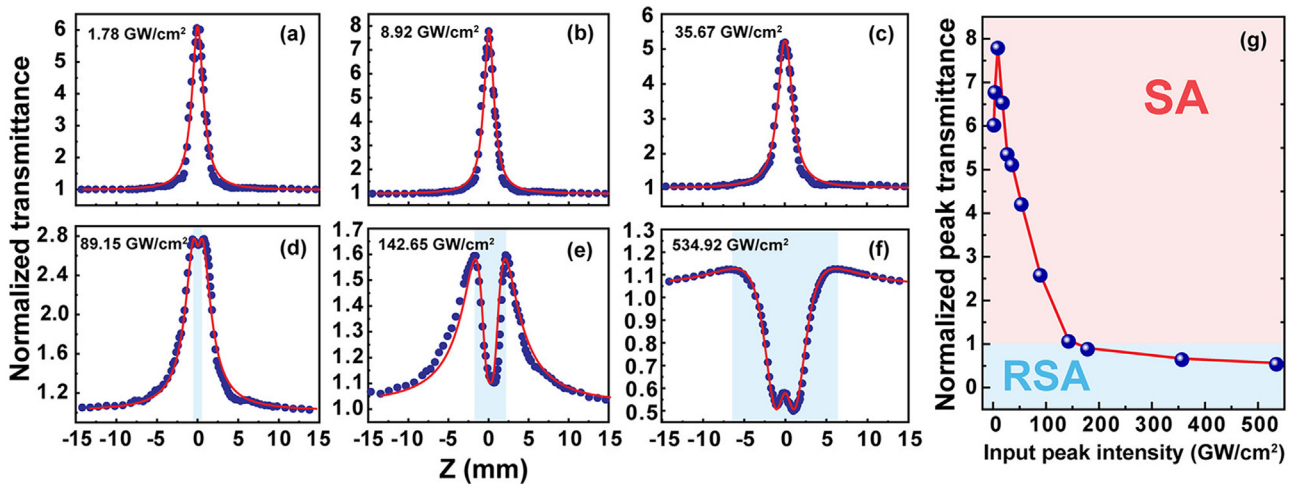

FIG. 12. Open-aperture Z-scan curves of porphyrin-based SURMOFs under different excitation intensities: (a) 1.78 GW/cm^2, (b) 8.92 GW/cm^2, (c) 35.67 GW/cm^2, (d) 89.15 GW/cm^2, (e) 142.65 GW/cm^2, and (f) 534.92 GW/cm^2. (g) The normalized transmittance at Z = 0 as a function of the input peak intensity. Reproduced with permission from Gu *et al.*, Nano Lett. **19**, 9095 (2019). Copyright 2018 American Chemical Society.[50]

III. ELECTRONIC AND IONIC CONDUCTION IN SURMOFs

Most MOF materials are insulators (conductivities $\leq 10^{-10}$ S/cm) due to their sizeable HOMO–LUMO gap.[233] However, with the large interest in electrically conducting MOFs, researchers have explored a huge variety of combinations of metal nodes and organic linkers to create frameworks with either metallic behavior or a small bandgap.[234] As a result of this intense effort during the last two decades, numerous conductive MOF materials have been reported. Most of them belong to one of the following categories: (1) conductivity based on metal-to-linker coordination,[233] (2) conductivity through intermolecular π–π stacking,[235] or (3) conductivity by introducing guest molecules.[236]

Progress in this field is to some extent hampered by the experimental difficulty of reliably determining the electrical conductivity of MOF materials.

However, preparing well-defined electrical contacts to powder particles is challenging. In this context, the attachment of electrical contacts to millimeter-sized MOF thin films, in particular SURMOFs, is fairly straightforward. Benefiting from LbL assembly, SURMOFs exhibit high structure quality and low defect densities. Several cases demonstrated that the charge transport mechanism can be better analyzed by low-defect SURMOFs in their electrical characterization, compared to the corresponding bulk MOF materials. Moreover, the highly oriented fabrication of SURMOFs is used to integrate the anisotropy properties, which are crucial to investigating the charge transport model in MOF materials.

A. Various strategies for conductive SURMOFs

The first work on charge transport through SURMOFs was reported by Wöll, Schlettwein *et al.* in 2012 using an electrochemical cell.[94] Whereas as-prepared HKUST-1 SURMOFs were observed to be highly insulating, the loading of ferrocene molecules into the pores was found to result in a strong conductivity increase. Later, Allendorf *et al.* demonstrated that loading TCNQ molecules (7,7,8,8-tetracyanoquinododimethane) into the pores of HKUST-1 SURMOFs increased their conductivity to 7 S/m, as shown in Fig. 13.[237] First-principles modeling and experimental spectroscopic data suggested that the conductivity increase resulted from the TCNQ molecules bridging the binuclear copper paddle wheels. In 2015, Mugnaini and Wöll *et al.* used the Hg-drop method to gently attach metal contacts to the top of HKUST-1 SURMOFs.[100] The results obtained from SURMOFs with different thicknesses demonstrated that the electric conductivity in empty HKUST-1 SURMOFs corresponds to incoherent multistep charge hopping. After loading with ferrocene, a noticeably increased conductivity was observed, which was attributed to the changes in the electronic and vibrational structure of the HKUST-1 in a hopping transport mechanism.

In 2016, Ballav and co-workers fabricated oriented and uniform SURMOFs in a straightforward manner using a TCNQ molecule as the organic MOF linker in the LPE LbL assembly.[61] The Cu-TCNQ SURMOF devices were produced by employing the electron-beam lithography technique on FTO and Au substrates and exhibited non-Ohmic conductivity ($\sim 10^{-5}$ S cm^{-1}). A remarkable rectification in the electrical conductance of Cu-TCNQ SURMOF devices was investigated as well upon exposure to iodine vapor, which would have been hard to achieve using the powder form of MOFs. In 2017, Xu and co-workers reported the fabrication of SURMOFs of the type $Cu_3(HHTP)_2$, (HHTP = 2,3,6,7,10,11-hexahydroxytriphenylene) by employing a spray LPE LbL method, as shown in Fig. 14(a).[88] The electrically conductive $Cu_3(HHTP)_2$ SURMOFs exhibited a high degree of orientation, good crystallinity, large single-crystal domain sizes, dense packing, and smooth surface. Also, the thickness could be tuned by adjusting the number of cycles. The room temperature

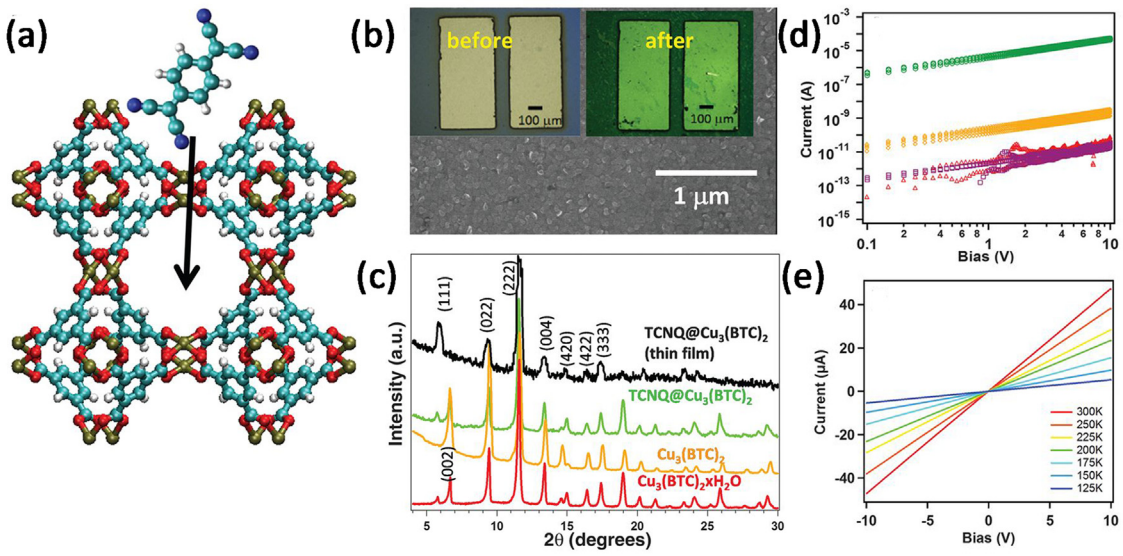

FIG. 13. (a) TCNQ guest molecules were loaded into the pores of HKUST-1 SURMOFs; (b) SEM image of HKUST-1 coated device; insets are photographs of HKUST-1 coated devices before and after TCNQ loading; (c) XRD patterns for HKUST-1 powders and HKUST-1 thin films; (d) I–V curves before loading guest molecules (red) and after loading with TCNQ (green), F4-TCNQ (orange), and H4-TCNQ (purple); and (e) temperature-dependent IV curves. Reproduced with permission from Talin *et al.*, Science **343**, 66 (2014). Copyright 2014 AAAS.[237]

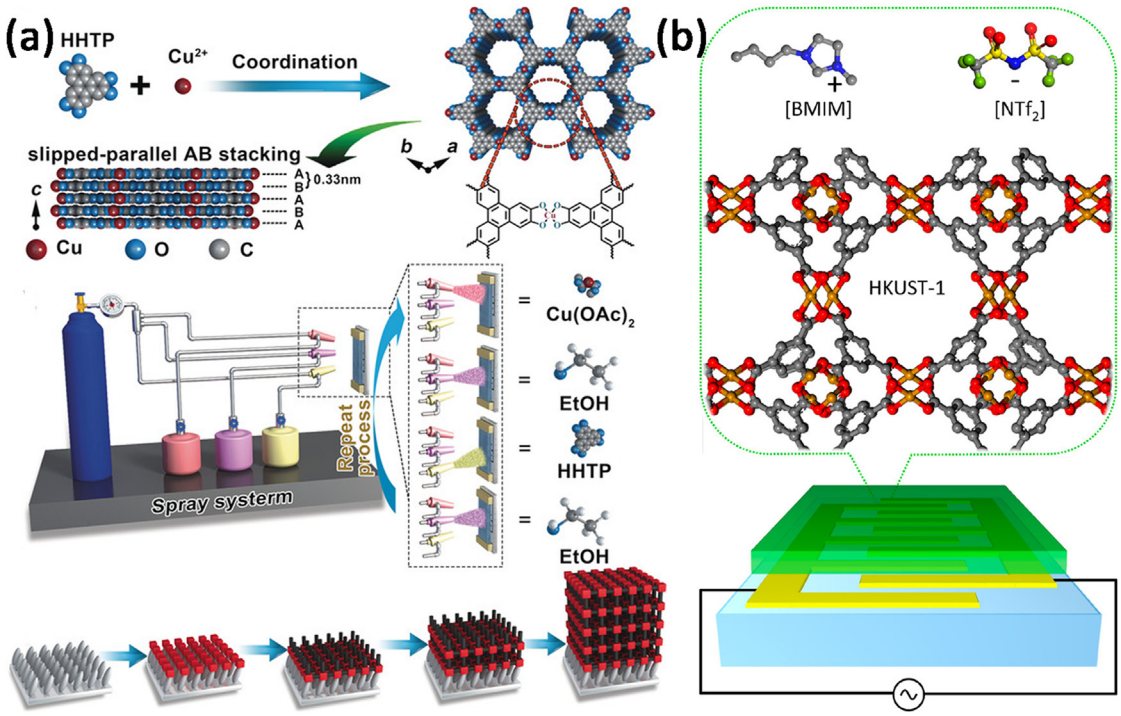

FIG. 14. (a) Illustration of the structure of $[Cu_3(HHTP)_2]_n$ SURMOF and the LbL assembly method of $[Cu_3(HHTP)_2]_n$ SURMOF gas sensors. Reproduced with permission from Yao *et al.*, Angew. Chem. Int. Ed. **56**, 16510 (2017). Copyright 2017 Wiley-VCH.[88] (b) Ionic liquid ([BMIM][NTf_2]) confined in regular nanopores of HKUST-1 MOF. Reproduced with permission from Kanj *et al.*, Nano Lett. **19**, 2114 (2019). Copyright 2019 American Chemical Society.[121]

conductivity of the $Cu_3(HHTP)_2$ SURMOF with 20 nm thickness amounted to 0.02 S/cm.

Wenzel and Heinke *et al.* investigated embedding of ionic liquids (ILs) in the pores of HKUST-1 SURMOFs to control the electric and ion conduction properties.[121] The experimental data combined with molecular dynamics (MD) simulations revealed the dynamic behavior of ILs embedded in HKUST-1 SURMOFs [see in Fig. 14(b)]. At low ionic liquid loading, ionic conduction occurs without significant interaction between the IL guest molecules. The conductivity of the IL at SURMOFs host/guest systems increased by many orders of magnitude relative to the empty SURMOFs. However, at high IL loadings, collective field-induced interactions occur between IL molecules, leading to a blocking of ionic transport in the IL at SURMOF samples. As a result, the ion conductivity of IL at SURMOFs was found to decrease tremendously.

Ruben and co-workers fabricated 1D conductive polymer chains within the channels of a Cu-BDC SURMOF (SURMOF-2 type) by potentiostatically electropolymerizing 1-hexyne monomers contained within the MOF pores.[51] Data from mass spectroscopy demonstrated successful polymerization. The electrical conductivity of this polymer at SURMOFs increased by 8 orders of magnitude relative to the empty SURMOFs. Theoretical work using DFT calculations revealed that this electrical conductivity was limited by hopping between the conductive oligomers. In another case, methyl propiolate was embedded in HKUST-1 SURMOFs and then polymerized. The resulting increase in electrical conductivity amounted to 6 orders of magnitude.[143]

B. Switching electrical conductivity

Introducing stimuli-responsive molecules into MOFs and SURMOFs allows the development of strategies for fabricating conductive MOF thin films in which the electrical resistance can be switched by remote control. In 2018, Heinke and co-workers presented a SURMOF and showed that its proton conduction could be switched by illumination with light (Fig. 15).[79] The key element to obtaining this functionality is the integration of an azobenzene-containing linker, F_2AzoBDC (F_2AzoBDC = (E)-2-((2,6-difluorophenyl)diazenyl)terephthalic acid), into the MOF lattice. F_2AzoBDC can be switched reversibly between trans and cis states. This switching also takes place inside the SURMOF and affects the behavior of guest molecules, 1,2,3-triazole and 1,4-butanediol, loaded into the MOF thin film. Electrical measurements revealed that illumination with light results in reversible changes of the conductivity, with higher conductivity for the trans state and reduced conductivity for the cis state. Experimental data combined with quantum chemical calculations showed that the light-switching effect results from breaking the rather strong hydrogen bonds of the guest molecules to the cis azobenzene moieties when switching to the trans conformation of the F_2AzoBDC linkers.

Later, Heinke and co-workers also introduced a spiropyran-functionalized SURMOF with large on-off ratio of proton conductivity.[78] The spiropyran group was incorporated into a Cu_2(e-BPDC)2(dabco) SURMOF (e-BPDC = 2-ethynyl-[1,10-biphenyl]-4,40-dicarboxylic) by

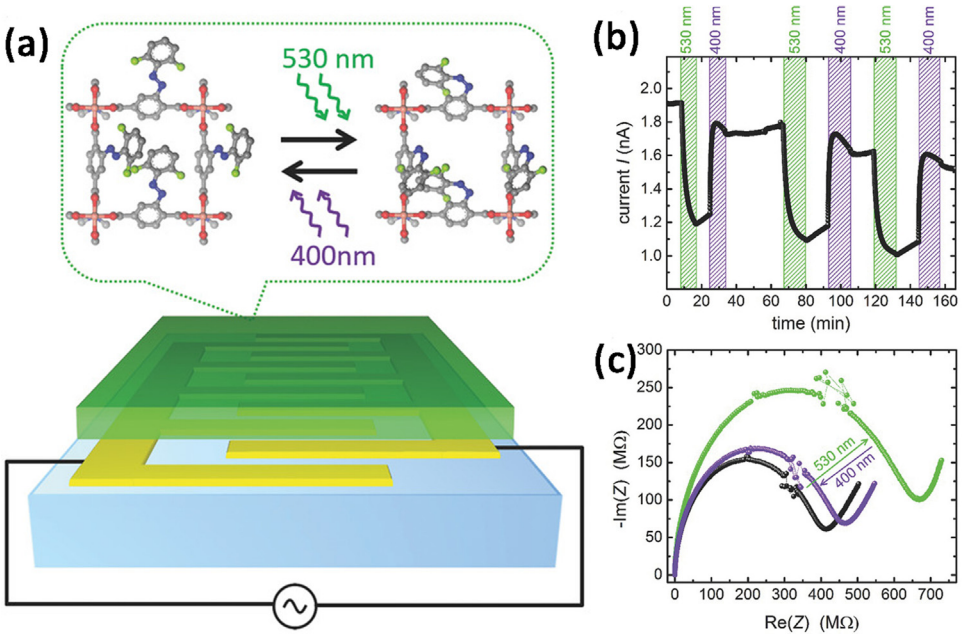

FIG. 15. (a) Sketch of the $Cu_2(F_2AzoBDC)_2(dabco)$ SURMOF film on the interdigitated gold electrodes. (b) The current (at 1 Hz and 1 V) of SURMOF film under green light (530 nm) and violet light (400 nm) irradiation. (c) Nyquist plot of impedance Z of butanediol at $Cu_2(F_2AzoBDC)_2(dabco)$ in the pristine sample (trans), under post-irradiation with green light (530 nm), and under post-irradiation with violet light (400 nm). Reproduced with permission from Müller *et al.*, Adv. Mater. **30**, 1706551 (2018). Copyright 2018 Wiley-VCH.[79]

post-synthetic modifications (PSM), as shown in Fig. 16. A reversible spiropyran-to-merocyanine isomerization in the host SURMOFs was induced by UV light (365 nm). The strong binding strength between the guests and the SURMOF suppressed the proton conduction when the structure isomerized from spiropyran form to merocyanine form. Thus, the mobility of the guests was decreased in the merocyanine form, and the proton conductivity could be photomodulated by up to 2 orders of magnitude.

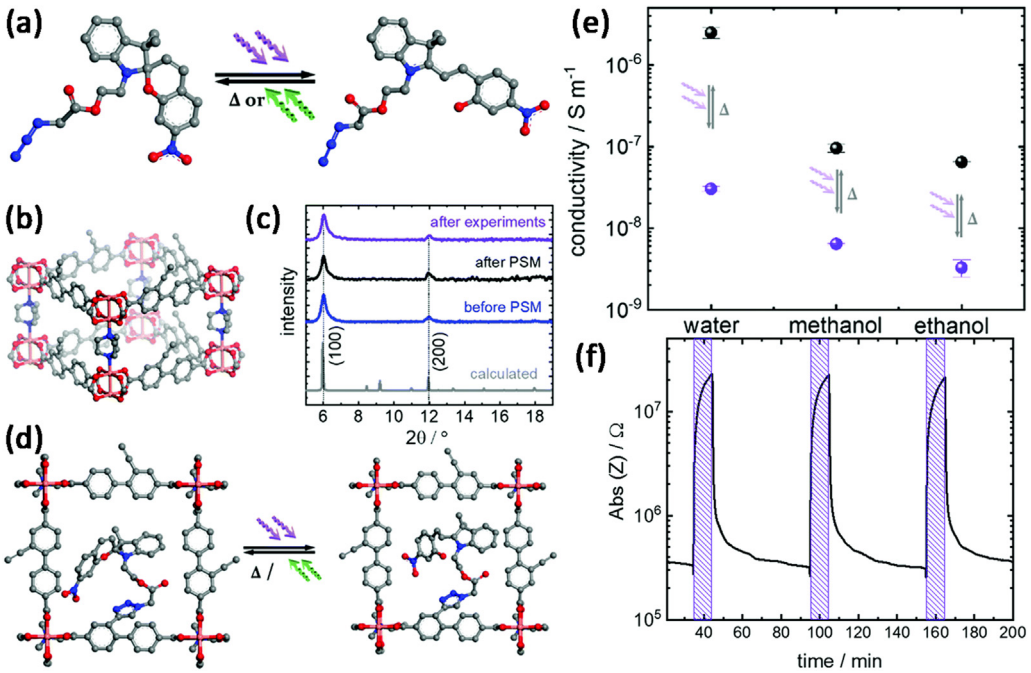

FIG. 16. (a) Schematic representation of the mechanism of photoswitching isomerization between the spiropyran (left) form and the merocyanine (right) form; (b) the structure of the host SURMOF; (c) XRD patterns of the SURMOFs; (d) the pore window of spiropyran-functionalized SURMOF under spiropyran (left) form and merocyanine (right) form; (e) conductivity of spiropyran-functionalized SURMOF with water, ethanol, and methanol in the spiropyran (black) form and the merocyanine (violet) form; and (f) absolute value of impedance Z of the spiropyran-functionalized SURMOF at 1 Hz vs time. Reproduced with permission from Kanj *et al.*, Chem. Sci. **11**, 1404 (2020). Copyright 2020 Royal Society of Chemistry.[78]

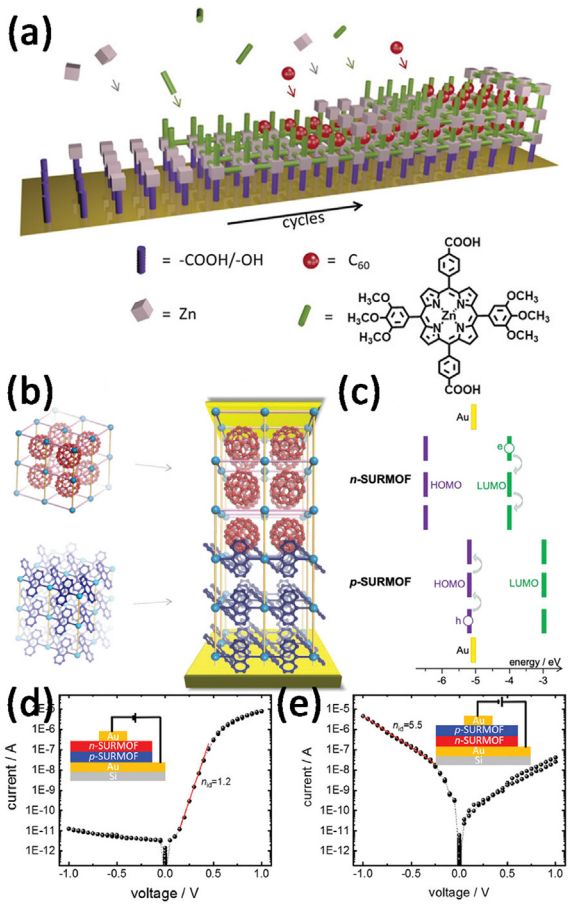

FIG. 17. (a) Schematic representation of the C_{60} encapsulation method in the LbL assembly methods. Reproduced with permission from Liu *et al.*, Angew. Chem. Int. Ed. **58**, 9590 (2019). Copyright 2019 Wiley-VCH.[41] (b) Schematic representation of n-SURMOF (fullerene-containing) and p-SURMOF (anthracene-containing). The bilayer heterostructure p–n-SURMOF with the top and bottom gold electrodes. (c) The HOMO and LUMO energy levels of the p- and n-SURMOF. Schematic representation and current–voltage curves of the (d) p–n-SURMOF and (e) n–p-SURMOF. Reproduced with permission from Chandresh *et al.*, Adv. Sci. **8**, 2001884 (2021). Copyright 2021 Wiley-VCH.[70]

Photoconductivity can be rendered to SURMOFs in a straightforward fashion by embedding C_{60} guests into porphyrin-based SURMOFs using the encapsulation LbL approach.[41] When using light at a wavelength of 455 nm, the photoconductivity of C_{60} at SURMOFs increased by 2 orders of magnitude. While the excitation of the porphyrin Soret band under blue light irradiation also occurs for the empty SURMOF, only after loading the C_{60} molecules (acting as acceptors) into the pores of the MOF charge transfer can take place. As confirmed by density functional theory calculations, the donor-acceptor interactions induce a rapid charge separation. After exciton dissociation, electrons and holes transport through different channels formed by C_{60} molecules and by porphyrin groups, respectively. The substantially larger on–off photocurrent ratio as compared to the empty SURMOF, thus, is a result of host–guest interactions.

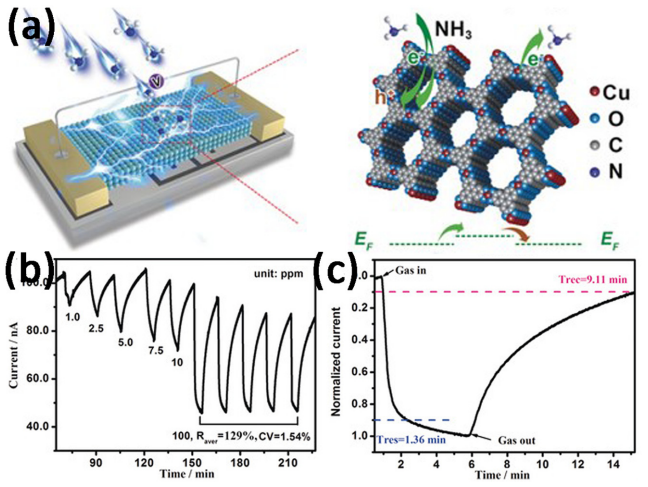

FIG. 18. (a) Schematic representation of gas-sensing mechanism; (b) current response toward NH_3 with different concentrations; and (c) response time and recovery time to 100 ppm NH_3. Reproduced with permission from Yao *et al.*, Angew. Chem. Int. Ed. **56**, 16510 (2017). Copyright 2017 Wiley-VCH.[88]

In a further step, the C_{60} at SURMOFs were used as a substrate for growing a second MOF thin film on top, creating an anthracene-based SURMOF.[70] As shown in Fig. 17, in this bilayer heterostructure, the junction between the n-type conducting C_{60} at SURMOFs and the p-type conducting anthracene-based SURMOF exhibited rectifying

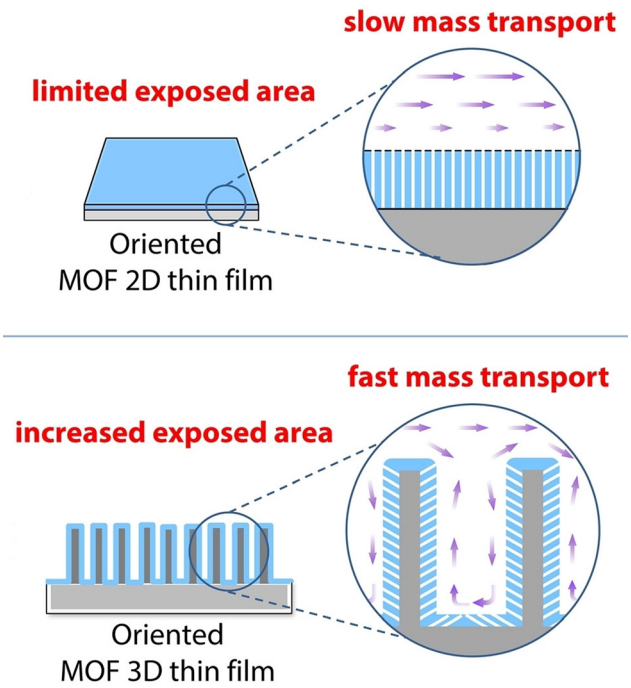

FIG. 19. Gas sensing mechanism of 2D Cu-HHTP SURMOF and 3D Cu-HHTP SURMOF. Reproduced with permission from Lin *et al.*, Angew. Chem. Int. Ed. **60**, 25758 (2021). Copyright 2021 Wiley-VCH.[89]

behavior. Using a gold substrate for SURMOF growth and then adding a top electrode, p–n as well as n–p devices could be fabricated, and the functioning MOF-diodes showed an on/off ratio of up to 6 orders of magnitude.

C. Electronic devices

Conductive SURMOF thin films possess a number of properties that make them attractive for chemical sensing applications, especially for gas detection devices. For such applications, their high surface area (resulting from the intrinsic porosity), easily controllable thickness, and enormous chemical variability are particularly important. The 2D conductive $Cu_3(HHTP)_2$ SURMOF, which was fabricated by the LPE LbL method (introduced in Sec. II A), exhibited selective detection of NH_3 against ten typical interference gases. As shown in Fig. 18, the average resistance increased ~129% toward 100 ppm NH_3 with good repeatability. In combination with the short response time (1.36 min), these properties demonstrate the huge potential of this SURMOF-based sensor for real-time monitoring of NH_3.

In 2021, Xu and co-workers introduced another strategy for building Cu-HHTP SURMOF-based sensing devices.[89] As shown in Fig. 19, they used 3D nanowire array substrates in the LPE LbL approach to increase the exposed area and optimize the charge and mass transport in the 3D SURMOFs. Compared to the above-mentioned 2D systems, the 3D sensors exhibited a 1000-fold improvement in the optimized limit of detection, 2.5-fold enhanced response (toward 1 ppm NH_3), and 1.3-fold improved response speed. In later work, the same group demonstrated a dual-ligand SURMOF strategy to further modulate the performance of the SURMOF gas sensor.[238] In this approach, a second hexagonal ligand, 2,3,6,7,10,11–hexaimino-triphenylene (HITP), was doped into the Cu-HHTP SURMOF during LbL growth. The selectivity and sensitivity toward benzene and NH_3 were further optimized in the HITP-doped Cu-HHTP SURMOFs. Large selectivity improvement (over 220%) was achieved for benzene when NH_3 was the interfering gas.

In 2021, Heinke and Krupke *et al.* reported a highly selective ethanol sensor. In contrast to the examples discussed above, this device was based on a graphene field-effect transistor (GFET), where the graphene was used as a substrate for SURMOF growth.[52] Large shifts (15 V) in the GFET Dirac point were observed when the SURMOF-on-graphed device was exposed to ethanol. Meanwhile, only very small shifts were observed for exposure to methanol, isopropanol, water, and other air constituents. Due to the countless variants of SURMOFs, this work demonstrated the potential of a new class of GFET-based SURMOF sensors with tailorable sensitivity and selectivity.

Organic field-effect transistors (OFETs) have attracted broad research interest as well as commercial interest for use in light-emitting transistors, phototransistors, and memory devices.[239–241] In general, an OFET consists of a dielectric layer, an organic semiconductor layer, and three electrodes (gate, source, and drain).[242] The use of an optimal dielectric layer material is crucial to obtaining OFETs that have competitive performance. In 2017, Zheng and Zhang *et al.* modified the dielectric layer by preparing a HKUST-1 SURMOF-on-SiO_2 using LbL assembly, creating a new dielectric layer material in OFET fabrication.[106] As shown in Fig. 20, by controlling the LbL deposition for the growth of HKUST-1 SURMOFs, the charge mobility, current on/off ratio, and threshold voltage were optimized and fine-tuned. Compared to the bare SiO_2-based OFETs, the SURMOF-modified SiO_2-based OFETs exhibited better performance. The enhancement was mainly attributed to the homogeneous and highly crystalline HKUST-1 SURMOFs with low dielectric constant deposited on the SiO/Si substrate, which induced smaller interface trap density in the SURMOF-modified OFETs.

A memristor (MR) is an electronic device whose internal states depend on the history of charge flowing through the device.[243,244] A memristor device has a sandwich structure usually consisting of a top electrode; an active, resistive layer; and a bottom electrode.[245] In pioneering work, Bufon and co-workers fabricated HKUST-1 SURMOFs in the form of rolled-up devices.[125] As shown in Fig. 21, a rolled-up tube electrode provided a robust and self-adjusted mechanical contact at the top of HKUST-1 SURMOFs. A stable and humidity-mediated

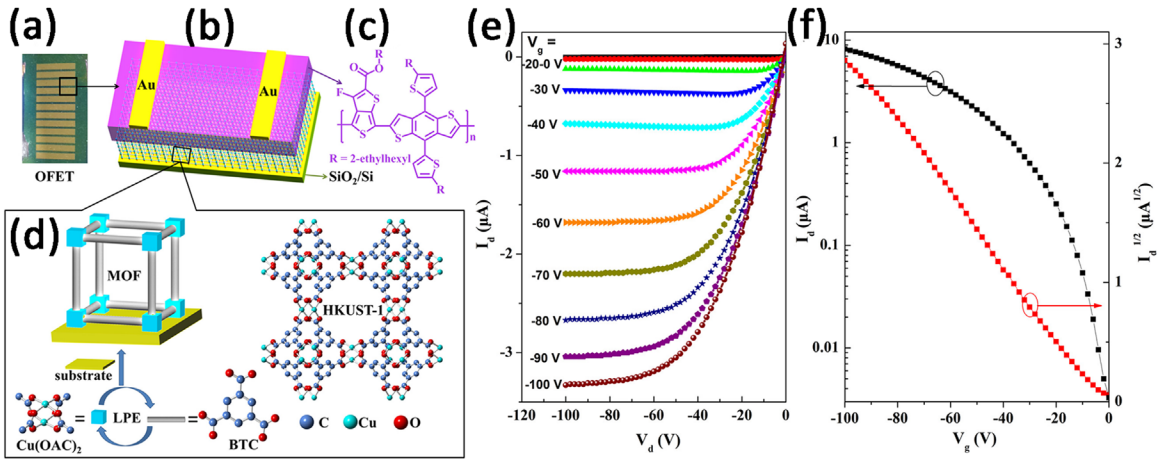

FIG. 20. (a) Photograph of OFET sample; (b) illustration of OFET with the SURMOF-modified interface of SiO_2 dielectric layers; (c) semiconducting polymer PTB7-Th; (d) schematic LbL growth of HKUST-1 SURMOFs; (e) output characteristic; and (f) transfer characteristic of SURMOF-modified OFET device. Reproduced with permission from Gu *et al.*, ACS Appl. Mater. Interfaces **9**, 7259 (2017). Copyright 2017 American Chemical Society.[106]

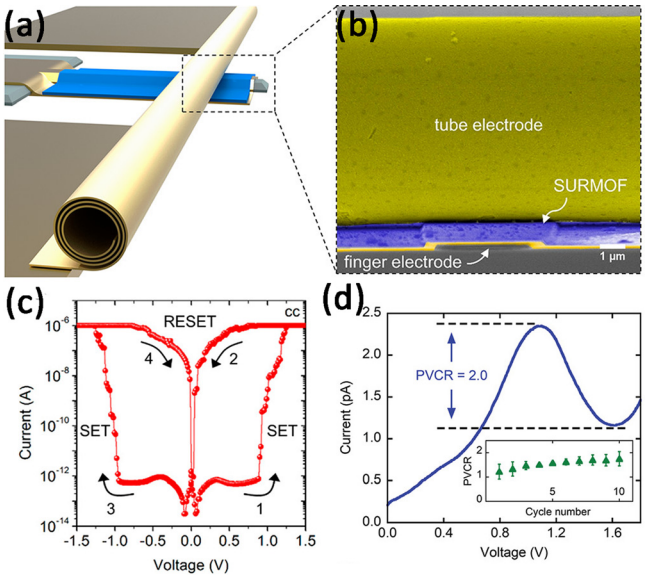

FIG. 21. (a) Schematic representation of a rolled-up Au/SURMOF vertical heterojunction; (b) SEM image showing the SURMOF in contact with the rolled-up tube electrode; (c) current–voltage characteristics at 90% humidity for the rolled-up Au/SURMOF vertical heterojunction. Reproduced with permission from Albano *et al.*, Nano Lett. **20**, 1080 (2020). Copyright 2020 American Chemical Society.[125] (d) Negative differential resistance behavior at 90% humidity after the conditioning process. Inset: Peak-to-valley current ratio in each cycle. Reproduced with permission from Albano *et al.*, Small **17**, 2101475 (2021). Copyright 2021 Wiley-VCH.[130]

ambipolar resistive switching was observed in this device. The on/off ratio under low threshold voltages (<1 V) and high humidity (90%) amounted to 6 orders of magnitude. DFT calculations suggested that the appearance of additional states in the bandgap region, caused by the structural defects attributed to the water molecules, played a key role in the resistivity switching. Later, the same group also reported a HKUST-I SURMOF-based room-temperature negative differential resistance (NDR) device.[130] As shown in Fig. 21(d), the peak-to-valley current ratio (PVCR), an important figure of merit of NDR devices, reached a value of around 2. DFT calculations revealed that the NDR effect appeared because the transition from metastable condition to field emission-like tunneling provided access to water-defect states near the Fermi level of the HKUST-1 SURMOF. These works demonstrated the potential of SURMOF-based devices for the next generation of logic circuits and scalable functional devices.

IV. PHOTOACTIVE SURMOFs

A response to external stimuli is a crucial factor for controlling functionality in devices in numerous application fields. Due to the large variety of building blocks, it is rather straightforward to render such responsiveness to MOFs, e.g., for chemical stimuli (redox, pH, reactive species, etc.) or physical stimuli (light, temperature, pressure, etc.).[246] Among the different types of external stimuli, light plays a special role. Remote optical control carries a lot of advantages, since it can be easily switched on and off and can work with high spatiotemporal resolution. In addition, varying the wavelength of the incident light offers the possibility of switching the type of response induced in the target material.[247] When photoresponsive materials are prepared in the form of SURMOFs, the thin MOF films exhibit even faster response than MOF powder particles. In particular, the problem of sufficient penetration depth can be avoided, which otherwise may occur in photon-triggered material responses.[248] In this section, we will introduce progress on SURMOF materials exhibiting properties amenable to switching by optical stimuli.

A. Reversible photoswitching of SURMOFs

Principally, three different strategies can be used to integrate photoresponsive moieties into SURMOFs: (1) designing organic ligands containing functionalized moieties suitable as a MOF linker, (2) adding functionalized moieties as a side group to photoinactive MOF ligands, and (3) diffusing/encapsulating functionalized moieties into the pores of SURMOFs. As discussed in the previous two sections, the first strategy, designing new MOF ligands with built-in functionality, is an attractive option for modifying the SURMOF backbones to achieve optical and electric/electronic properties. However, the use of MOF linkers that show photoisomerization may lead to problems, since the switching from one isomeric form to another may modify the MOF backbone, causing pronounced mechanical stress and potentially leading to a collapse of the structure. Therefore, to date, SURMOFs showing reversible photoswitching have been presented only according to the second two strategies.

In 2014, Wöll and co-workers reported a heteroepitaxial SURMOF system based on a MOF linker with a photoswitchable side group for the optically triggered release of guest molecules.[63] In this work, 2-azobenzene was attached to a BPDC ligand according to above-mentioned second strategy. Using these AB-BPDC (AB-BPDC = 2-azobenzene-4,4'-biphenyldicarboxylic acid) linkers, photoswitchable SURMOFs were grown on the top of SURMOFs with BPDC ligands, with the latter acting as a container that could be loaded and emptied through the top AP-BPDC SURMOF. XRD results revealed the presence of a perfect SURMOF-on-SURMOF bilayer system. The switching of the azobenzene side group between trans and cis states was first characterized using UV-Vis and IR spectroscopy and then used to control the uptake and release of guest molecules by illuminating with light at 365 (for opening the channels) and 560 nm (for closing). In 2015, another photoactive MOF ligand, AzoBipyB (AzoBipyB: 4,4′-(2-(phenyldiazenyl)-1,4-phenylene)dipyridine), also carrying an azobenzene as side group,[249] was designed. The corresponding AzoBipyB SURMOFs exhibited a substantial increase in the uptake of polar guest molecules when the azobenzene group switched from the trans to the cis state. No or only very small changes were seen for nonpolar molecules. These observations were attributed to dipole–dipole interactions between the polar guest molecules and the rather large dipole of the cis isomer of azobenzene. There is no dipole in the trans state, which thus strongly reduces the binding energy for polar guest molecules. A similar strategy was also used for other MOF linkers that are suitable for building pillared-layer SURMOFs for guest uptake.[67,250]

Switching the azobenzene side groups also affects the diffusivity of guest species inside SURMOFs. The fact that this effect can be different for different guest species was exploited to fabricate SURMOF-based membranes showing switchable selective permeance.[66] In this work, Wang and co-workers deposited pillared-layer SURMOFs built from linkers with azobenzene moieties as a side group onto mesoporous aluminum oxide supports. The obtained membranes exhibited

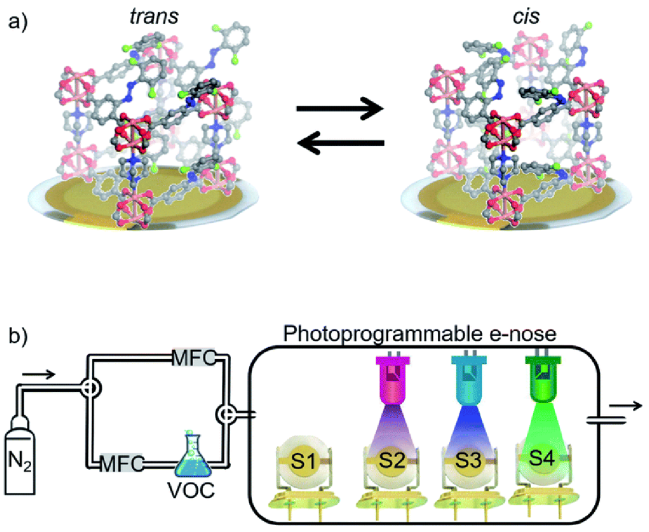

FIG. 22. (a) The $Cu_2(F_2AzoBDC)_2(dabco)$ SURMOF on a QCM sensor. The azobenzene side groups can isomerize from the trans form to the cis form and vice versa. (b) Schematic representation of the sensor array setup. The four photoprogrammable sensor chips can be selectively irradiated in the cell. Reproduced with permission from Qin *et al.*, Chem. Sci. **12**, 15700 (2021). Copyright 2021 Royal Society of Chemistry.[81]

dynamic control of the permeance and selectivity by photoswitching the azobenzene moieties in the pore. The separation factor of this membrane for a hydrogen/carbon dioxide mixture was reversibly switched between 3 and 8 when inducing a transition from the cis to the trans state. Later, Knebel and Heinke *et al.* introduced fluorinated azobenzene side groups and obtained $Cu_2(F_2AzoBDC)_2(dabco)$ SURMOFs, which also showed highly interesting performance related to photoswitchable separation.[65] The main advantage of the fluorinated azobenzene side groups is that not only the trans-to-cis but also the cis-to-trans switching can be induced with light in the visible regime, whereas for the non-fluorinated compound, UV light is needed for the back switching. For the fluorinated compound, the unwanted UV-induced ligand-to-metal charge transfer can be avoided, thus substantially increasing the yield of the photoswitching process.

Loading photoactive guest molecules into the SURMOF pores represents another strategy to render remote optical control to these porous thin films. Heinke and co-workers loaded azobenzene and o-tetrafluoroazobenzene into HKUST-1 SURMOFs to obtain thin films with switchable optical absorbance and guest molecule uptake.[65] For the azobenzene guests, reversible switching was achieved by UV light and blue light illumination, whereas for the o-tetrafluoroazobenzene at SURMOF, the use of light with two different wavelengths colors in the visible regime was sufficient.

Switching the interaction of frameworks with guest molecules can also be combined with MOF-based detectors to yield programmable sensor devices. To this end, Heinke and co-workers designed an array of gravimetric sensors monitoring volatile organic compounds (VOCs).[81] As shown in Fig. 22, the array consisted of four QCM sensors that were coated by $Cu_2(F_2AzoBDC)_2(dabco)$ SURMOFs. The selectivity of the sensor device was achieved by illuminating each of the four sensor chips with different colors of light. This resulted in a different trans-to-cis ratio for each sensor chip.

B. Photochemical post-synthetic modification of SURMOFs

MOF thin films provide an excellent platform for solid-state photochemical reactions, including optical lithography. Here, the small, adjustable thickness ensures that the incident light reaches reactants; thus, self-absorption effects can be largely avoided. In 2018, Wöll and co-workers reported selective oxidative photocyclization of a tetraarylethylene moiety by supramolecular control in SURMOFs.[190] As shown in Fig. 23, for the solvated tetraarylethylene linker, illumination leads

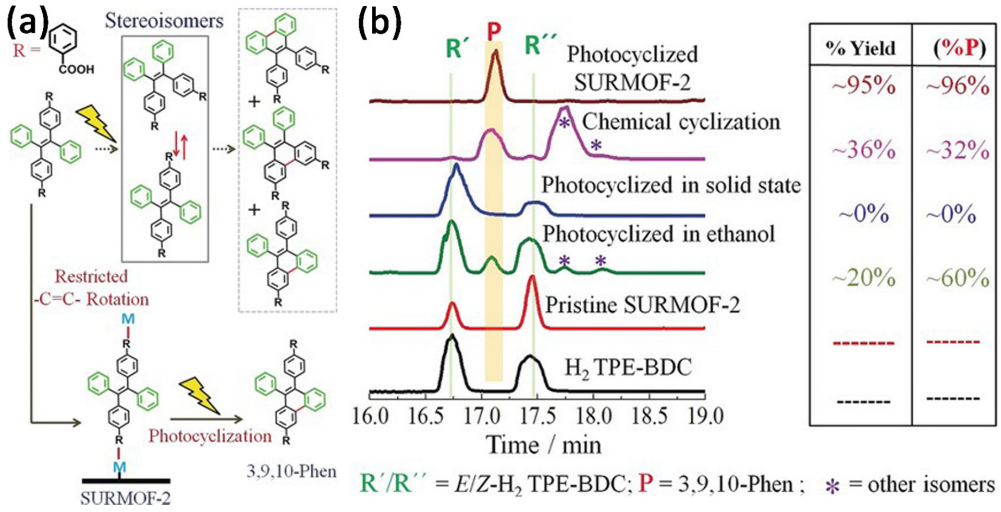

FIG. 23. (a) Different behaviors of E-H2 TPE-BDC free state and E-H2 TPE-BDC linker of SURMOF-2 in oxidative photocyclization reaction. (b) Liquid chromatography–mass spectrometry profiles of TPE-BDC under different conditions. Right: Total reaction yields and percentage of 3,9,10-phen isomer formed in different conditions. Reproduced with permission from Haldar *et al.*, Angew. Chem. Int. Ed. **57**, 13662 (2018). Copyright 2018 Wiley-VCH.[190]

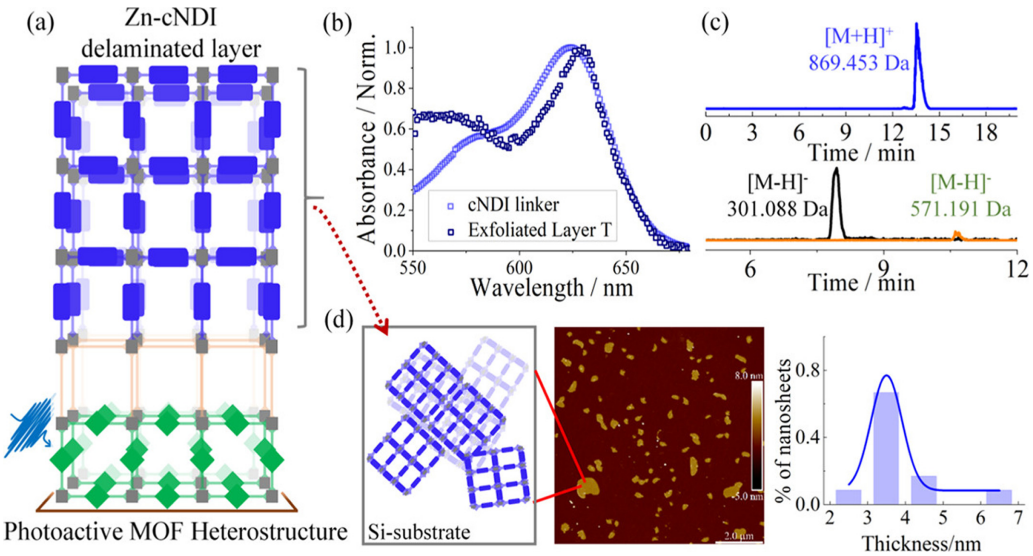

FIG. 24. (a) Illustration of the heteroepitaxial structure Zn-cNDI (blue) on the Zn-PPY-TPE; (b) UV-vis absorbance spectra of the Zn-cNDI layer and the cNDI linker in ethanol; (c) liquid chromatography–mass spectrometry profiles of the delaminated Zn-cNDI top layer; and (d) left: schematic illustration of delaminated Zn-cNDI 2D MOF sheets; middle: AFM image of the delaminated Zn-cNDI 2D MOF sheets; right: distribution of the 2D nanosheet thicknesses. Reproduced with permission from Liu *et al.*, ACS Appl. Mater. Interfaces **13**, 57768 (2021). Copyright 2021 American Chemical Society.[182]

to an oxidative photocyclization of the produced three isomers, depending on the rotation of –C = C– before the ring closure step, with slow kinetics. Different behavior was observed after assembling the linker into a SURMOF. In this case, illumination with light at 365 nm yielded only one of the phenanthrene isomers, and the selectivity amounted to ∼96%. Moreover, much faster reaction kinetics were observed within the SURMOF.

Photoinduced reactions inside SURMOFs also profit from the combination of a second SURMOF in MOF-on-MOF thin-film heterostructures. In the paper by Hupp and co-workers,[187,215,232] a reactive oxygen species produced by incident light in a photoactive first (bottom) layer was used to drive a chemical reaction in a second layer. In this case, the spatio-selective generation of reactive oxygen species reacted with the MOF linkers in the second (top) layer so that delamination occurred.[183] As shown in Fig. 24, a porphyrinic SURMOF was used to create the reactive oxygen species, which then reacted with the tetraphenylethylene (TPE)-top SURMOF. Reactive oxygen species formed upon illumination with visible light in the presence of oxygen gas, leading to a cleavage of the TPE MOF linkers and yielding 2D MOF sheets of well-defined thickness.

V. SURMOF-DERIVED MATERIALS

Metal-organic frameworks, as porous and periodic structure materials with well-defined compositions, also provide a starting point for obtaining other materials by calcination. In this context, SURMOFs provide the advantage that the calcination products are obtained in the form of thin films with well-defined thicknesses, which may be difficult to prepare with other approaches. Depending on the MOF material and the type of atmosphere present during calcination, different types of thin films can be obtained, including porous carbons,[251,252] metal oxides,[253,254] organic-inorganic hybrid materials,[255] and polymers.[256,257]

A. SURMOF-derived polymer

Surface-anchored polymeric gels (SURGELs) were produced from a SURMOF precursor via covalent cross-linking and subsequent removal of the metal ions, as schematically depicted in Fig. 25(a).[57] These metal-free SURMOF-derived polymer thin films combine the advantages of SURMOFs, including precisely controlled structure and high porosity, with the intrinsic beneficial properties of polymers, such as soft texture and pronounced stability in biological/aqueous environments. The porosity of these thin films can be exploited by loading bioactive compounds into SURGELs for biotechnological processes (such as biotransformation) or for biomedical applications (such as spatially confined delivery of high concentrations of bioactive molecules, particularly drugs).

Another instructive example is the fabrication of 2D polymer films composed of interwoven linear fibers using a sophisticated three-layer SURMOF architecture [see Figs. 25(b) and 25(c)].[176] In this case, quadritopic linkers were first assembled into SURMOFs. Then, in a second step, UV illumination was used to induce a Glaser–Hay coupling of the triple bonds to yield linear, interwoven polymer chains. In a final step, 2D textile sheets were obtained by removing the metal ions.

Porphyrin-based polymer thin films with high antimicrobial activity were reported via the SURMOF-derived strategy.[171] Bisazido-functionalized porphyrin linkers were adopted in LbL SURMOF fabrication. Afterward, secondary linkers were covalently connected between each porphyrin unit of the SURMOFs, and the SURMOF-derived porphyrin-based polymer thin films were produced after removal of the metal nodes. The obtained polymer thin films exhibited high antibacterial activity in bacteria experiments, due to the reactive oxygen species generated under visible light illumination.

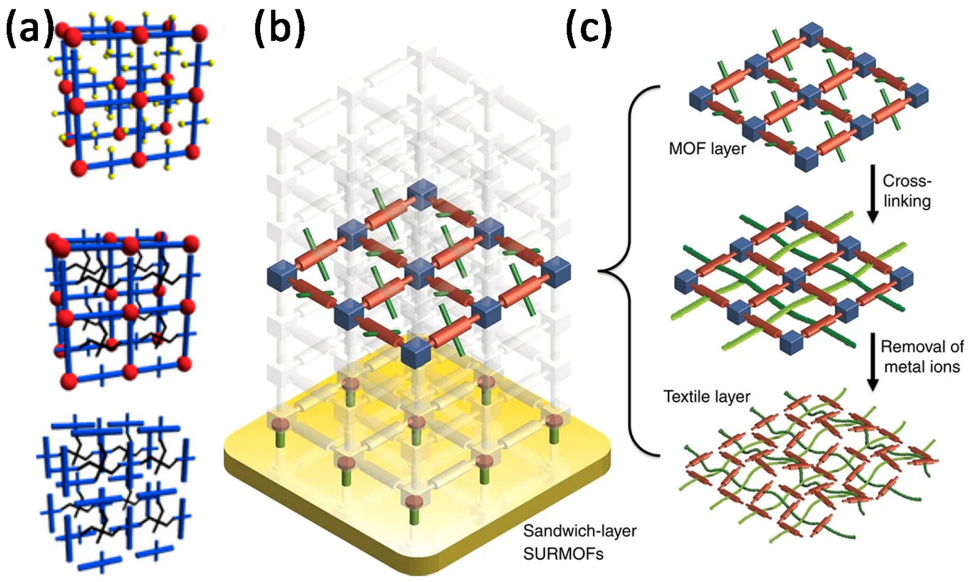

FIG. 25. (a) Schematic representation of the SURMOF-2 structure (top), SURMOF structure after the cross-linking process (middle), and SURGELs after removal of the metal ions (bottom). Reproduced with permission from Tsotsalas *et al.*, J. Am. Chem. Soc. **136**, 8 (2014). Copyright 2014 American Chemical Society.[57] Schematic illustration of (b) the heteroepitaxial sandwich-layer SURMOFs and (c) the formation procedure of molecular weaving in the active MOF layer embedded between two sacrificial layers. Reproduced with permission from Wang *et al.*, Nat. Commun. **8**, 1 (2017). Copyright 2017 Spring Nature.[178]

The porosity of the parent SURMOF is transferred to the corresponding SURGEL membranes and can be used for applications as membranes.[59] The SURGEL membranes exhibited interesting size-dependent permeabilities, in combination with high mechanical and chemical stability.

B. SURMOF-derived oxy-hydroxides

Thin layers of oxides are of pronounced interest with regard to electrocatalysis.[258] Methods to yield well-defined thin films with low densities of pinholes are required to fabricate devices. A straightforward manufacturing strategy to reach this goal was reported by Bandarenka and Fischer in 2019, who fabricated mixed nickel/cobalt hydroxide sheets with impressive performance in electrocatalysts. The thin films were prepared from nickel-cobalt-BDC SURMOFs.[153] The prefabricated SURMOFs were transformed into SURMOF-derived materials by immersion into alkaline electrolyte solution (0.1 M KOH aqueous solution). Compared to industrial and state-of-the-art relevant oxygen evolution reaction (OER) electrocatalysts (such as IrO_2), the converted SURMOF oxy-hydroxide thin films revealed outstanding performance in the OER, mass activity (mass-normalized OER activity), and prominent durability. Thus, the obtained mass activity ($\sim$2.5 mA μg^{-1}) at the defined overpotential of 300 mV is one order of magnitude higher than the mass activity of IrO_2 electrocatalyst and 3.5 times higher than that of reported NiFe-, FeCoW-, or NiCo-based electrocatalysts.

Subsequently, the same group used nickel–iron-BDC SURMOFs as parent system to fabricate bifunctional nickel/iron hydroxide electrocatalysts with high performance in the oxygen reduction reaction (ORR) and the OER.[154] By introducing additional functional groups, such as –Br, $-OCH_3$, and $-NH_2$, into the SURMOF by attaching the side groups to the MOF linkers, the performance of the resulting electrocatalytically active thin films could be further tuned, leading to an increase in the overall OER activity. The materials exhibited an OER activity of 200 mA cm^{-2} at an overpotential of only $\approx$210 mV. Operational long-term stability of SURMOFDs was demonstrated even at a high current density of 500 mA cm^{-2}. A narrow overpotential window ΔEORR-OER (0.69 V) was also exhibited in 0.1 M KOH with a mass loading two orders of magnitude lower than the mass loading of benchmark electrocatalysts.

More recently, heterostructured Ni|Fe-BDC-SURMOFs (Fe-BDC-SURMOF on Ni-BDC-SURMOF) were converted to oxy-hydroxide thin films via immersion in the alkaline electrolyte solution.[156] This work demonstrated partial leaching of the BDC linker and generation of NiFe hydroxides/oxyhydroxides during the alkaline derivation treatment, as shown in Fig. 26. The obtained Ni|Fe-SURMOFDs exhibited an OER activity ($\approx$2.90 kA/g) at an overpotential of 300 mV. Their excellent performance, namely, a low apparent activation energy and a large electroactivity, was attributed to the

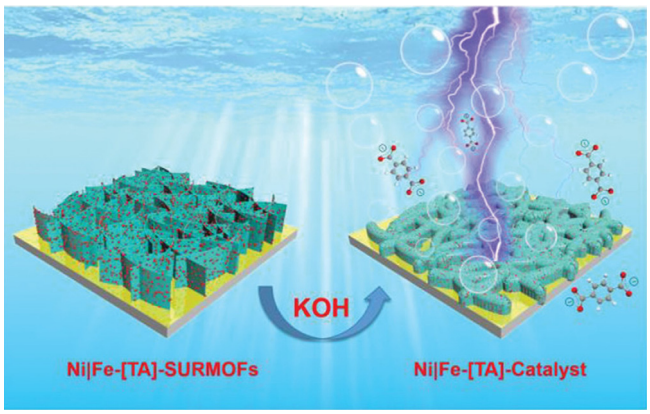

FIG. 26. Schematic illustration showing the prefabricated SURMOFs are transformed into SURMOF-derived catalysts by immersion into alkaline electrolyte solution. Reproduced with permission from Hou *et al.*, Adv. Mater. **33**, 2103218 (2021). Copyright 2021 Wiley-VCH.[156]

particular structure of the resulting thin films, which contained a high Ni content in a high oxidation state. In other work, the alkali metal cations in the OER were also demonstrated to impact the oxygen evolution activity of SURMOFD thin films.[155] The OER activity of the SURMOFDs was sensitive to the alkali metal cations in the alkaline electrolyte solution, with the following order: $Cs^+ > K^+ > Na^+ > Li^+$. The cation-dependent catalytic activity was closely associated with the Ni–O bond variable length of the SURMOFDs. By introducing a laser-induced current transient technique, it was also demonstrated that the alkali metal cations impact the interfacial water layer structure.

VI. CONCLUSIONS AND PERSPECTIVES

As highlighted in this review, during the past decade SURMOFs have not only attracted interest in basic research for studying photophysical phenomena but also found applications in basically all fields where well-defined MOF thin films are required. The layer-by-layer assembly using alternating contact with solutions of the MOF constituents allows the thin-film formation to be steered in a number of different directions and, in particular, offers the possibility of encapsulating large guests using layer-by-layer encapsulation. When compared to other MOF thin film fabrication strategies, the LbL process yields monolithic thin films with a high degree of orientation and defect densities, which in several cases are much smaller than those for the corresponding bulk materials. Recent advances in the application of SURMOF materials can be placed into three groups: (1) optical application of high-optical-quality SURMOF materials with controllable chromophore aggregation or well-defined metal node assembly, (2) conductive SURMOF thin-film fabrications and applications based on the low-defect properties and straightforward realization of heteromultilayers, and (3) photo-modifiable MOF thin films using the flexible LbL assembly and the ultrathin thickness of SURMOF materials.

Due to the SURMOFs' enormous structural flexibility, a property inherited from their parent MOF materials, SURMOFs have the huge potential for optimization with regard to specific applications, can be integrated into devices with industrial relevance, and can overcome present limitations in as-yet unexplored fields. We foresee future pronounced impact of SURMOFs in the following areas: (1) the fabrication of extremely stable SURMOF thin films (in particular, UiO-68, NU-1000, etc.) manufactured using a mild synthetic condition, (2) encapsulation of biomolecules (e.g., enzymes) or nanoparticles into SURMOF materials for catalysis applications, (3) high-resolution lithographical printing of SURMOF materials as optical filters or optical anti-counterfeiting materials, (4) combinations of photo-click moieties as highly efficient light-triggered click chemistry materials, (5) low-defect separation thin-film materials with high selective separation efficiency and repeatability, and (6) design from a structure point of view to achieve highly conductive thin-film materials.

An important aspect of LbL growth as compared to solvothermal synthesis at temperature typically above 150 °C is that SURMOF synthesis is carried out at much lower temperatures, in many cases at room temperature. The deposition process therefore largely occurs under kinetic control, and the structural parameters of the deposited films depend strongly on details of synthesis parameters, e.g., concentrations, immersion times, and duration of the rinsing process. The optimization of these parameters is a rather tedious process, which, in general, will be different for each type of MOF. Recently, a breakthrough has been achieved by introducing machine learning (ML) strategies combined with a robot-based synthesis in a glovebox.[259] In this work, it is demonstrated that by using genetic algorithms, structural parameters of the deposited films can be changed and optimized. We also see a huge potential of AI (artificial intelligence) based approaches for the synthesis of SURMOFs—recently, it has been demonstrated that AI approaches can be successfully used to predict synthesis conditions for bulk MOF materials by analyzing the published synthesis protocols for similar materials.[260] We expect that a combination of these strategies will make it easier in the future to develop strategies for depositing SURMOFs for MOF types where so far only the bulk form is known and then to optimize structural parameters like orientation, defect density, and surface roughness.

Finally, we would like to point out that the planar outer surfaces of SURMOFs exhibit a well-defined structure and an unusually large spacing of anchoring sites. Such flat substrates are of potential interest for a number of different purposes. For example, the attachment of photoswitchable compounds during the last step of LbL deposition might yield a collective motion of azobenzene moieties on the top SURMOF layer, thus realizing a "command surface" where light-induced switching of azobenzene groups leads to a change of surface properties.[261]

ACKNOWLEDGMENTS

The authors acknowledge support by the Helmholtz program "Materials Systems Engineering" (MSE) at the Karlsruhe Institute of Technology. C.W. acknowledges support from Deutsche Forschungsgemeinschaft (DFG, German Research Foundation) under Germany's Excellence Strategy—2082/1—390761711. We thank L. Heinke, M. Tsotsalas, P. G. Weidler, T. Hashem, L. Pilz, D. Wonanke, Y. Luo, and N. Prasetya for comments on this manuscript.

AUTHOR DECLARATIONS

Conflict of Interest

The authors have no conflicts to disclose.

Author Contributions

Donghui Chen: Writing – original draft (equal); Writing – review & editing (equal). **Hartmut Gliemann:** Writing – review & editing (equal). **Christof Woll:** Writing – review & editing (equal).

DATA AVAILABILITY

Data sharing is not applicable to this article as no new data were created or analyzed in this study.

REFERENCES

[1]O. M. Yaghi, G. Li, and H. Li, "Selective binding and removal of guests in a microporous metal–organic framework," Nature **378**, 703 (1995).
[2]X. Zhang, Z. Chen, X. Liu, S. L. Hanna, X. Wang, R. Taheri-Ledari, A. Maleki, P. Li, and O. K. Farha, "A historical overview of the activation and porosity of metal–organic frameworks," Chem. Soc. Rev. **49**, 7406 (2020).
[3]T. L. Easun, F. Moreau, Y. Yan, S. Yang, and M. Schröder, "Structural and dynamic studies of substrate binding in porous metal–organic frameworks," Chem. Soc. Rev. **46**, 239 (2017).

[4]H. K. Chae, D. Y. Siberio-Pérez, J. Kim, Y. Go, M. Eddaoudi, A. J. Matzger, M. O'Keeffe, and O. M. Yaghi, "A route to high surface area, porosity and inclusion of large molecules in crystals," Nature **427**, 523 (2004).
[5]T. Jia, Y. Gu, and F. Li, "Progress and potential of metal-organic frameworks (MOFs) for gas storage and separation: A review," J. Environ. Chem. Eng. **10**, 108300 (2022).
[6]K. Kuruvinashetti, J. Li, Y. Zhang, H. Bemana, M. McKee, and N. Kornienko, "Emerging opportunities with metal-organic framework electrosynthetic platforms," Chem. Phys. Rev. **3**, 021306 (2022).
[7]K. A. Forrest, G. Verma, Y. Ye, J. Ren, S. Ma, T. Pham, and B. Space, "Methane storage in flexible and dynamical metal–organic frameworks," Chem. Phys. Rev. **3**, 021308 (2022).
[8]D.-H. Chen, C. Zhuo, Y.-H. Wen, L. Lin, Y.-X. Zhang, S.-M. Hu, R.-B. Fu, and X.-T. Wu, "Porous metal–organic frameworks based on 3, 6-bis (4-benzoic acid)-N-(4-benzoic acid) carbazole for HPLC separation of small organic molecules," Mater. Chem. Front. **2**, 1508 (2018).
[9]D. Zacher, O. Shekhah, C. Wöll, and R. A. Fischer, "Thin films of metal–organic frameworks," Chem. Soc. Rev. **38**, 1418 (2009).
[10]D. Bradshaw, A. Garai, and J. Huo, "Metal–organic framework growth at functional interfaces: Thin films and composites for diverse applications," Chem. Soc. Rev. **41**, 2344 (2012).
[11]Y. Cheng, S. J. Datta, S. Zhou, J. Jia, O. Shekhah, and M. Eddaoudi, "Advances in metal–organic framework-based membranes," Chem. Soc. Rev. **51**, 8300 (2022).
[12]E. Virmani, J. M. Rotter, A. Mähringer, T. V. Zons, A. Godt, T. Bein, S. Wuttke, and D. D. Medina, "On-surface synthesis of highly oriented thin metal–organic framework films through vapor-assisted conversion," J. Am. Chem. Soc. **140**, 4812 (2018).
[13]H. Tian, H. Fan, M. Li, and L. Ma, "Zeolitic imidazolate framework coated ZnO nanorods as molecular sieving to improve selectivity of formaldehyde gas sensor," ACS Sens. **1**, 243 (2016).
[14]Y. Zhao, N. Kornienko, Z. Liu, C. Zhu, S. Asahina, T.-R. Kuo, W. Bao, C. Xie, A. Hexemer, O. Terasaki, P. Yang, and O. M. Yaghi, "Mesoscopic constructs of ordered and oriented metal–organic frameworks on plasmonic silver nanocrystals," J. Am. Chem. Soc. **137**, 2199 (2015).
[15]J. Liu and C. Wöll, "Metal–organic framework thin films: Electrochemical fabrication techniques and corresponding applications and perspectives," Chem. Soc. Rev. **46**, 5730 (2017).
[16]W.-J. Li, M. Tu, R. Cao, and R. A. Fischer, "Elaboration of metal organic framework hybrid materials with hierarchical porosity by electrochemical deposition–dissolution," J. Mater. Chem. A **4**, 12356 (2016).
[17]C. Warakulwit, S. Yadnum, C. Boonyuen, C. Wattanakit, A. Karajic, P. Garrigue, N. Mano, D. Bradshaw, J. Limtrakul, and A. Kuhn, "On the electrochemical deposition of metal–organic frameworks," CrystEngComm **18**, 5095 (2016).
[18]N. Campagnol, T. R. Van Assche, M. Li, L. Stappers, M. Dincă, J. F. Denayer, K. Binnemans, D. E. De Vos, and J. Fransaer, "Surface-supported metal–organic framework thin films: Fabrication methods, applications, and challenges," J. Mater. Chem. A **4**, 3914 (2016).
[19]K. B. Blodgett, "Properties of built-up films of barium stearate," J. Phys. Chem. **41**, 975 (1937).
[20]L. Wågberg and J. Erlandsson, "The use of layer-by-layer self-assembly and nanocellulose to prepare advanced functional materials," Adv. Mater. **33**, 2001474 (2021).
[21]J. Lipton, G.-M. Weng, J. A. Röhr, H. Wang, and A. D. Taylor, "Layer-by-layer assembly of two-dimensional materials: Meticulous control on the nanoscale," Matter **2**, 1148 (2020).
[22]G. Decher and J. Hong, "Buildup of ultrathin multilayer films by a self-assembly process, 1 consecutive adsorption of anionic and cationic bipolar amphiphiles on charged surfaces," Makromol. Chem. Macromol. Symp. **46**, 321 (1991).
[23]H. Agarwal, W. M. Breining, and D. M. Lynn, "Continuous fabrication of slippery liquid-infused coatings on rolls of flexible materials," ACS Appl. Polym. Mater. **4**, 787 (2022).
[24]M. Morita, S. Toyoda, H. Kiuchi, T. Abe, K. Kumagai, T. Saida, and K. Fukuda, "Chromogenic amorphous MoO_{3-x} nanosheets and their nanostructured films for smart window applications," ACS Appl. Nano Mater. **4**, 8781 (2021).
[25]J. Wu, H. Zeng, X. Li, X. Xiang, Y. Liao, Z. Xue, Y. Ye, and X. Xie, "Ultralight layer-by-layer self-assembled MoS_2-polymer modified separator for simultaneously trapping polysulfides and suppressing lithium dendrites," Adv. Energy Mater. **8**, 1802430 (2018).
[26]M. D. Ward, "Bulk crystals to surfaces: Combining x-ray diffraction and atomic force microscopy to probe the structure and formation of crystal interfaces," Chem. Rev. **101**, 1697 (2001).
[27]R. K. Smith, P. A. Lewis, and P. S. Weiss, "Patterning self-assembled monolayers," Prog. Surf. Sci. **75**, 1 (2004).
[28]O. Shekhah, H. Wang, S. Kowarik, F. Schreiber, M. Paulus, M. Tolan, C. Sternemann, F. Evers, D. Zacher, R. A. Fischer, and C. Wöll, "Step-by-step route for the synthesis of metal-organic frameworks," J. Am. Chem. Soc. **129**, 15118 (2007).
[29]L. Messe, S. M. Clarke, T. Arnold, C. Dong, R. K. Thomas, and A. Inaba, "Mixing behavior at the solid/liquid interface: Binary monolayers of linear alcohols adsorbed on graphite," Langmuir **18**, 4010 (2002).
[30]Y.-F. Liu and Y.-L. Lee, "Adsorption characteristics of OH-terminated alkanethiol and arenethiol on Au (111) surfaces," Nanoscale **4**, 2093 (2012).
[31]N. Stock and S. Biswas, "Synthesis of metal-organic frameworks (MOFs): Routes to various MOF topologies, morphologies, and composites," Chem. Rev. **112**, 933 (2012).
[32]H. K. Arslan, O. Shekhah, D. F. Wieland, M. Paulus, C. Sternemann, M. A. Schroer, S. Tiemeyer, M. Tolan, R. A. Fischer, and C. Wöll, "Intercalation in layered metal–organic frameworks: Reversible inclusion of an extended π-system," J. Am. Chem. Soc. **133**, 8158 (2011).
[33]H. K. Arslan, O. Shekhah, J. Wohlgemuth, M. Franzreb, R. A. Fischer, and C. Wöll, "High-throughput fabrication of uniform and homogenous MOF coatings," Adv. Funct. Mater. **21**, 4228 (2011).
[34]V. Chernikova, O. Shekhah, and M. Eddaoudi, "Advanced fabrication method for the preparation of MOF thin films: Liquid-phase epitaxy approach meets spin coating method," ACS Appl. Mater. Interfaces **8**, 20459 (2016).
[35]K. Müller, J. S. Malhi, J. Wohlgemuth, R. A. Fischer, C. Wöll, H. Gliemann, and L. Heinke, "Water as a modulator in the synthesis of surface-mounted metal–organic framework films of type HKUST-1," Dalton Trans. **47**, 16474 (2018).
[36]Z.-G. Gu, A. Pfriem, S. Hamsch, H. Breitwieser, J. Wohlgemuth, L. Heinke, H. Gliemann, and C. Wöll, "Transparent films of metal-organic frameworks for optical applications," Microporous Mesoporous Mater. **211**, 82 (2015).
[37]O. Zybaylo, O. Shekhah, H. Wang, M. Tafipolsky, R. Schmid, D. Johannsmann, and C. Wöll, "A novel method to measure diffusion coefficients in porous metal–organic frameworks," Phys. Chem. Chem. Phys. **12**, 8093 (2010).
[38]L. Heinke and C. Wöll, "Adsorption and diffusion in thin films of nanoporous metal–organic frameworks: Ferrocene in SURMOF $Cu_2(ndc)_2(dabco)$," Phys. Chem. Chem. Phys. **15**, 9295 (2013).
[39]Z. Wang, J. Liu, B. Lukose, Z. Gu, P. G. Weidler, H. Gliemann, T. Heine, and C. Wöll, "Nanoporous designer solids with huge lattice constant gradients: Multiheteroepitaxy of metal–organic frameworks," Nano Lett. **14**, 1526 (2014).
[40]J. Wang, W. Wang, Z. Fan, S. Chen, A. Nefedov, S. Heißler, R. A. Fischer, C. Wöll, and Y. Wang, "Defect-engineered metal–organic frameworks: A thorough characterization of active sites using CO as a probe molecule," J. Phys. Chem. C **125**, 593 (2021).
[41]X. Liu, M. Kozlowska, T. Okkali, D. Wagner, T. Higashino, G. Brenner-Weiß, S. M. Marschner, Z. Fu, Q. Zhang, H. Imahori, S. Bräse, W. Wenzel, C. Wöll, and L. Heinke, "Photoconductivity in metal–organic framework (MOF) thin films," Angew. Chem. Int. Ed. **58**, 9590 (2019).
[42]R. Haldar, Z. Fu, R. Joseph, D. Herrero, L. Martín-Gomis, B. S. Richards, I. A. Howard, A. Sastre-Santos, and C. Wöll, "Guest-responsive polaritons in a porous framework: Chromophoric sponges in optical QED cavities," Chem. Sci. **11**, 7972 (2020).
[43]Y. Ma, Z. Dong, M. You, Y. Zhang, X. Feng, X. Ma, and J. Meng, "Formation of a thin and continuous MOF membrane with 2-D MOF nanosheets as seeds via layer-by-layer growth," Chem. Commun. **55**, 10146 (2019).
[44]M.-H. Li, Z. Yang, Z. Li, J.-R. Wu, B. Yang, and Y.-W. Yang, "Construction of hydrazone-linked macrocycle-enriched covalent organic frameworks for highly efficient photocatalysis," Chem. Mater. **34**, 5726 (2022).

[45]J. Gao, W. Wei, Y. Yin, M. Liu, C. Zheng, Y. Zhang, and P. Deng, "Continuous ultrathin UiO-66-NH_2 coatings on a polymeric substrate synthesized by a layer-by-layer method: A kind of promising membrane for oil–water separation," Nanoscale **12**, 6658 (2020).
[46]J. Zhuang, J. Friedel, and A. Terfort, "The oriented and patterned growth of fluorescent metal–organic frameworks onto functionalized surfaces," Beilstein J. Nanotechnol. **3**, 570 (2012).
[47]J. Zhuang, D. Ceglarek, S. Pethuraj, and A. Terfort, "Rapid room-temperature synthesis of metal–organic framework HKUST-1 crystals in bulk and as oriented and patterned thin films," Adv. Funct. Mater. **21**, 1442 (2011).
[48]T. Ladnorg, A. Welle, S. Heißler, C. Wöll, and H. Gliemann, "Site-selective growth of surface-anchored metal-organic frameworks on self-assembled monolayer patterns prepared by AFM nanografting," Beilstein J. Nanotechnol. **4**, 638 (2013).
[49]J. Ou, J. Xiang, J. Liu, and L. Sun, "Surface-supported metal–organic framework thin-film-derived transparent $CoS_{1.097}$ at N-doped carbon film as an efficient counter electrode for bifacial dye-sensitized solar cells," ACS Appl. Mater. Interfaces **11**, 14862 (2019).
[50]C. Gu, H. Zhang, P. You, Q. Zhang, G. Luo, Q. Shen, Z. Wang, and J. Hu, "Giant and multistage nonlinear optical response in porphyrin-based surface-supported metal–organic framework nanofilms," Nano Lett. **19**, 9095 (2019).
[51]S. Klyatskaya, A. B. Kanj, C. Molina-Jirón, S. Heidrich, L. Velasco, C. Natzeck, H. Gliemann, S. Heissler, P. Weidler, W. Wenzel, C. C. B. Bufon, L. Heinke, C. Wöll, and M. Ruben, "Conductive metal–organic framework thin film hybrids by electropolymerization of monosubstituted acetylenes," ACS Appl. Mater. Interfaces **12**, 30972 (2020).
[52]S. Kumar, Y. Pramudya, K. Müller, A. Chandresh, S. Dehm, S. Heidrich, A. Fediai, D. Parmar, D. Perera, M. Rommel, L. Heinke, W. Wenzel, C. Wöll, and R. Krupke, "Sensing molecules with metal–organic framework functionalized graphene transistors," Adv. Mater. **33**, 2103316 (2021).
[53]M. P. Arpa Sancet, M. Hanke, Z. Wang, S. Bauer, C. Azucena, H. K. Arslan, M. Heinle, H. Gliemann, C. Wöll, and A. Rosenhahn, "Surface anchored metal-organic frameworks as stimulus responsive antifouling coatings," Biointerphases **8**, 29 (2013).
[54]M. Hanke, H. K. Arslan, S. Bauer, O. Zybaylo, C. Christophis, H. Gliemann, A. Rosenhahn, and C. Wöll, "The biocompatibility of metal–organic framework coatings: An investigation on the stability of SURMOFs with regard to water and selected cell culture media," Langmuir **28**, 6877 (2012).
[55]S. Friedländer, J. Liu, M. Addicoat, P. Petkov, N. Vankova, R. Rüger, A. Kuc, W. Guo, W. Zhou, B. Lukose, Z. Wang, P. G. Weidler, A. Pöppl, M. Ziese, T. Heine, and C. Wöll, "Linear chains of magnetic ions stacked with variable distance: Ferromagnetic ordering with a Curie temperature above 20 K," Angew. Chem. Int. Ed. **55**, 12683 (2016).
[56]E. Frederick, T. W. Shaw, M. G. Frith, and S. L. Bernasek, "Synthesis of a surface mounted metal–organic framework on gold using a Au–carbene self-assembled monolayer linkage," Mater. Chem. Front. **3**, 636 (2019).
[57]M. Tsotsalas, J. Liu, B. Tettmann, S. Grosjean, A. Shahnas, Z. Wang, C. Azucena, M. Addicoat, T. Heine, J. Lahann, J. Overhage, S. Bräse, H. Gliemann, and C. Wöll, "Fabrication of highly uniform gel coatings by the conversion of surface-anchored metal–organic frameworks," J. Am. Chem. Soc. **136**, 8 (2014).
[58]S. Schmitt, J. Hümmer, S. Kraus, A. Welle, S. Grosjean, M. Hanke-Roos, A. Rosenhahn, S. Bräse, C. Wöll, C. Lee-Thedieck, and M. Tsotsalas, "Tuning the cell adhesion on biofunctionalized nanoporous organic frameworks," Adv. Funct. Mater. **26**, 8455 (2016).
[59]S. Schmitt, S. Shishatskiy, P. Krolla, Q. An, S. Begum, A. Welle, T. Hashem, S. Grosjean, V. Abetz, S. Bräse, C. Wöll, and M. Tsotsalas, "Synthesis, transfer, and gas separation characteristics of MOF-templated polymer membranes," Membranes **9**, 124 (2019).
[60]J. Liu, S. Heidrich, J. Liu, B. Guo, M. Zharnikov, U. Simon, W. Wenzel, and C. Wöll, "Encapsulation of Au_{55} clusters within surface-supported metal–organic frameworks for catalytic reduction of 4-nitrophenol," ACS Appl. Nano Mater. **4**, 522 (2021).
[61]S. Rana, R. Rajendra, B. Dhara, P. K. Jha, and N. Ballav, "Highly hydrophobic and chemically rectifiable surface-anchored metal-organic framework thin-film devices," Adv. Mater. Interfaces **3**, 1500738 (2016).
[62]S. Lei, L.-M. Chang, Z.-G. Gu, and J. Zhang, "A metal-porphyrinic framework film as an efficient optical limiting layer in an electro-optical switchable device," Chem. Commun. **57**, 10166 (2021).
[63]L. Heinke, M. Cakici, M. Dommaschk, S. Grosjean, R. Herges, S. Bräse, and C. Wöll, "Photoswitching in two-component surface-mounted metal–organic frameworks: Optically triggered release from a molecular container," ACS Nano **8**, 1463 (2014).
[64]W. Guo, M. Zha, Z. Wang, E. Redel, Z. Xu, and C. Wöll, "Improving the loading capacity of metal–organic framework thin films using optimized linkers," ACS Appl. Mater. Interfaces **8**, 24699 (2016).
[65]K. Müller, A. Knebel, F. Zhao, D. Bléger, J. Caro, and L. Heinke, "Switching thin films of azobenzene-containing metal–organic frameworks with visible light," Chem. Eur. J. **23**, 5434 (2017).
[66]Z. Wang, A. Knebel, S. Grosjean, D. Wagner, S. Bräse, C. Wöll, J. Caro, and L. Heinke, "Tunable molecular separation by nanoporous membranes," Nat. Commun. **7**(1), 13872 (2016).
[67]X. Yu, Z. Wang, M. Buchholz, N. Füllgrabe, S. Grosjean, F. Bebensee, S. Bräse, C. Wöll, and L. Heinke, "cis-to-trans isomerization of azobenzene investigated by using thin films of metal–organic frameworks," Phys. Chem. Chem. Phys. **17**, 22721 (2015).
[68]B. D. McCarthy, T. Liseev, A. M. Beiler, K. L. Materna, and S. Ott, "Facile orientational control of M_2L_2P SURMOFs on ⟨100⟩ silicon substrates and growth mechanism insights for defective MOFs," ACS Appl. Mater. Interfaces **11**, 38294 (2019).
[69]X.-J. Yu, Y.-M. Xian, C. Wang, H.-L. Mao, M. Kind, T. Abu-Husein, Z. Chen, S.-B. Zhu, B. Ren, A. Terfort, and J.-L. Zhuang, "Liquid-phase epitaxial growth of highly oriented and multivariate surface-attached metal–organic frameworks," J. Am. Chem. Soc. **141**, 18984 (2019).
[70]A. Chandresh, X. Liu, C. Wöll, and L. Heinke, "Programmed molecular assembly of abrupt crystalline organic/organic heterointerfaces yielding metal-organic framework diodes with large on-off ratios," Adv. Sci. **8**, 2001884 (2021).
[71]X. Li, C. Jiang, Y. Yao, Q. Zhang, S. Dai, Y. Ying, and J. Ping, "Growth-controllable triboelectric nanogenerator based on surface-attached metal-organic framework layer on living leaf," Small **17**, 2103430 (2021).
[72]J. Liu, B. Lukose, O. Shekhah, H. K. Arslan, P. Weidler, H. Gliemann, S. Bräse, S. Grosjean, A. Godt, X. Feng, K. Mullen, I.-B. Magdau, T. Heine, and C. Wöll, "A novel series of isoreticular metal organic frameworks: Realizing metastable structures by liquid phase epitaxy," Sci. Rep. **2**, 921 (2012).
[73]R. Haldar, B. Sen, S. Hurrle, T. Kitao, R. Sankhla, B. Kühl, A. Welle, S. Heissler, G. Brenner-Weiß, P. Thissen, T. Uemura, H. Gliemann, C. Barner-Kowollik, and C. Wöll, "Oxidative polymerization of terthiophene and a substituted thiophene monomer in metal-organic framework thin films," Eur. Polym. J. **109**, 162 (2018).
[74]A. B. Kanj, J. Bürck, S. Grosjean, S. Bräse, and L. Heinke, "Switching the enantioselectivity of nanoporous host materials by light," Chem. Commun. **55**, 8776 (2019).
[75]S. Okur, P. Qin, A. Chandresh, C. Li, Z. Zhang, U. Lemmer, and L. Heinke, "An enantioselective e-nose: An array of nanoporous homochiral MOF films for stereospecific sensing of chiral odors," Angew. Chem. Int. Ed. **60**, 3566 (2021).
[76]Z. Gu, J. Bürck, A. Bihlmeier, J. Liu, O. Shekhah, P. G. Weidler, C. Azucena, Z. Wang, S. Heissler, H. Gliemann, W. Klopper, A. S. Ulrich, and C. Wöll, "Oriented circular dichroism analysis of chiral surface-anchored metal–organic frameworks grown by liquid-phase epitaxy and upon loading with chiral guest compounds," Chem. Eur. J. **20**, 9879 (2014).
[77]Z. Wang, K. Müller, M. Valášek, S. Grosjean, S. Bräse, C. Wöll, M. Mayor, and L. Heinke, "Series of photoswitchable azobenzene-containing metal–organic frameworks with variable adsorption switching effect," J. Phys. Chem. C **122**, 19044 (2018).
[78]A. B. Kanj, A. Chandresh, A. Gerwien, S. Grosjean, S. Bräse, Y. Wang, H. Dube, and L. Heinke, "Proton-conduction photomodulation in spiropyran-functionalized MOFs with large on–off ratio," Chem. Sci. **11**, 1404 (2020).
[79]K. Müller, J. Helfferich, F. Zhao, R. Verma, A. B. Kanj, V. Meded, D. Bléger, W. Wenzel, and L. Heinke, "Switching the proton conduction in nanoporous, crystalline materials by light," Adv. Mater. **30**, 1706551 (2018).

[80]Z. Zhang, K. Müller, S. Heidrich, M. Koenig, T. Hashem, T. Schlöder, D. Bleger, W. Wenzel, and L. Heinke, "Light-switchable one-dimensional photonic crystals based on MOFs with photomodulatable refractive index," J. Phys. Chem. Lett. **10**, 6626 (2019).
[81]P. Qin, S. Okur, C. Li, A. Chandresh, D. Mutruc, S. Hecht, and L. Heinke, "A photoprogrammable electronic nose with switchable selectivity for VOCs using MOF films," Chem. Sci. **12**, 15700 (2021).
[82]J.-L. Zhuang, M. Kind, C. M. Grytz, F. Farr, M. Diefenbach, S. Tussupbayev, M. C. Holthausen, and A. Terfort, "Insight into the oriented growth of surface-attached metal–organic frameworks: Surface functionality, deposition temperature, and first layer order," J. Am. Chem. Soc. **137**, 8237 (2015).
[83]Q. Li, J. Gies, X. Yu, Y. Gu, A. Terfort, and M. Kind, "Concentration-dependent seeding as a strategy for fabrication of densely packed surface-mounted metal–organic frameworks (SURMOF) layers," Chem. Eur. J. **26**, 5185 (2020).
[84]O. Lugier, U. Pokharel, and S. Castellanos, "Impact of synthetic conditions on the morphology and crystallinity of FDMOF-1 (Cu) thin films," Cryst. Growth Des. **20**, 5302 (2020).
[85]J. Liu, O. Shekhah, X. Stammer, H. K. Arslan, B. Liu, B. Schüpbach, A. Terfort, and C. Wöll, "Deposition of metal-organic frameworks by liquid-phase epitaxy: The influence of substrate functional group density on film orientation," Materials **5**, 1581 (2012).
[86]B. Liu, M. Tu, D. Zacher, and R. A. Fischer, "Multi variant surface mounted metal–organic frameworks," Adv. Funct. Mater. **23**, 3790 (2013).
[87]M. Tu, S. Wannapaiboon, and R. A. Fischer, "Programmed functionalization of SURMOFs via liquid phase heteroepitaxial growth and post-synthetic modification," Dalton Trans. **42**, 16029 (2013).
[88]M. Yao, X. Lv, Z. Fu, W. Li, W. Deng, G. Wu, and G. Xu, "Layer-by-layer assembled conductive metal–organic framework nanofilms for room-temperature chemiresistive sensing," Angew. Chem. Int. Ed. **56**, 16510 (2017).
[89]Y. Lin, W. Li, Y. Wen, G. Wang, X. Ye, and G. Xu, "Layer-by-layer growth of preferred-oriented MOF thin film on nanowire array for high-performance chemiresistive sensing," Angew. Chem. Int. Ed. **60**, 25758 (2021).
[90]R. Zheng, Z. Fu, W. Deng, Y. Wen, A. Wu, X. Ye, and G. Xu, "The growth mechanism of a conductive MOF thin film in spray-based layer-by-layer liquid phase epitaxy," Angew. Chem. Int. Ed. **61**, e202212797 (2022).
[91]S. Schmitt, M. Silvestre, M. Tsotsalas, A.-L. Winkler, A. Shahnas, S. Grosjean, F. Laye, H. Gliemann, J. Lahann, S. Bräse, M. Franzreb, and C. Wöll, "Hierarchically functionalized magnetic core/multishell particles and their postsynthetic conversion to polymer capsules," ACS Nano **9**, 4219 (2015).
[92]O. Shekhah, H. Wang, M. Paradinas, C. Ocal, B. Schüpbach, A. Terfort, D. Zacher, R. A. Fischer, and C. Wöll, "Controlling interpenetration in metal–organic frameworks by liquid-phase epitaxy," Nat. Mater. **8**, 481 (2009).
[93]O. Shekhah, "Layer-by-layer method for the synthesis and growth of surface mounted metal-organic frameworks (SURMOFs)," Materials **3**, 1302 (2010).
[94]A. Dragässer, O. Shekhah, O. Zybaylo, C. Shen, M. Buck, C. Wöll, and D. Schlettwein, "Redox mediation enabled by immobilised centres in the pores of a metal–organic framework grown by liquid phase epitaxy," Chem. Commun. **48**, 663 (2012).
[95]H. C. Streit, M. Adlung, O. Shekhah, X. Stammer, H. K. Arslan, O. Zybaylo, T. Ladnorg, H. Gliemann, M. Franzreb, C. Wöll, and C. Wickleder, "Surface-anchored MOF-based photonic antennae," ChemPhysChem **13**, 2699 (2012).
[96]P. St. Petkov, G. N. Vayssilov, J. Liu, O. Shekhah, Y. Wang, C. Wöll, and T. Heine, "Defects in MOFs: A thorough characterization," ChemPhysChem **13**, 2025 (2012).
[97]W. Guo, J. Liu, P. G. Weidler, J. Liu, T. Neumann, D. Danilov, W. Wenzel, C. Feldmann, and C. Wöll, "Loading of ionic compounds into metal–organic frameworks: A joint theoretical and experimental study for the case of La^{3+}," Phys. Chem. Chem. Phys. **16**, 17918 (2014).
[98]J. P. Best, J. Michler, J. Liu, Z. Wang, M. Tsotsalas, X. Maeder, S. Röse, V. Oberst, J. Liu, S. Walheim, H. Gliemann, P. G. Weidler, E. Redel, and C. Wöll, "Nanomechanical investigation of thin-film electroceramic/metal-organic framework multilayers," Appl. Phys. Lett. **107**, 101902 (2015).
[99]J. Liu, E. Redel, S. Walheim, Z. Wang, V. Oberst, J. Liu, S. Heissler, A. Welle, M. Moosmann, T. Scherer, M. Bruns, H. Gliemann, and C. Wöll, "Monolithic high performance surface anchored metal-organic framework Bragg reflector for optical sensing," Chem. Mater. **27**, 1991 (2015).
[100]J. Liu, T. Wächter, A. Irmler, P. G. Weidler, H. Gliemann, F. Pauly, V. Mugnaini, M. Zharnikov, and C. Wöll, "Electric transport properties of surface-anchored metal–organic frameworks and the effect of ferrocene loading," ACS Appl. Mater. Interfaces **7**, 9824 (2015).
[101]Z. Wang, P. G. Weidler, C. Azucena, L. Heinke, and C. Wöll, "Negative, anisotropic thermal expansion in monolithic thin films of crystalline metal-organic frameworks," Microporous Mesoporous Mater. **222**, 241 (2016).
[102]Z. Wang, D. Nminibapiel, P. Shrestha, J. Liu, W. Guo, P. G. Weidler, H. Baumgart, C. Wöll, and E. Redel, "Resistive switching nanodevices based on metal–organic frameworks," ChemNanoMat **2**, 67 (2016).
[103]W. Guo, Z. Chen, C. Yang, T. Neumann, C. Kübel, W. Wenzel, A. Welle, W. Pfleging, O. Shekhah, C. Wöll, and E. Redel, "Bi_2O_3 nanoparticles encapsulated in surface mounted metal–organic framework thin films," Nanoscale **8**, 6468 (2016).
[104]K. Müller, K. Fink, L. Schöttner, M. Koenig, L. Heinke, and C. Wöll, "Defects as color centers: The apparent color of metal–organic frameworks containing Cu^{2+}-based paddle-wheel units," ACS Appl. Mater. Interfaces **9**, 37463 (2017).
[105]L. J. Brower, L. K. Gentry, A. L. Napier, and M. E. Anderson, "Tailoring the nanoscale morphology of HKUST-1 thin films via codeposition and seeded growth," Beilstein J. Nanotechnol. **8**, 2307 (2017).
[106]Z.-G. Gu, S.-C. Chen, W.-Q. Fu, Q. Zheng, and J. Zhang, "Epitaxial growth of MOF thin film for modifying the dielectric layer in organic field-effect transistors," ACS Appl. Mater. Interfaces **9**, 7259 (2017).
[107]Z.-G. Gu, D.-X. Zhang, W.-Q. Fu, Z.-H. Fu, M. I. Vohra, L. Zhang, C. Wöll, and J. Zhang, "Facile synthesis of metal-loaded porous carbon thin films via carbonization of surface-mounted metal–organic frameworks," Inorg. Chem. **56**, 3526 (2017).
[108]K. Müller, J. Wadhwa, J. S. Malhi, L. Schöttner, A. Welle, H. Schwartz, D. Hermann, U. Ruschewitz, and L. Heinke, "Photoswitchable nanoporous films by loading azobenzene in metal–organic frameworks of type HKUST-1," Chem. Commun. **53**, 8070 (2017).
[109]X. Chen, Z. Wang, Z. M. Hassan, P. Lin, K. Zhang, H. Baumgart, and E. Redel, "Seebeck coefficient measurements of polycrystalline and highly ordered metal-organic framework thin films," ECS J. Solid State Sci. Technol. **6**, 150 (2017).
[110]H. Yoo, A. Welle, W. Guo, J. Choi, and E. Redel, "Electrodeposition of WO_3 nanoparticles into surface mounted metal–organic framework HKUST-1 thin films," Nanotechnology **28**, 115605 (2017).
[111]S. Hurrle, S. Friebe, J. Wohlgemuth, C. Wöll, J. Caro, and L. Heinke, "Sprayable, large-area metal–organic framework films and membranes of varying thickness," Chem. Eur. J. **23**, 2294 (2017).
[112]M. Saghanejhadtehrani, E. K. Schneider, and L. Heinke, "Multi-component uptake of dye molecules by films of nanoporous metal–organic frameworks," ChemPhysChem **18**, 3548 (2017).
[113]Z.-G. Gu, W.-Q. Fu, M. Liu, and J. Zhang, "Surface-mounted MOF templated fabrication of homochiral polymer thin film for enantioselective adsorption of drugs," Chem. Commun. **53**, 1470 (2017).
[114]B. H. Bowser, L. J. Brower, M. L. Ohnsorg, L. K. Gentry, C. K. Beaudoin, and M. E. Anderson, "Comparison of surface-bound and free-standing variations of HKUST-1 MOFs: Effect of activation and ammonia exposure on morphology, crystallinity, and composition," Nanomaterials **8**, 650 (2018).
[115]G. Delen, Z. Ristanović, L. D. Mandemaker, and B. M. Weckhuysen, "Mechanistic insights into growth of surface-mounted metal-organic framework films resolved by infrared (nano-) spectroscopy," Chem. Eur. J. **24**, 187 (2018).
[116]R. P. Brand, L. D. Mandemaker, G. Delen, N. Rijnveld, and B. M. Weckhuysen, "Behavior of a metal organic framework thin-film at elevated temperature and pressure as studied with an autoclave-inserted atomic force microscope," ChemPhysChem **19**, 2397 (2018).
[117]H. Chen, Z.-G. Gu, S. Mirza, S.-H. Zhang, and J. Zhang, "Hollow Cu–TiO_2/C nanospheres derived from a Ti precursor encapsulated MOF coating for efficient photocatalytic hydrogen evolution," J. Mater. Chem. A **6**, 7175 (2018).
[118]G. Bolla and A. S. Myerson, "SURMOF induced morphological crystal engineering of substituted benzamides," Cryst. Growth Des. **18**, 7048 (2018).

[119]G. Bolla and A. S. Myerson, "SURMOF induced polymorphism and crystal morphological engineering of acetaminophen polymorphs: Advantage of heterogeneous nucleation," CrystEngComm **20**, 2084 (2018).
[120]Q. Zhao, Y. Fan, Y. Zhang, J. Liu, W. Li, and Y. Weng, "Copper-based SURMOFs for nitric oxide generation: Hemocompatibility, vascular cell growth, and tissue response," ACS Appl. Mater. Interfaces **11**, 7872 (2019).
[121]A. B. Kanj, R. Verma, M. Liu, J. Helfferich, W. Wenzel, and L. Heinke, "Bunching and immobilization of ionic liquids in nanoporous metal–organic framework," Nano Lett. **19**, 2114 (2019).
[122]T. P. Vello, M. Strauss, C. A. R. Costa, C. C. Corrêa, and C. C. B. Bufon, "Deterministic control of surface mounted metal–organic framework growth orientation on metallic and insulating surfaces," Phys. Chem. Chem. Phys. **22**, 5839 (2020).
[123]L. D. Mandemaker, M. Rivera-Torrente, G. Delen, J. P. Hofmann, M. Lorenz, A. Belianinov, and B. M. Weckhuysen, "Nanoweb surface-mounted metal–organic framework films with tunable amounts of acid sites as tailored catalysts," Chem. Eur. J. **26**, 691 (2020).
[124]X.-J. Yu, H. Zhong, Y.-M. Xian, Z.-P. Wang, S. Schneider, J. Scherr, T. Abu-Husein, Z. Zhang, and A. Terfort, "Highly oriented and polyoxometalate-incorporating surface-attached metal–organic frameworks for efficient dye adsorption and water oxidation," Dalton Trans. **49**, 16627 (2020).
[125]L. G. Albano, T. P. Vello, D. H. de Camargo, R. M. da Silva, A. C. Padilha, A. Fazzio, and C. C. Bufon, "Ambipolar resistive switching in an ultrathin surface-supported metal–organic framework vertical heterojunction," Nano Lett. **20**, 1080 (2020).
[126]H. Ohara, S. Yamamoto, D. Kuzuhara, T. Koganezawa, H. Oikawa, and M. Mitsuishi, "Layer-by-layer growth control of metal–organic framework thin films assembled on polymer films," ACS Appl. Mater. Interfaces **12**, 50784 (2020).
[127]L. D. Mandemaker, M. Rivera-Torrente, R. Geitner, C. M. Vis, and B. M. Weckhuysen, "In situ spectroscopy of calcium fluoride anchored metal–organic framework thin films during gas sorption," Angew. Chem. Int. Ed. **59**, 19545 (2020).
[128]Z. Wang, S. Henke, M. Paulus, A. Welle, Z. Fan, K. Rodewald, B. Rieger, and R. A. Fischer, "Defect creation in surface-mounted metal–organic framework thin films," ACS Appl. Mater. Interfaces **12**, 2655 (2020).
[129]O. Lugier, N. Thakur, L. Wu, M. Vockenhuber, Y. Ekinci, and S. Castellanos, "Bottom-up nanofabrication with extreme-ultraviolet light: Metal–organic frameworks on patterned monolayers," ACS Appl. Mater. Interfaces **13**, 43777 (2021).
[130]L. G. Albano, D. H. de Camargo, G. R. Schleder, S. G. Deeke, T. P. Vello, L. D. Palermo, C. C. Corrêa, A. Fazzio, C. Wöll, and C. C. Bufon, "Room-temperature negative differential resistance in surface-supported metal-organic framework vertical heterojunctions," Small **17**, 2101475 (2021).
[131]A. Oliveira, J. Ribeiro, D. Vasconcelos, P. Weidler, and W. Vasconcelos, "Room temperature and ambient pressure deposition of Cu-BTC MOF on SBA-15 functionalized silica supports by simple spray layer-by-layer method," Mater. Today Commun. **27**, 102388 (2021).
[132]T. Koehler, I. Strauss, A. Mundstock, J. Caro, and F. Marlow, "Reversible photoalignment of azobenzene in the SURMOF HKUST-1," J. Phys. Chem. Lett. **12**, 8903 (2021).
[133]W. Li, G. Yang, A. Terzis, S. Mukherjee, C. He, X. An, J. Wu, B. Weigand, and R. A. Fischer, "In situ tracking of wetting-front transient heat release on a surface-mounted metal–organic framework," Adv. Mater. **33**, 2006980 (2021).
[134]R. M. da Silva, L. G. Albano, T. P. Vello, W. W. de Araújo, D. H. de Camargo, L. D. Palermo, C. C. Corrêa, C. Wöll, and C. C. Bufon, "Surface-supported metal-organic framework as low-dielectric-constant thin films for novel hybrid electronics," Adv. Electron. Mater. **8**, 2200175 (2022).
[135](a) A. Z. Li, J. Liu, L. Feng, Y. Pan, J. Tang, H. Li, G. Cheng, Z. Li, J. Shi, Y. Xu, and W. Liu, "Monolithic MOF-based metal-insulator-metal resonator for filtering and sensing," Nano Lett. **23**, 637 (2023); (b) Z. Li, J. Liu, X. Yi, W. Wu, F. Liu, Z. Zhu, H. Li, J. Shi, Y. Xu, F. Zhou, and W. Liu, "Metal-organic frameworks-based Fabry—Pérot cavity encapsulated TiO_2 nanoparticles for selective chemical sensing," Adv. Funct. Mater. **32**, 2109541 (2022); (c) Z. Li, J. Liu, H. Wu, J. Tang, Z. Li, Y. Xu, F. Zhou, and W. Liu, "Photonic crystals constructed by isostructural metal-organic framework films," Nano Res. (published online, 2023).
[136]X. Chen, K. Zhang, Z. M. Hassan, E. Redel, and H. Baumgart, "Charge. Transport, conductivity and Seebeck coefficient in pristine and TCNQ loaded preferentially grown metal-organic framework films," J. Phys.: Condens. Matter **34**, 404001 (2022).
[137]M. Tu and R. A. Fischer, "Heteroepitaxial growth of surface mounted metal–organic framework thin films with hybrid adsorption functionality," J. Mater. Chem. A **2**, 2018 (2014).
[138]Z. Wang, S. Wannapaiboon, K. Rodewald, M. Tu, B. Rieger, and R. A. Fischer, "Directing the hetero-growth of lattice-mismatched surface-mounted metal–organic frameworks by functionalizing the interface," J. Mater. Chem. A **6**, 21295 (2018).
[139]E. Redel, Z. Wang, S. Walheim, J. Liu, H. Gliemann, and C. Wöll, "On the dielectric and optical properties of surface-anchored metal-organic frameworks: A study on epitaxially grown thin films," Appl. Phys. Lett. **103**, 091903 (2013).
[140]Z. Wang, S. Wannapaiboon, S. Henke, M. Paulus, K. Rodewald, B. Rieger, and R. A. Fischer, "The synergistic effect of heterostructured dissimilar metal–organic framework thin films on adsorption properties," J. Mater. Chem. A **8**, 12990 (2020).
[141]S. Okur, C. Li, Z. Zhang, S. Vaidurya Pratap, M. Sarheed, A. Kanbar, L. Franke, F. Geislhöringer, L. Heinke, U. Lemmer, P. Nick, and C. Wöll, "Sniff species: SURMOF-based sensor array discriminates aromatic plants beyond the genus level," Chemosensors **9**, 171 (2021).
[142]S. Okur, Z. Zhang, M. Sarheed, P. Nick, U. Lemmer, and L. Heinke, "Towards a MOF e-Nose: A SURMOF sensor array for detection and discrimination of plant oil scents and their mixtures," Sens. Actuators, B **306**, 127502 (2020).
[143]B. Sen, J. C. Santos, R. Haldar, Q. Zhang, T. Hashem, P. Qin, Y. Li, F. Kirschhöfer, G. Brenner-Weiss, H. Gliemann, L. Heinke, C. Barner-Kowollik, A. Knebel, and C. Wöll, "Introducing electrical conductivity to metal–organic framework thin films by templated polymerization of methyl propiolate," Nanoscale **12**, 24419 (2020).
[144]Z. Wang, K. Rodewald, R. Medishetty, B. Rieger, and R. A. Fischer, "Control of water content for enhancing the quality of copper paddle-wheel-based metal–organic framework thin films grown by layer-by-layer liquid-phase epitaxy," Cryst. Growth Des. **18**, 7451 (2018).
[145]W. Guo, Z. M. Hassan, C. Kübel, R. Haldar, P. G. Weidler, S. Heissler, K. Peikert, M. Fröba, E. Redel, and C. Wöll, "MOF-templated synthesis of 3D Bi_2O_3 supracrystals with bcc packing," Nanoscale **10**, 17099 (2018).
[146]M. Drost, F. Tu, L. Berger, C. Preischl, W. Zhou, H. Gliemann, C. Wöll, and H. Marbach, "Surface-anchored metal–organic frameworks as versatile resists for gas-assisted e-beam lithography: Fabrication of sub-10 nanometer structures," ACS Nano **12**, 3825 (2018).
[147]G. Delen, M. Monai, F. Meirer, and B. M. Weckhuysen, "In situ nanoscale infrared spectroscopy of water adsorption on nanoislands of surface-anchored metal-organic frameworks," Angew. Chem. Int. Ed. **60**, 1620 (2021).
[148]L.-M. Chang, Q. Li, P. Weidler, Z.-G. Gu, C. Wöll, and J. Zhang, "Surface-oriented assembly of cyclodextrin metal–organic framework film for enhanced peptide-enantiomers sensing," CCS Chem. **4**, 3472 (2022).
[149]J. C. Santos, Y. Pramudya, M. Krstic, D.-H. Chen, B. L. Neumeier, C. Feldmann, W. Wenzel, and E. Redel, "Halogenated terephthalic acid 'antenna effects' in lanthanide-SURMOF thin films," ACS Appl. Mater. Interfaces **12**, 52166 (2020).
[150]D. Chen, R. Haldar, B. L. Neumeier, Z. Fu, C. Feldmann, C. Wöll, and E. Redel, "Tunable emission in heteroepitaxial Ln-SURMOFs," Adv. Funct. Mater. **29**, 1903086 (2019).
[151]D. Chen, A. E. Sedykh, G. E. Gomez, B. L. Neumeier, J. C. Santos, V. Gvilava, R. Maile, C. Feldmann, C. Wöll, C. Janiak, K. Müller-Buschbaum, and E. Redel, "SURMOF devices based on heteroepitaxial architectures with white-light emission and luminescent thermal-dependent performance," Adv. Mater. Interfaces **7**, 2000929 (2020).
[152]B. H. Monjezi, S. Okur, R. Limbach, A. Chandresh, K. Sen, T. Hashem, M. Schwotzer, L. Wondraczek, C. Wöll, and A. Knebel, "Fast dynamic synthesis of MIL-68(In) thin films in high optical quality for optical cavity sensing," ChemRxiv
[153]W. Li, S. Watzele, H. A. El-Sayed, Y. Liang, G. Kieslich, A. S. Bandarenka, K. Rodewald, B. Rieger, and R. A. Fischer, "Unprecedented high oxygen

evolution activity of electrocatalysts derived from surface-mounted metal–organic frameworks," J. Am. Chem. Soc. **141**, 5926 (2019).
[154]W. Li, S. Xue, S. Watzele, S. Hou, J. Fichtner, A. L. Semrau, L. Zhou, A. Welle, A. S. Bandarenka, and R. A. Fischer, "Advanced bifunctional oxygen reduction and evolution electrocatalyst derived from surface-mounted metal–organic frameworks," Angew. Chem. Int. Ed. **59**, 5837 (2020).
[155]S. Hou, L. Xu, X. Ding, R. M. Kluge, T. K. Sarpey, R. W. Haid, B. Garlyyev, S. Mukherjee, J. Warnan, M. Koch, S. Zhang, W. Li, A. S. Bandarenka, and R. A. Fischer, "Dual in situ laser techniques underpin the role of cations in impacting electrocatalysts," Angew. Chem. Int. Ed. **61**, e202201610 (2022).
[156]S. Hou, W. Li, S. Watzele, R. M. Kluge, S. Xue, S. Yin, X. Jiang, M. Döblinger, A. Welle, B. Garlyyev, M. Koch, P. Müller-Buschbaum, C. Wöll, A. S. Bandarenka, and R. A. Fischer, "Metamorphosis of heterostructured surface-mounted metal–organic frameworks yielding record oxygen evolution mass activities," Adv. Mater. **33**, 2103218 (2021).
[157]Y. Xiao, P. Weidler, S. Lin, C. Wöll, Z. Gu, and J. Zhang, "Chiral metal–organic cluster induced high circularly polarized luminescence of metal–organic framework thin film," Adv. Funct. Mater. **32**, 2204289 (2022).
[158]T. Hashem, E. P. Valadez Sánchez, P. G. Weidler, H. Gliemann, M. H. Alkordi, and C. Wöll, "Liquid-phase quasi-epitaxial growth of highly stable, monolithic UiO-66-NH_2 MOF thin films on solid substrates," ChemistryOpen **9**, 524 (2020).
[159]T. Hashem, E. P. V. Sanchez, E. Bogdanova, A. Ugodchikova, A. Mohamed, M. Schwotzer, M. H. Alkordi, and C. Wöll, "Stability of monolithic mof thin films in acidic and alkaline aqueous media," Membranes **11**, 207 (2021).
[160]A. Micero, T. Hashem, H. Gliemann, and A. Léon, "Hydrogen separation performance of UiO-66-NH_2 membranes grown via liquid-phase epitaxy layer-by-layer deposition and one-pot synthesis," Membranes **11**, 735 (2021).
[161]A. L. Semrau and R. A. Fischer, "High-quality thin films of UiO-66-NH_2 by coordination modulated layer-by-layer liquid phase epitaxy," Chem. Eur. J. **27**, 8509 (2021).
[162]A. L. Semrau, S. Wannapaiboon, S. P. Pujari, P. Vervoorts, B. Albada, H. Zuilhof, and R. A. Fischer, "Highly porous nanocrystalline UiO-66 thin films via coordination modulation controlled step-by-step liquid-phase growth," Cryst. Growth Des. **19**, 1738 (2019).
[163]E. P. Valadez Sánchez, H. Gliemann, K. Haas-Santo, C. Wöll, and R. Dittmeyer, "ZIF-8 SURMOF membranes synthesized by Au-assisted liquid phase epitaxy for application in gas separation," Chem. Ing. Tech. **88**, 1798 (2016).
[164]E. P. V. Sanchez, H. Gliemann, K. Haas-Santo, W. Ding, E. Hansjosten, J. Wohlgemuth, C. Wöll, and R. Dittmeyer, "α-Al_2O_3-supported ZIF-8 SURMOF membranes: Diffusion mechanism of ethene/ethane mixtures and gas separation performance," J. Membr. Sci. **594**, 117421 (2020).
[165]B. M. Weckhuysen, Z. Öztürk, R. P. Brand, J. M. Boereboom, and F. Meirer, "Vibrational fingerprinting of defects sites in thin films of zeolitic imidazolate frameworks," Chem. Eur. J. **25**, 8070 (2019).
[166]E. P. Valadez Sánchez, A. Knebel, L. Izquierdo Sánchez, M. Klumpp, C. Wöll, and R. Dittmeyer, "Studying ZIF-8 SURMOF thin films with a langatate crystal microbalance: Single-component gas adsorption isotherms measured at elevated temperatures and pressures," Langmuir **36**, 8444 (2020).
[167]L. Ye, J. Liu, Y. Gao, C. Gong, M. Addicoat, T. Heine, C. Wöll, and L. Sun, "Highly oriented MOF thin film-based electrocatalytic device for the reduction of CO_2 to CO exhibiting high faradaic efficiency," J. Mater. Chem. A **4**, 15320 (2016).
[168]S. Ahmad, J. Liu, C. Gong, J. Zhao, and L. Sun, "Photon up-conversion via epitaxial surface-supported metal–organic framework thin films with enhanced photocurrent," ACS Appl. Energy Mater. **1**, 249 (2018).
[169]S. Ahmad, J. Liu, W. Ji, and L. Sun, "Metal–organic framework thin film-based dye sensitized solar cells with enhanced photocurrent," Materials **11**, 1868 (2018).
[170]M. Kozlowska, Y. Pramudya, M. Jakoby, S. Heidrich, L. Pan, B. S. Richards, I. A. Howard, C. Wöll, R. Haldar, and W. Wenzel, "Crystalline assembly of perylene in metal–organic framework thin film: J-aggregate or excimer? Insight into the electronic structure," J. Phys.: Condens. Matter **33**, 034001 (2021).
[171]W. Zhou, S. Begum, Z. Wang, P. Krolla, D. Wagner, S. Bräse, C. Wöll, and M. Tsotsalas, "High antimicrobial activity of metal–organic framework-templated porphyrin polymer thin films," ACS Appl. Mater. Interfaces **10**, 1528 (2018).
[172]S. Begum, T. Hashem, M. Tsotsalas, C. Wöll, and M. H. Alkordi, "Electrolytic conversion of sacrificial metal–organic framework thin films into an electrocatalytically active monolithic oxide coating for the oxygen-evolution reaction," Energy Technol. **7**, 1900967 (2019).
[173]M. Oldenburg, A. Turshatov, D. Busko, M. Jakoby, R. Haldar, K. Chen, G. Emandi, M. Senge, C. Wöll, J. Hodgkiss, B. S. Richards, and I. A. Howard, "Enhancing the photoluminescence of surface anchored metal–organic frameworks: Mixed linkers and efficient acceptors," Phys. Chem. Chem. Phys. **20**, 11564 (2018).
[174]A. Windischbacher, L. Steiner, R. Haldar, C. Wöll, E. Zojer, and A.-M. Kelterer, "Exciton coupling and conformational changes impacting the excited state properties of metal organic frameworks," Molecules **25**, 4230 (2020).
[175]M. Oldenburg, A. Turshatov, D. Busko, S. Wollgarten, M. Adams, N. Baroni, A. Welle, E. Redel, C. Wöll, B. S. Richards, and I. A. Howard, "Photon upconversion at crystalline organic–organic heterojunctions," Adv. Mater. **28**, 8477 (2016).
[176]Z. Wang, A. Błaszczyk, O. Fuhr, S. Heissler, C. Wöll, and M. Mayor, "Molecular weaving via surface-templated epitaxy of crystalline coordination networks," Nat. Commun. **8**, 14442 (2017).
[177]S. Schmitt, S. Diring, P. G. Weidler, S. Begum, S. Heißler, S. Kitagawa, C. Wöll, S. Furukawa, and M. Tsotsalas, "Localized conversion of metal–organic frameworks into polymer gels via light-induced click chemistry," Chem. Mater. **29**, 5982 (2017).
[178]Z. M. Hassan, P. G. Weidler, A. Nefedov, Y. Luo, S. Heißler, M. Tsotsalas, R. Haldar, and C. Wöll, "Spectroscopic investigation of bianthryl-based metal–organic framework thin films and their photoinduced topotactic transformation," Adv. Mater. Interfaces **9**, 2102441 (2022).
[179]R. Haldar, A. Mazel, R. Joseph, M. Adams, I. A. Howard, B. S. Richards, M. Tsotsalas, E. Redel, S. Diring, F. Odobel, and C. Wöll, "Excitonically coupled states in crystalline coordination networks," Chem. Eur. J. **23**, 14316 (2017).
[180]R. Haldar, A. Mazel, M. Krstić, Q. Zhang, M. Jakoby, I. A. Howard, B. S. Richards, N. Jung, D. Jacquemin, S. Diring, W. Wenzel, F. Odobel, and C. Wöll, "A de novo strategy for predictive crystal engineering to tune excitonic coupling," Nat. Commun. **10**, 2048 (2019).
[181]R. Haldar, H. Chen, A. Mazel, D. Chen, G. Gupta, N. Dua, S. Diring, F. Odobel, and C. Wöll, "Antenna doping: The key for achieving efficient optical wavelength conversion in crystalline chromophoric heterolayers," Adv. Mater. Interfaces **8**, 2100262 (2021).
[182]X. Liu, A. Mazel, S. Marschner, Z. Fu, M. Muth, F. Kirschhöfer, G. Brenner-Weiss, S. Bräse, S. Diring, F. Odobel, R. Haldar, and C. Wöll, "Photoinduced delamination of metal–organic framework thin films by spatioselective generation of reactive oxygen species," ACS Appl. Mater. Interfaces **13**, 57768 (2021).
[183]R. Haldar, M. Jakoby, M. Kozlowska, M. Rahman Khan, H. Chen, Y. Pramudya, B. S. Richards, L. Heinke, W. Wenzel, F. Odobel, S. Diring, I. A. Howard, U. Lemmer, and C. Wöll, "Tuning optical properties by controlled aggregation: Electroluminescence assisted by thermally-activated delayed fluorescence from thin films of crystalline chromophores," Chem. Eur. J. **26**, 17016 (2020).
[184]Z. Wang, J. Liu, S. Grosjean, D. Wagner, W. Guo, Z. Gu, L. Heinke, H. Gliemann, S. Bräse, and C. Wöll, "Monolithic, crystalline MOF coating: An excellent patterning and photoresist material," ChemNanoMat **1**, 338 (2015).
[185]R. Haldar, K. Batra, S. M. Marschner, A. B. Kuc, S. Zahn, R. A. Fischer, S. Bräse, T. Heine, and C. Wöll, "Bridging the green gap: Metal–organic framework heteromultilayers assembled from porphyrinic linkers identified by using computational screening," Chem. Eur. J. **25**, 7847 (2019).
[186]I. N. Meshkov, A. I. Zvyagina, A. A. Shiryaev, M. S. Nickolsky, A. E. Baranchikov, A. A. Ezhov, A. G. Nugmanova, Y. Y. Enakieva, Y. G. Gorbunova, V. V. Arslanov, and M. A. Kalinina, "Understanding self-assembly of porphyrin-based SURMOFs: How layered minerals can be useful," Langmuir **34**, 5184 (2018).
[187]S. Goswami, M. Chen, M. R. Wasielewski, O. K. Farha, and J. T. Hupp, "Boosting transport distances for molecular excitons within photoexcited metal–organic framework films," ACS Appl. Mater. Interfaces **10**, 34409 (2018).
[188]Y. Wang, S. Chen, R. Haldar, C. Wöll, Z. Gu, and J. Zhang, "van der Waals epitaxial growth of 2D metal–porphyrin framework derived thin films for dye-sensitized solar cells," Adv. Mater. Interfaces **5**, 1800985 (2018).

[189]A. Kutenina, A. Zvyagina, O. Raitman, Y. Enakieva, and M. Kalinina, "Layer-by-layer assembly of SAM-supported porphyrin-based metal organic frameworks for molecular recognition," Colloid J. **81**, 401 (2019).
[190]R. Haldar, S. Diring, P. K. Samanta, M. Muth, W. Clancy, A. Mazel, S. Schlabach, F. Kirschhöfer, G. Brenner-Weiß, S. K. Pati, F. Odobel, and C. Wöll, "Enhancing selectivity and kinetics in oxidative photocyclization by supramolecular control," Angew. Chem. Int. Ed. **57**, 13662 (2018).
[191]M. Adams, N. Baroni, M. Oldenburg, F. Kraffert, J. Behrends, R. W. MacQueen, R. Haldar, D. Busko, A. Turshatov, G. Emandi, M. O. Senge, C. Wöll, K. Lips, B. S. Richards, and I. A. Howard, "Reaction of porphyrin-based surface-anchored metal–organic frameworks caused by prolonged illumination," Phys. Chem. Chem. Phys. **20**, 29142 (2018).
[192]M. Adams, M. Kozlowska, N. Baroni, M. Oldenburg, R. Ma, D. Busko, A. Turshatov, G. Emandi, M. O. Senge, R. Haldar, C. Wöll, G. U. Nienhaus, B. S. Richards, and I. A. Howard, "Highly efficient one-dimensional triplet exciton transport in a palladium–porphyrin-based surface-anchored metal–organic framework," ACS Appl. Mater. Interfaces **11**, 15688 (2019).
[193]X. Li, C. Gong, G. G. Gurzadyan, M. F. Gelin, J. Liu, and L. Sun, "Ultrafast relaxation dynamics in zinc tetraphenylporphyrin surface-mounted metal organic framework," J. Phys. Chem. C **122**, 50 (2018).
[194]X. Li, G. G. Gurzadyan, M. F. Gelin, W. Domcke, C. Gong, J. Liu, and L. Sun, "Enhanced S_2 fluorescence from a free-base tetraphenylporphyrin surface-mounted metal organic framework," J. Phys. Chem. C **122**, 23321 (2018).
[195]B. Liu, O. Shekhah, H. K. Arslan, J. Liu, C. Wöll, and R. A. Fischer, "Enantiopure metal–organic framework thin films: Oriented SURMOF growth and enantioselective adsorption," Angew. Chem. Int. Ed. **51**, 807 (2012).
[196]N. Baroni, A. Turshatov, M. Oldenburg, D. Busko, M. Adams, R. Haldar, A. Welle, E. Redel, C. Wöll, B. S. Richards, and I. A. Howard, "Facile loading of thin-film surface-anchored metal-organic frameworks with Lewis-base guest molecules," Mater. Chem. Front. **1**, 1888 (2017).
[197]N. Baroni, A. Turshatov, M. Adams, E. A. Dolgopolova, S. Schlisske, G. Hernandez-Sosa, C. Wöll, N. B. Shustova, B. S. Richards, and I. A. Howard, "Inkjet-printed photoluminescent patterns of aggregation-induced-emission chromophores on surface-anchored metal–organic frameworks," ACS Appl. Mater. Interfaces **10**, 25754 (2018).
[198]S.-M. Chen, L.-M. Chang, X.-K. Yang, T. Luo, H. Xu, Z.-G. Gu, and J. Zhang, "Liquid-phase epitaxial growth of azapyrene-based chiral metal–organic framework thin films for circularly polarized luminescence," ACS Appl. Mater. Interfaces **11**, 31421 (2019).
[199]Z. Wang, J. Liu, H. K. Arslan, S. Grosjean, T. Hagendorn, H. Gliemann, S. Bräse, and C. Wöll, "Post-synthetic modification of metal–organic framework thin films using click chemistry: The importance of strained C–C triple bonds," Langmuir **29**, 15958 (2013).
[200]A. I. Zvyagina, A. A. Shiryaev, A. E. Baranchikov, V. V. Chernyshev, Y. Y. Enakieva, O. A. Raitman, A. A. Ezhov, IN. Meshkov, D. A. Grishanov, O. S. Ivanova, Y. G. Gorbunova, V. V. Arslanov, and M. A. Kalinina, "Layer-by-layer assembly of porphyrin-based metal–organic frameworks on solids decorated with graphene oxide," New J. Chem. **41**, 948 (2017).
[201]S. Wannapaiboon, M. Tu, and R. A. Fischer, "Liquid phase heteroepitaxial growth of moisture-tolerant MOF-5 isotype thin films and assessment of the sorption properties by quartz crystal microbalance," Adv. Funct. Mater. **24**, 2696 (2014).
[202]H. Kuhn, "Present status and future prospects of Langmuir-Blodgett film research," Thin Solid Films **178**, 1 (1989).
[203]H. Kaur, S. Sundriyal, V. Pachauri, S. Ingebrandt, K.-H. Kim, A. L. Sharma, and A. Deep, "Luminescent metal-organic frameworks and their composites: Potential future materials for organic light emitting displays," Coord. Chem. Rev. **401**, 213077 (2019).
[204]C. Peng, X. Song, J. Yin, G. Zhang, and H. Fei, "Intrinsic white-light-emitting metal–organic frameworks with structurally deformable secondary building units," Angew. Chem. Int. Ed. **58**, 7818 (2019).
[205]H. Yoon, M. Park, J. Kim, T. G. Novak, S. Lee, and S. Jeon, "Toward highly efficient luminescence in graphene quantum dots for optoelectronic applications," Chem. Phys. Rev. **2**, 031303 (2021).
[206]Y. Zheng, F. Sun, X. Han, J. Xu, and X. Bu, "Recent progress in 2D metal-organic frameworks for optical applications," Adv. Opt. Mater. **8**, 2000110 (2020).
[207]T. N. Nguyen, F. M. Ebrahim, and K. C. Stylianou, "Photoluminescent, upconversion luminescent and nonlinear optical metal-organic frameworks: From fundamental photophysics to potential applications," Coord. Chem. Rev. **377**, 259 (2018).
[208]K. C. Stylianou, R. Heck, S. Y. Chong, J. Bacsa, J. T. Jones, Y. Z. Khimyak, D. Bradshaw, and M. J. Rosseinsky, "A guest-responsive fluorescent 3D microporous metal-organic framework derived from a long-lifetime pyrene core," J. Am. Chem. Soc. **132**, 4119 (2010).
[209]D.-H. Chen, L. Lin, T.-L. Sheng, Y.-H. Wen, S.-M. Hu, R.-B. Fu, C. Zhuo, H.-R. Li, and X.-T. Wu, "Syntheses, structures and luminescence properties of five coordination polymers based on designed 2,7-bis (4-benzoic acid)-N-(4-benzoic acid) carbazole," CrystEngComm **19**, 2632 (2017).
[210]H.-Q. Yin, X.-Y. Wang, and X.-B. Yin, "Rotation restricted emission and antenna effect in single metal–organic frameworks," J. Am. Chem. Soc. **141**, 15166 (2019).
[211]D.-H. Chen, L. Lin, T.-L. Sheng, Y.-H. Wen, X.-Q. Zhu, L.-T. Zhang, S.-M. Hu, R.-B. Fu, and X.-T. Wu, "Syntheses, structures, luminescence and magnetic properties of seven isomorphous metal–organic frameworks based on 2,7-bis(4-benzoic acid)-N-(4-benzoic acid)carbazole," New J. Chem. **42**, 2830 (2018).
[212]J. Dong, P. Shen, S. Ying, Z.-J. Li, Y. D. Yuan, Y. Wang, X. Zheng, S. B. Peh, H. Yuan, G. Liu, Y. Cheng, Y. Pan, L. Shi, J. Zhang, D. Yuan, B. Liu, Z. Zhao, B. Z. Tang, and D. Zhao, "Aggregation-induced emission-responsive metal––organic frameworks," Chem. Mater. **32**, 6706 (2020).
[213]Y. Shu, Q. Ye, T. Dai, Q. Xu, and X. Hu, "Encapsulation of luminescent guests to construct luminescent metal–organic frameworks for chemical sensing," ACS Sens. **6**, 641 (2021).
[214]N. J. Hestand and F. C. Spano, "Expanded theory of H-and J-molecular aggregates: The effects of vibronic coupling and intermolecular charge transfer," Chem. Rev. **118**, 7069 (2018).
[215]R. Haldar and C. Wöll, "Hierarchical assemblies of molecular frameworks—MOF-on-MOF epitaxial heterostructures," Nano Res. **14**, 355 (2021).
[216]R. Haldar, M. Jakoby, A. Mazel, Q. Zhang, A. Welle, T. Mohamed, P. Krolla, W. Wenzel, S. Diring, F. Odobel, B. S. Richards, I. A. Howard, and C. Wöll, "Anisotropic energy transfer in crystalline chromophore assemblies," Nat. Commun. **9**, 4332 (2018).
[217]K. Binnemans, "Lanthanide-based luminescent hybrid materials," Chem. Rev. **109**, 4283 (2009).
[218]S. Weissman, "Intramolecular energy transfer the fluorescence of complexes of europium," J. Chem. Phys. **10**, 214 (1942).
[219]M. D. Allendorf, C. A. Bauer, R. Bhakta, and R. Houk, "Luminescent metal–organic frameworks," Chem. Soc. Rev. **38**, 1330 (2009).
[220]K. Liu, X. Zhang, X. Meng, W. Shi, P. Cheng, and A. K. Powell, "Constraining the coordination geometries of lanthanide centers and magnetic building blocks in frameworks: A new strategy for molecular nanomagnets," Chem. Soc. Rev. **45**, 2423 (2016).
[221]A. Karmakar, P. Samanta, S. Dutta, and S. K. Ghosh, "Fluorescent 'Turn-on' sensing based on metal–organic frameworks (MOFs)," Chem. Asian J. **14**, 4506 (2019).
[222]M. Pan, Y. Zhu, K. Wu, L. Chen, Y. Hou, S. Yin, H. Wang, Y. Fan, and C. Su, "Epitaxial growth of hetero-Ln-MOF hierarchical single crystals for domain- and orientation-controlled multicolor luminescence 3D coding capability," Angew. Chem. Int. Ed. **56**, 14582 (2017).
[223]Z. Gao, S. Yang, B. Xu, T. Zhang, S. Chen, W. Zhang, X. Sun, Z. Wang, X. Wang, X. Meng, and Y. S. Zhao, "Laterally engineering lanthanide-MOFs epitaxial heterostructures for spatially resolved planar 2D photonic barcoding," Angew. Chem. Int. Ed. **60**, 24519 (2021).
[224]Z.-G. Gu, Z. Chen, W.-Q. Fu, F. Wang, and J. Zhang, "Liquid-phase epitaxy effective encapsulation of lanthanide coordination compounds into MOF film with homogeneous and tunable white-light emission," ACS Appl. Mater. Interfaces **7**, 28585 (2015).
[225]T. M. Reineke, M. Eddaoudi, M. Fehr, D. Kelley, and O. Yaghi, "From condensed lanthanide coordination solids to microporous frameworks having accessible metal sites," J. Am. Chem. Soc. **121**, 1651 (1999).
[226]B. Zerulla, M. Krstić, D. Beutel, C. Holzer, C. Wöll, C. Rockstuhl, and I. Fernandez-Corbaton, "A multi-scale approach for modeling the optical

response of molecular materials inside cavities," Adv. Mater. **34**, 2200350 (2022).
[227]S. S. Rajasree, X. Li, and P. Deria, "Physical properties of porphyrin-based crystalline metal–organic frameworks," Commun. Chem. **4**, 47 (2021).
[228]J. Chen, Y. Zhu, and S. Kaskel, "Porphyrin-based metal–organic frameworks for biomedical applications," Angew. Chem. Int. Ed. **60**, 5010 (2021).
[229]J. Liu, W. Zhou, J. Liu, I. Howard, G. Kilibarda, S. Schlabach, D. Coupry, M. Addicoat, S. Yoneda, Y. Tsutsui, T. Sakurai, S. Seki, Z. Wang, P. Lindemann, E. Redel, T. Heine, and C. Wöll, "Photoinduced charge-carrier generation in epitaxial MOF thin films: High efficiency as a result of an indirect electronic band gap?," Angew. Chem. Int. Ed. **54**, 7441 (2015).
[230]J. Liu, W. Zhou, J. Liu, Y. Fujimori, T. Higashino, H. Imahori, X. Jiang, J. Zhao, T. Sakurai, Y. Hattori, W. Matsuda, S. Seki, S. K. Garlapati, S. Dasgupta, E. Redel, L. Sun, and C. Wöll, "A new class of epitaxial porphyrin metal– organic framework thin films with extremely high photocarrier generation efficiency: Promising materials for all-solid-state solar cells," J. Mater. Chem. A **4**, 12739 (2016).
[231]E. A. Dolgopolova, A. M. Rice, C. R. Martin, and N. B. Shustova, "Photochemistry and photophysics of MOFs: Steps towards MOF-based sensing enhancements," Chem. Soc. Rev. **47**, 4710 (2018).
[232]S. Goswami, L. Ma, A. B. Martinson, M. R. Wasielewski, O. K. Farha, and J. T. Hupp, "Toward metal–organic framework-based solar cells: Enhancing directional exciton transport by collapsing three-dimensional film structures," ACS Appl. Mater. Interfaces **8**, 30863 (2016).
[233]L. Sun, M. G. Campbell, and M. Dincă, "Electrically conductive porous metal–organic frameworks," Angew. Chem. Int. Ed. **55**, 3566 (2016).
[234]D.-W. Lim and H. Kitagawa, "Rational strategies for proton-conductive metal–organic frameworks," Chem. Soc. Rev. **50**, 6349 (2021).
[235]L. S. Xie, E. V. Alexandrov, G. Skorupskii, D. M. Proserpio, and M. Dincă, "Diverse π–π stacking motifs modulate electrical conductivity in tetrathiafulvalene-based metal–organic frameworks," Chem. Sci. **10**, 8558 (2019).
[236]X. Mu, W. Wang, C. Sun, J. Wang, C. Wang, and M. Knez, "Recent progress on conductive metal-organic framework films," Adv. Mater. Interfaces **8**, 2002151 (2021).
[237]A. A. Talin, A. Centrone, A. C. Ford, M. E. Foster, V. Stavila, P. Haney, R. A. Kinney, V. Szalai, F. E. Gabaly, H. P. Yoon, F. Léonard, and M. D. Allendorf, "Tunable electrical conductivity in metal-organic framework thin-film devices," Science **343**, 66 (2014).
[238]A.-Q. Wu, W.-Q. Wang, H.-B. Zhan, L.-A. Cao, X.-L. Ye, J.-J. Zheng, P. N. Kumar, K. Chiranjeevulu, W.-H. Deng, G.-E. Wang, M. Yao, and G. Xu, "Layer-by-layer assembled dual-ligand conductive MOF nano-films with modulated chemiresistive sensitivity and selectivity," Nano Res. **14**, 438 (2021).
[239]W. Tang, Y. Huang, L. Han, R. Liu, Y. Su, X. Guo, and F. Yan, "Recent progress in printable organic field effect transistors," J. Mater. Chem. C **7**, 790 (2019).
[240]S. Maiti, M. van der Laan, D. Poonia, P. Schall, S. Kinge, and L. D. Siebbeles, "Emergence of new materials for exploiting highly efficient carrier multiplication in photovoltaics," Chem. Phys. Rev. **1**, 011302 (2020).
[241]Z. A. Lamport, H. F. Haneef, S. Anand, M. Waldrip, and O. D. Jurchescu, "Tutorial: Organic field-effect transistors: Materials, structure and operation," J. Appl. Phys. **124**, 071101 (2018).
[242]H. Chen, W. Zhang, M. Li, G. He, and X. Guo, "Interface engineering in organic field-effect transistors: Principles, applications, and perspectives," Chem. Rev. **120**, 2879 (2020).
[243]K. Sun, J. Chen, and X. Yan, "The future of memristors: Materials engineering and neural networks," Adv. Funct. Mater. **31**, 2006773 (2021).
[244]D. B. Strukov, G. S. Snider, D. R. Stewart, and R. S. Williams, "The missing memristor found," Nature **453**, 80 (2008).
[245]Y. Zhang, Z. Wang, J. Zhu, Y. Yang, M. Rao, W. Song, Y. Zhuo, X. Zhang, M. Cui, L. Shen, R. Huang, and J. Yang, "Brain-inspired computing with memristors: Challenges in devices, circuits, and systems," Appl. Phys. Rev. **7**, 011308 (2020).
[246]S. S. Nagarkar, A. V. Desai, and S. K. Ghosh, "Stimulus-responsive metal–organic frameworks," Chem. Asian J. **9**, 2358 (2014).
[247]D.-H. Qu, Q.-C. Wang, Q.-W. Zhang, X. Ma, and H. Tian, "Photoresponsive host–guest functional systems," Chem. Rev. **115**, 7543 (2015).
[248]G. S. Kumar and Q. Lin, "Light-triggered click chemistry," Chem. Rev. **121**, 6991 (2021).
[249]Z. Wang, S. Grosjean, S. Bräse, and L. Heinke, "Photoswitchable adsorption in metal–organic frameworks based on polar guest–host interactions," ChemPhysChem **16**, 3779 (2015).
[250]Z. Wang, L. Heinke, J. Jelic, M. Cakici, M. Dommaschk, R. J. Maurer, H. Oberhofer, S. Grosjean, R. Herges, S. Bräse, K. Reuter, and C. Wöll, "Photoswitching in nanoporous, crystalline solids: An experimental and theoretical study for azobenzene linkers incorporated in MOFs," Phys. Chem. Chem. Phys. **17**, 14582 (2015).
[251]Y. V. Kaneti, J. Tang, R. R. Salunkhe, X. Jiang, A. Yu, K. C. Wu, and Y. Yamauchi, "Nanoarchitectured design of porous materials and nanocomposites from metal-organic frameworks," Adv. Mater. **29**, 1604898 (2017).
[252]M.-L. Hu, M. Y. Masoomi, and A. Morsali, "Template strategies with MOFs," Coord. Chem. Rev. **387**, 415 (2019).
[253]T. K. Kim, K. J. Lee, J. Y. Cheon, J. H. Lee, S. H. Joo, and H. R. Moon, "Nanoporous metal oxides with tunable and nanocrystalline frameworks via conversion of metal–organic frameworks," J. Am. Chem. Soc. **135**, 8940 (2013).
[254]X. Yu, L. Yu, H. B. Wu, and X. W. Lou, "Formation of nickel sulfide nanoframes from metal–organic frameworks with enhanced pseudocapacitive and electrocatalytic properties," Angew. Chem. Int. Ed. **54**, 5331 (2015).
[255]L. Chen, R. Luque, and Y. Li, "Controllable design of tunable nanostructures inside metal–organic frameworks," Chem. Soc. Rev. **46**, 4614 (2017).
[256]C. Lu, T. Ben, S. Xu, and S. Qiu, "Electrochemical synthesis of a microporous conductive polymer based on a metal–organic framework thin film," Angew. Chem. Int. Ed. **53**, 6454 (2014).
[257]X. Guo, S. Geng, M. Zhuo, Y. Chen, M. J. Zaworotko, P. Cheng, and Z. Zhang, "The utility of the template effect in metal-organic frameworks," Coord. Chem. Rev. **391**, 44 (2019).
[258]B. D. L. Campéon and N. Yabuuchi, "Fundamentals of metal oxide/oxyfluoride electrodes for Li-/Na-ion batteries," Chem. Phys. Rev. **2**, 041306 (2021).
[259]L. Pilz, C. Natzeck, J. Wohlgemuth, N. Scheuermann, P. G. Weidler, I. Wagner, C. Wöll, and M. Tsotsalas, "Fully automated optimization of robot-based MOF thin film growth via machine learning approaches," Adv. Mater. Interfaces (published online 2022).
[260]Y. Luo, S. Bag, O. Zaremba, A. Cierpka, J. Andreo, S. Wuttke, P. Friederich, and M. Tsotsalas, "MOF synthesis prediction enabled by automatic data mining and machine learning," Angew. Chem. Int. Ed. **61**, e202200242 (2022).
[261]K. Ichimura, Y. Suzuki, T. Seki, A. Hosoki, and K. Aoki, "Reversible change in alignment mode of nematic liquid crystals regulated photochemically by command surfaces modified with an azobenzene monolayer," Langmuir **4**, 1214 (1988).